Fundamental Limits of Wideband Localization

by

Yuan Shen

Submitted to the Department of Electrical Engineering and Computer Science
in partial fulfillment of the requirements for the degree of

Master of Science in Electrical Engineering

at the

MASSACHUSETTS INSTITUTE OF TECHNOLOGY

Feb 2008
[February 2008]

Author ....
Department of Electrical Engineering and Computer Science
Jan 18, 2008

⌃

Certified by....................
⌣Moe Z. Win
Associate Professor
Thesis Supervisor

Accepted by ....
⁄
Terry P. Orlando
Chairman, Department Committee on Graduate Students
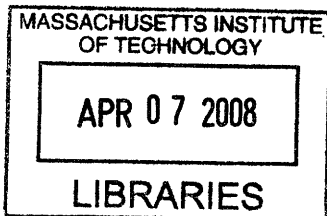
Fundamental Limits of Wideband Localization

by

Yuan Shen

Submitted to the Department of Electrical Engineering and Computer Science
on Jan 18, 2008, in partial fulfillment of the
requirements for the degree of
Master of Science in Electrical Engineering

Abstract

Location-awareness is essential for many wireless network applications. However, determining nodes' positions precisely is a challenging task, especially in harsh multipath propagation environments. To address this problem, wide bandwidth signals are envisioned to be used in future localization systems, since such signals can provide accurate range measurements. In this paper, we investigate the localization performance of wideband networks and proposed a performance measure called the squared position error bound (SPEB) to characterize the localization accuracy. We derive the SPEB succinctly by applying the notion of equivalent Fisher information (EFI). The EFI provides insights into the essence of localization problem by unifying the localization information from individual anchors and that from *a priori* knowledge of the agent's position in a canonical form. We also investigate the use of wideband antenna arrays and the effect of clock asynchronism on the localization accuracy. Our analysis begins with the received waveforms themselves rather than utilizing only signal metrics, such as time-of-arrival and received signal strength, extracted from the waveforms. Our framework exploits all the information inherent in the received waveforms, and therefore the SPEB serves as a fundamental limit of localization accuracy.

Thesis Supervisor: Moe Z. Win
Title: Associate Professor

Acknowledgments

I would like to gratefully acknowledge all people who contributed to this thesis.

First and foremost, I would like to express my deep and sincere gratitude to my advisor, Professor Moe Win, for his patient guidance and encouragement over the past two years. From him, I have gained invaluable insights and self-confidence with respective to both my work and my life, which has made research life smooth and rewarding for me. Professor Win has been a wonderful mentor and friend. I cannot overstate my gratitude for his support.

I am greatly indebted to Henk Wymeersch and Wesley Gifford for their inspiration and help. Without their generous help with research techniques, as well as with grammar, this thesis would not have been possible. I especially want to thank Wes for sharing his broad knowledge and experience on topics ranging from course study to carpentry and from VNA operation to car suspension, since the very first day I joined the group.

I am grateful to all the members of the W group-Tony, Ae, Wee-Peng, Pedro, Jaime, Kampol, Ulric, Stephano, and Pisit-for their friendship and support. I have truly enjoyed getting to know each of you, both in and outside work. Thank you for sharing your knowledge, for making the office a fun place to be, and for organizing each of the fantastic group activities.

To all my friends, old and new, thank you for sharing both the ups and the downs of this process with empathy and laughter.

Finally, I cannot express the full extent of my gratitude to my parents, Zhongchen and Yiqin, for their love, persistent confidence, and unwavering support in everything I do.

Contents

List of Figures

11

Abbreviations

AoA	angle-of-arrival
CRB	Cramér-Rao bound
EFI	equivalent Fisher information
EFIM	equivalent Fisher information matrix
FIM	Fisher information matrix
GPS	Global Positioning System
LoS	line-of-sight
NLoS	non-line-of-sight
RI	ranging information
RII	ranging information intensity
RSS	Received signal strength
SOEB	squared orientation error bound
SPEB	squared position error bound
TDoA	time-difference-of-arrival
ToA	time-of-arrival
UWB	ultra-wide bandwidth

Chapter 1

Introduction

Location-awareness is essential for many wireless network applications, such as the localization service in next generation cellular networks [1], search-and-rescue operations [2, 3], logistics [4], and blue force tracking in battlefields [5]. Although localization in the absolute frame through the Global Positioning System (GPS) has found applications in many different fields [6], the effectiveness of GPS is limited in harsh environments, such as in buildings, in urban canyons, under tree canopies, and in caves [7]. In these environments, line-of-sight (LoS) signals from GPS satellites are often unavailable due to the inability of GPS signals to penetrate most obstacles. Hence, new localization techniques are required to meet the increasing need for accurate localization in such harsh environments [7, 8].

Wideband wireless networks are capable of providing accurate localization in GPS-denied environments [7–12]. A wireless location-aware network consists of two kinds of nodes: anchors and agents. Anchors are the nodes with known positions (for example, through GPS or system design), and agents are the nodes with unknown positions, as shown in Fig.1-1. Each node is equipped with a transceiver, and localization is accomplished using signals passed between agents and their neighboring anchors. Wide bandwidth or ultra-wide bandwidth (UWB) signals are particularly well-suited for localization, since they can provide accurate and reliable range measurements due to their fine delay resolution and robustness in harsh environments [13–25].

Since agents are localized using the received signals from anchors, their position
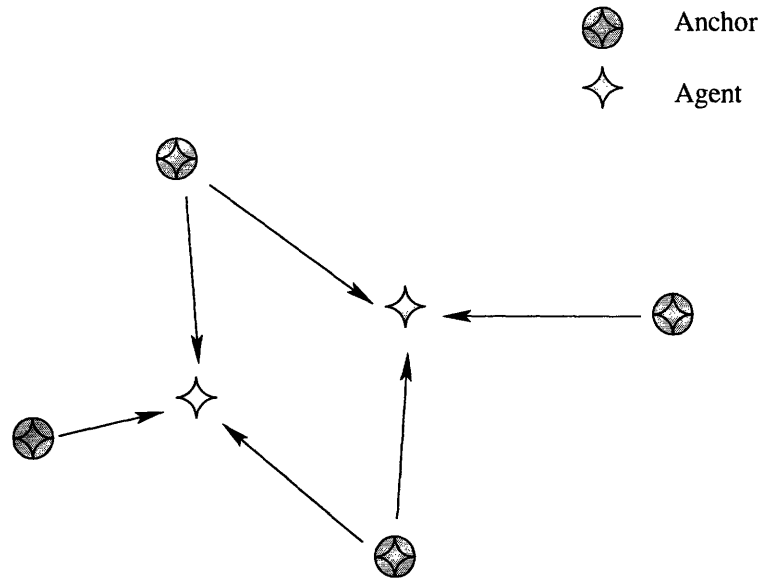
Figure 1-1: Wireless location-aware networks: each arrow denotes the flow of ranging information from anchor to agent.

estimates are subject to uncertainty due to noise and environment-dependent phenomena, such as fading, shadowing, and multipath propagation. To characterize the localization performance, two measures are commonly used, the geometric dilution of precision (GDOP) [6] and the Cramér-Rao bound (CRB) [26]. The GDOP provides a way to compare geometric configurations of anchors [27]. The CRB sets a lower bound on the variance of estimators for deterministic parameters [28, 29]. These two measures are equivalent only if the ranging error is Gaussian [30].

To localize an agent, a number of signals transmitting from anchors to the agent are needed, and the agent's position relative to the anchors is extracted from these signals using a variety of metrics. Commonly used signal metrics for localization include time-of-arrival (ToA) [7–9, 23–25], time-difference-of-arrival (TDoA) [31, 32], angle-of-arrival (AoA) [8, 33], and received signal strength (RSS) [8, 34, 35].

Time-based metrics, ToA and TDoA, are obtained by measuring the signal propagation time between nodes. In ideal scenarios, the estimated distance equals the product of the known propagation speed and the measured signal propagation time. The ToA metric gives possible positions of an agent on a circle with the anchor at the

16

center, and two common way to measure ToA are either the one-way time-of-flight of a signal in a synchronized network [24, 36, 37], or the roundtrip time-of-flight in non-synchronized network [17, 38]. Alternatively, the TDoA metric provides possible positions of an agent on the hyperbola, determined by the difference in the ToA's from two anchors located at the foci. Note that TDoA techniques require synchronization among anchors but not necessarily with the agent.

Since time-based metrics depend on the direct path signal from the anchors to the agent, they are subject to errors caused by multipath and non-line-of-sight (NLoS) conditions [39, 40]. Multipath refers to a propagation phenomenon in which signals reach the receiving antenna via multiple paths, including reflecting off the surroundings. The superposition of these arriving paths results in fading and interference, complicating the detection of the direct path. NLoS conditions, created by physical obstructions in the direct path, produce a positive bias in the measurement of propagation time, which can severely degrade the localization accuracy. Several types of algorithms have been proposed to deal with NLoS conditions: 1) treat the NLoS bias as additive noise modeled by experimental data [7, 41]; 2) identify the NLoS signals, and then remove these signals or weigh the importance of these signals [42–47]; or 3) consider the NLoS bias as a parameter to be estimated [8, 10, 11, 36, 37, 48–50]. In the third type, the NLoS biases and amplitudes of multipath components are modeled as parameters to be estimated for determining the first-arriving path.

Relatively few studies have investigated the effect of multipath and NLoS conditions on the accuracy of ToA-based localization [7, 8, 10, 11, 36, 37, 50, 51]. In [51], the CRB for the position in NLoS environments was derived assuming that the signals are received in line-of-sight (LoS) conditions with biases injected as small perturbations in attempt to account for NLoS effects.[1] The authors in [7, 8, 36, 37] showed that NLoS signals do not improve localization accuracy unless *a priori* knowledge of the NLoS biases is available, but their results were restricted to specific models and did not provide in-depth analysis of the effect of multipath conditions on ranging accuracy.

---

[1] In practice, however, a NLoS induced bias can be as much as a few kilometers depending on the propagation environment [39, 42], and small perturbation may not compensate for NLoS induced error.

The angle at which a signal arrives at the agent, known as AoA, provides information about the agent's position relative to the anchor. AoA can be obtained using an array of antennas, based on the signals' ToA at each antenna.[2] The use of the AoA metric for localization has been investigated, and many hybrid systems have been proposed. These include hybrid ToA/AoA systems [49, 56], and hybrid TDoA/AoA systems [57]. However, these studies either are restricted to narrowband signals, or approximate wide bandwidth signals using narrowband models. Such approaches are not applicable for wideband antenna arrays, since typical assumptions for narrowband array signal processing are not valid for wide bandwidth signals.

RSS is also a useful metric for localization, since the propagation distance between nodes can be estimated from the strength of the received signal [8, 34, 38]. This technique has been widely implemented due to its low complexity, but has limited accuracy [4, 8]. Although RSS can be measured by the receiver during data communication, accurate channel model is needed in order to obtain reliable range estimates.

Note that all these signal metrics are obtained from the received waveforms, and the specific measurement processes used to extract these metrics may discard relevant information for localization. Moreover, the models for the signal metrics depend heavily on the measurement processes. For instance, the ranging error of the ToA metric is commonly modeled as additive Gaussian [7, 49, 58]. However, it has been shown that the ranging error is not Gaussian [20, 24, 59, 60], and this has been further verified by experiments [7, 23]. Therefore, in deriving the fundamental limits of localization accuracy, it is necessary to start from the received waveforms rather than from signal metrics extracted from the waveforms [10, 11, 36, 37].

In this thesis, we investigate the localization accuracy of wideband wireless networks. Our analysis begins with the received waveforms themselves rather than utilizing only signal metrics, such as ToA, TDoA, AoA, and RSS, extracted from the waveforms.

---

[2]There are two ways to obtain the AoA metric: the first is directly through measurement by a directional antenna, and the second is indirectly through ToA measurements using an antenna array [52–55]. Wideband directional antennas that satisfy size and cost requirements are difficult to implement, since they are required to work across a large bandwidth [38]. As such, antenna arrays are more commonly used, when angle measurement for wide bandwidth signals is necessary.

The main contributions of this thesis are as follows:

- We derive the fundamental limits of localization accuracy for wideband wireless networks in terms of a performance measure called the squared position error bound (SPEB).

- We propose the notion of equivalent Fisher information (EFI), which enables us to succinctly derive the SPEB. This methodology also provides insights into the essence of the localization problem by unifying the localization information from anchors and that from the *a priori* knowledge of the agent's position in a canonical form.

- We characterize the *a priori* knowledge of the channel parameters from realistic wideband propagation models and determine its contribution to the localization accuracy.

- We quantify the effects of multipath propagation and path-overlap on localization accuracy, and show that the NLoS components can be beneficial when *a priori* channel knowledge is available.

- We derive the fundamental limits of localization and orientation accuracy for localization systems employing wideband antenna arrays. We prove that AoA metrics obtained from antenna arrays do not increase the localization accuracy beyond that achieved by ToA metrics alone.

- We quantify the effect of clock asynchronism between the anchors and the agents on localization accuracy, using both a single antenna and an array of antennas.

The rest of the thesis is organized as follows. In Chapter 2, we present the our system model and propose the notion of the SPEB to characterize localization accuracy. Chapter 3 provides the derivation of the FIM for the SPEB, for both deterministic and random parameter cases. Then, in Chapter 4, we introduce the notion of EFI, and show how it can simplify the derivation of the SPEB and give insights into the

19

localization problem. In Chapter 5, we investigate the performance of localization systems employing wideband antenna arrays. Chapter 6 investigates the effect of clock asynchronism between the anchors and the agents. Finally, numerical illustrations are given in Chapter 7, and conclusions are drawn in the last chapter.

Chapter 2

Squared Position Error Bound in Multipath Environments

In this chapter, we briefly describe the wideband channel model [15–18, 61] and introduce the SPEB, a performance measure for localization accuracy.

2.1 System Model

Consider a wireless network consisting of $N_\circledast$ anchors and multiple agents. Each anchor has perfect knowledge of its position, and each agent attempts to estimate its position based on the received wide bandwidth waveforms from neighboring anchors. Radio signals traveling from anchors to agents are subject to multipath propagation. The agents estimate their positions independently, and hence without loss of generality, our analysis focuses on one agent in the network.

Let $\mathbf{p} \in \mathbb{R}^n$ for $n = 2$ or 3 denote the coordinates of the agent's position, which are to be estimated, and let $\mathcal{N}_\circledast = \{1, 2, \cdots, N_\circledast\}$ denote the set of all anchors whose positions $\mathbf{p}_k \in \mathbb{R}^n$ ($k \in \mathcal{N}_\circledast$) are precisely known. Without loss of generality, we let $\mathcal{N}_\mathrm{L} = \{1, 2, \cdots, M\}$ denote the set of anchors from which the agent receives LoS signals ($0 \leq M \leq N_\circledast$) and let $\mathcal{N}_\mathrm{NL} = \{M + 1, M + 2, \cdots, N_\circledast\}$ denote the remaining anchors from which the agent receives NLoS signals. We first focus on two dimensional case ($n = 2$) and then extend the results to $n = 3$. For $n = 2$, we have $\mathbf{p} \triangleq [\, x \ y \,]^T$

and $\mathbf{p}_k \triangleq [\, x_k \; y_k \,]^T$.

The received waveform at the agent from the kth anchor can be written as

$$r_k(t) = \sum_{l=1}^{L_k} \alpha_k^{(l)} \cdot s\left(t - \tau_k^{(l)}\right) + z_k(t)\,, \qquad t \in [\, 0, T_{\mathrm{ob}}) \tag{2.1}$$

where $s(t)$ is a known wideband waveform whose Fourier transform is denoted by $S(f)$, $\alpha_k^{(l)}$ and $\tau_k^{(l)}$ are the amplitude and delay, respectively, of the lth path, L_k is the number of multipath components,[1] $z_k(t)$ represents the observation noise modeled as additive white Gaussian processes with two-side power spectral density $N_0/2$, and $[\, 0, T_{\mathrm{ob}})$ is the observation interval. The relationship between the agent's position and the delay of the lth path is given by

$$\tau_k^{(l)} = \frac{1}{c}\left[\, \|\mathbf{p} - \mathbf{p}_k\| + b_k^{(l)} \,\right], \tag{2.2}$$

where $\| \cdot \|$ is the Euclidean distance, c is the speed of light, and $b_k^{(l)} \geq 0$ is a range bias. Range bias $b_k^{(1)} = 0$ for LoS propagation, whereas $b_k^{(l)} > 0$ for NLoS propagation. Our analysis is based on the received signal of the form given in (2.1), and hence the parameter set includes the agent's position and the nuisance multipath parameters, i.e.,

1. The agent's position $\mathbf{p} = [\, x \; y \,]^T$;

2. The biases associated with NLoS paths,[2] denoted by $\mathbf{b} = \left[\, \mathbf{b}_1^T \;\; \mathbf{b}_2^T \;\; \cdots \;\; \mathbf{b}_{N_\circledast}^T \,\right]^T$, where the individual element is

$$\mathbf{b}_a = \begin{cases} \left[\, b_k^{(2)} \;\; b_k^{(3)} \;\; \cdots \;\; b_k^{(L_k)} \,\right]^T, & \text{for } \; k \in \mathcal{N}_{\mathrm{L}} \\ \left[\, b_k^{(1)} \;\; b_k^{(2)} \;\; b_k^{(3)} \;\; \cdots \;\; b_k^{(L_k)} \,\right]^T, & \text{for } \; k \in \mathcal{N}_{\mathrm{NL}}. \end{cases} \tag{2.3}$$

Note that we exclude $b_k^{(1)}$ from the parameter vector $\boldsymbol{\theta}$ for LoS signals since

---

[1]The number of multipath components L_k in $r_k(t)$ depends on the transmission bandwidth as well as the physical environment.

[2]Note that throughout this paper, we will make a distinction between signals and paths. In a LoS signal, the first path is called a LoS path, whereas the remaining paths are referred to as NLoS paths. In a NLoS signal, all paths are NLoS paths.

$$b_k^{(1)} = 0;$$

3. The amplitudes of multipath components $\boldsymbol{\alpha} = \begin{bmatrix} \boldsymbol{\alpha}_1^T & \boldsymbol{\alpha}_2^T & \cdots & \boldsymbol{\alpha}_{N_\circledast}^T \end{bmatrix}^T$, where

$$\boldsymbol{\alpha}_k = \begin{bmatrix} \alpha_k^{(1)} & \alpha_k^{(2)} & \cdots & \alpha_k^{(L_k)} \end{bmatrix}^T, \quad k \in \mathcal{N}_\circledast. \tag{2.4}$$

For notational convenience, we collect all parameters into the vector

$$\boldsymbol{\theta} = \begin{bmatrix} \mathbf{p}^T & \boldsymbol{\kappa}_1^T & \boldsymbol{\kappa}_2^T & \cdots & \boldsymbol{\kappa}_{N_\circledast}^T \end{bmatrix}^T \tag{2.5}$$

where $\boldsymbol{\kappa}_k$ is the vector of the multipath parameters associated with $r_k(t)$,

$$\boldsymbol{\kappa}_k = \begin{cases} \begin{bmatrix} \alpha_k^{(1)} & b_k^{(2)} & \alpha_k^{(2)} & \cdots & b_k^{(L_k)} & \alpha_k^{(L_k)} \end{bmatrix}^T, & k \in \mathcal{N}_{\mathrm{L}} \\ \begin{bmatrix} b_k^{(1)} & \alpha_k^{(1)} & b_k^{(2)} & \alpha_k^{(2)} & \cdots & b_k^{(L_k)} & \alpha_k^{(L_k)} \end{bmatrix}^T, & k \in \mathcal{N}_{\mathrm{NL}} \end{cases}. \tag{2.6}$$

2.2 Squared Position Error Bound

Let $\hat{\boldsymbol{\theta}}$ denote an estimate of the parameter vector $\boldsymbol{\theta}$ based on the $N_\circledast$ received waveforms, given by the vector

$$\mathbf{r}(t) = \begin{bmatrix} r_1(t) & r_2(t) & \cdots & r_{N_\circledast}(t) \end{bmatrix}^T, \quad t \in [0, T_{\mathrm{ob}}). \tag{2.7}$$

This continuous random process $\mathbf{r}(t)$ can be represented by the random vector

$$\mathbf{r} = \begin{bmatrix} \mathbf{r}_1^T & \mathbf{r}_2^T & \cdots & \mathbf{r}_{N_\circledast}^T \end{bmatrix}^T, \tag{2.8}$$

where $\mathbf{r}_k$ is obtained from the Karhunen-Loeve expansion of $r_k(t)$ [28, 29]. The mean squared error (MSE) matrix of $\hat{\boldsymbol{\theta}}$ satisfies the Information Inequality[3] [28, 29, 62]

$$\mathbb{E}_{\mathbf{r},\boldsymbol{\theta}} \left\{ (\hat{\boldsymbol{\theta}} - \boldsymbol{\theta})(\hat{\boldsymbol{\theta}} - \boldsymbol{\theta})^T \right\} \succeq \mathbf{J}_{\boldsymbol{\theta}}^{-1}. \tag{2.9}$$

---

[3]The notation $\mathbb{E}_{\mathbf{r},\boldsymbol{\theta}}\{\cdot\}$ is the expectation operator with respect to the random vectors $\mathbf{r}$ and $\boldsymbol{\theta}$, and the notation $\mathbf{A} \succeq \mathbf{B}$ denotes that the matrix $\mathbf{A} - \mathbf{B}$ is positive semi-definite.

where $\mathbf{J}_\theta$ is the Fisher information matrix (FIM) for the parameter vector $\boldsymbol{\theta}$.[4] Note that (2.9) holds for both deterministic and random parameter vectors under some regularity conditions [28]. Moreover, if the parameter vector is hybrid, i.e., some of its elements are deterministic and others are random, the above inequality still holds and provides lower bound on the MSE matrix of any unbiased estimates of the deterministic parameters and any estimates of the random parameters [62].[5]

Definition 1. *The squared position error bound (SPEB) is defined to be*[6]

$$\mathcal{P}(\mathbf{p}) \triangleq tr\left\{ \left[\mathbf{J}_\theta^{-1} \right]_{2\times 2} \right\}. \tag{2.10}$$

Note that the above definition is natural, since (2.9) implies that the MSE matrix of the position estimate $\hat{\mathbf{p}} = [\, \hat{x} \;\; \hat{y} \,]^T$ satisfies [10]

$$\mathbb{E}_{\mathbf{r},\theta} \left\{ (\hat{\mathbf{p}} - \mathbf{p})(\hat{\mathbf{p}} - \mathbf{p})^T \right\} \succeq \left[\mathbf{J}_\theta^{-1} \right]_{2\times 2}, \tag{2.11}$$

and thus we have[7]

$$\mathbb{E}_{\mathbf{r},\theta} \left\{ \|\hat{\mathbf{p}} - \mathbf{p}\|^2 \right\} \geq tr\left\{ \left[\mathbf{J}_\theta^{-1} \right]_{2\times 2} \right\}. \tag{2.12}$$

Thus, to obtain the SPEB, we need to derive the FIM for the parameter vector $\boldsymbol{\theta}$.

---

[4]More precisely, $\mathbf{J}_\theta$ is called the Bayesian information matrix if all or some parameters in $\boldsymbol{\theta}$ are random, and the corresponding lower bound is called the Bayesian Cramèr-Rao bound or the hybrid Bayesian Cramèr-Rao bound, respectively. In this work, we do not distinguish the names.

[5]With a slight abuse of notation, $\mathbb{E}_{\mathbf{r},\theta}\{\cdot\}$ in (2.9) will be used for both deterministic and hybrid cases with the understanding that the expectation operation is not performed over the deterministic elements of $\boldsymbol{\theta}$.

[6]The notation $tr\{\cdot\}$ is the trace of a square matrix, and $[\,\cdot\,]_{n\times n}$ denotes the upper left $n \times n$ submatrix of its argument.

[7]Note that for a three-dimensional localization problem, the SPEB is defined using the 3×3 matrix $\left[\mathbf{J}_\theta^{-1} \right]_{3\times 3}$.

24

Chapter 3

Fisher Information Matrix

In this chapter, we derive the Fisher information matrix for both deterministic and random parameter estimation. The former case corresponds to the situation where there is no *a priori* knowledge of the parameters, whereas in the latter case, such knowledge is available. This knowledge will be shown to increase the estimation accuracy.

3.1 Fisher Information Matrix without *A Priori* Knowledge

The FIM for the deterministic parameter vector $\boldsymbol{\theta}$ is given by [28]

$$\mathbf{J}_{\boldsymbol{\theta}} \triangleq \mathbb{E}_{\mathbf{r}} \left\{ \left[\frac{\partial}{\partial \boldsymbol{\theta}} \ln f(\mathbf{r}|\boldsymbol{\theta}) \right] \cdot \left[\frac{\partial}{\partial \boldsymbol{\theta}} \ln f(\mathbf{r}|\boldsymbol{\theta}) \right]^{T} \right\}, \tag{3.1}$$

where $f(\mathbf{r}|\boldsymbol{\theta})$ is the likelihood ratio of the random vector $\mathbf{r}$ conditioned on $\boldsymbol{\theta}$. Since the received waveforms from different anchors are independent, the likelihood ratio can be written as [29]

$$f(\mathbf{r}|\boldsymbol{\theta}) = \prod_{k \in \mathcal{N}_\circledast} f(\mathbf{r}_k|\boldsymbol{\theta}), \tag{3.2}$$

where

$$f(\mathbf{r}_k|\boldsymbol{\theta}) \propto \exp\left\{\frac{2}{N_0}\int_0^{T_{\text{ob}}} r_k(t) \cdot \sum_{l=1}^{L_k} \alpha_k^{(l)} s\left(t - \tau_k^{(l)}\right) dt - \frac{1}{N_0}\int_0^{T_{\text{ob}}} \left[\sum_{l=1}^{L_k} \alpha_k^{(l)} s\left(t - \tau_k^{(l)}\right)\right]^2 dt\right\}.$$

$$(3.3)$$

Definition 2. *An agent is said to be localizable if its position can be determined by the signal metrics extracted from waveforms received from neighboring anchors.*

To facilitate the analysis, we consider a mapping from $\boldsymbol{\theta}$ into another parameter vector

$$\boldsymbol{\eta} = \left[\begin{array}{cccc} \boldsymbol{\eta}_1^T & \boldsymbol{\eta}_2^T & \cdots & \boldsymbol{\eta}_{N_\oplus}^T \end{array}\right]^T,$$

$$(3.4)$$

where

$$\boldsymbol{\eta}_k = \left[\begin{array}{cccccccc} \tau_k^{(1)} & \tilde{\alpha}_k^{(1)} & \tau_k^{(2)} & \tilde{\alpha}_k^{(2)} & \cdots & \tau_k^{(L_k)} & \tilde{\alpha}_k^{(L_k)} \end{array}\right]^T,$$

$$(3.5)$$

and $\tilde{\alpha}_k^{(l)} \triangleq \alpha_k^{(l)}/c$. When the agent is localizable,[1] this mapping is a bijection and provides an alternative expression for the FIM as

$$\mathbf{J}_{\boldsymbol{\theta}} = \mathbf{T} \cdot \mathbf{J}_{\boldsymbol{\eta}} \cdot \mathbf{T}^T,$$

$$(3.6)$$

where $\mathbf{J}_{\boldsymbol{\eta}}$ is the FIM for $\boldsymbol{\eta}$, and $\mathbf{T}$ is the Jacobian matrix for the transformation from $\boldsymbol{\theta}$ to $\boldsymbol{\eta}$, given respectively by

$$\mathbf{J}_{\boldsymbol{\eta}} \triangleq \mathbb{E}_{\mathbf{r}}\left\{\left[\frac{\partial}{\partial\boldsymbol{\eta}}\ln f(\mathbf{r}|\boldsymbol{\theta})\right] \cdot \left[\frac{\partial}{\partial\boldsymbol{\eta}}\ln f(\mathbf{r}|\boldsymbol{\theta})\right]^T\right\} = \left[\begin{array}{cc} \boldsymbol{\Lambda}_{\text{L}} & \mathbf{0} \\ \mathbf{0} & \boldsymbol{\Lambda}_{\text{NL}} \end{array}\right],$$

$$(3.7)$$

---

[1]Note that the agent is localizable, i.e., trilateration is possible, when $M \geq 3$, or in some special cases when $M = 2$.

$$\mathbf{T} = \frac{\partial \boldsymbol{\eta}}{\partial \boldsymbol{\theta}} \triangleq \frac{1}{c} \begin{bmatrix} \mathbf{T_L} & \mathbf{T_{NL}} \\ \mathbf{0} & \mathbf{I} \end{bmatrix}, \tag{3.8}$$

where $\mathbf{0}$ is a matrix of all zeros, $\mathbf{I}$ is an identity matrix, and block matrices $\boldsymbol{\Lambda_L}$, $\boldsymbol{\Lambda_{NL}}$, $\mathbf{T_L}$ and $\mathbf{T_{NL}}$ are given in Appendix A.1. Substituting (3.7) and (3.8) into (3.6), we have

$$\mathbf{J}_{\boldsymbol{\theta}} = \frac{1}{c^2} \begin{bmatrix} \mathbf{T_L}\boldsymbol{\Lambda_L}\mathbf{T}_L^T + \mathbf{T_{NL}}\boldsymbol{\Lambda_{NL}}\mathbf{T}_{NL}^T & \mathbf{T_{NL}}\boldsymbol{\Lambda_{NL}} \\ \boldsymbol{\Lambda_{NL}}\mathbf{T}_{NL}^T & \boldsymbol{\Lambda_{NL}} \end{bmatrix}. \tag{3.9}$$

3.2 Fisher Information Matrix with *A Priori* Knowledge

We now incorporate the *a priori* knowledge for localization, which is known to increase the estimation accuracy. By exploiting the propagation channel models, we can characterize the *a priori* channel knowledge in terms of probability density functions (p.d.f.'s). The propagation models for wideband channels [38,55,61] and UWB channels [15–18,38] have been established by experimental efforts. We briefly summarize them and derive the joint *a priori* p.d.f. of the multipath parameters in Appendix A.2.

Since the multipath parameters $\boldsymbol{\kappa}_k$ for different k are independent *a priori*, the joint p.d.f. of $\boldsymbol{\theta}$ can be written as[2]

$$g(\boldsymbol{\theta}) = g_{\mathrm{p}}(\mathbf{p}) \cdot \prod_{k \in \mathcal{N}_\circledast} g_k(\boldsymbol{\kappa}_k | \mathbf{p}), \tag{3.10}$$

where $g_{\mathrm{p}}(\mathbf{p})$ is the p.d.f. of the agent's position, and $g_k(\boldsymbol{\kappa}_k | \mathbf{p})$ is the joint p.d.f. of the multipath parameters conditioned on the agent's position, given by (A.17). Using (3.2) and (3.10), the joint p.d.f. of the observation $\mathbf{r}$ and the parameter $\boldsymbol{\theta}$ can be

---

[2]This is a general expression of the joint p.d.f., where all parameters are random. If some parameters are deterministic, their corresponding $g(\cdot)$ are eliminated from (3.10).

27

written as

$$f(\mathbf{r}, \boldsymbol{\theta}) = f(\mathbf{r}|\boldsymbol{\theta}) \cdot g(\boldsymbol{\theta}), \tag{3.11}$$

and the FIM for localization can then be expressed as

$$\mathbf{J}_{\boldsymbol{\theta}} = \mathbf{J}_{\mathrm{w}} + \mathbf{J}_{\mathrm{p}}, \tag{3.12}$$

where $\mathbf{J}_{\mathrm{w}}$ and $\mathbf{J}_{\mathrm{p}}$ are the FIM's from the received waveforms and the *a priori* knowledge, respectively, given by[3]

$$\mathbf{J}_{\mathrm{w}} \triangleq \mathbb{E}_{\mathbf{r}, \boldsymbol{\theta}} \left\{ \left[\frac{\partial}{\partial \boldsymbol{\theta}} \ln f(\mathbf{r}|\boldsymbol{\theta}) \right] \cdot \left[\frac{\partial}{\partial \boldsymbol{\theta}} \ln f(\mathbf{r}|\boldsymbol{\theta}) \right]^{T} \right\}, \tag{3.13}$$

$$\mathbf{J}_{\mathrm{p}} \triangleq \mathbb{E}_{\boldsymbol{\theta}} \left\{ \left[\frac{\partial}{\partial \boldsymbol{\theta}} \ln g(\boldsymbol{\theta}) \right] \cdot \left[\frac{\partial}{\partial \boldsymbol{\theta}} \ln g(\boldsymbol{\theta}) \right]^{T} \right\}. \tag{3.14}$$

The FIM $\mathbf{J}_{\mathrm{w}}$ can be obtained by taking the expectation of $\mathbf{J}_{\boldsymbol{\theta}}$ in (3.9) over the random parameter vector $\boldsymbol{\theta}$. Substituting (3.10) in (3.14), we obtain

$$\mathbf{J}_{\mathrm{p}} = \begin{bmatrix} \Xi_{\mathrm{p}} + \sum_{k \in \mathcal{N}_{\oplus}} \Xi_{\mathrm{p,p}}^{k} & \Xi_{\mathrm{p},\kappa}^{1} & \cdots & \Xi_{\mathrm{p},\kappa}^{N_{\oplus}} \\ \Xi_{\mathrm{p},\kappa}^{1\,T} & \Xi_{\kappa,\kappa}^{1} & & \mathbf{0} \\ \vdots & & \ddots & \\ \Xi_{\mathrm{p},\kappa}^{N_{\oplus}\,T} & \mathbf{0} & & \Xi_{\kappa,\kappa}^{N_{\oplus}} \end{bmatrix}, \tag{3.15}$$

---

[3]Note from (3.13) and (3.14) that the FIM $\mathbf{J}_{\boldsymbol{\theta}}$ for random parameters requires averaging over these parameters, whereas the FIM in (3.1) is in general a function of the deterministic parameter vector $\boldsymbol{\theta}$.

where the FIM's $\Xi_{\mathbf{p}}$, $\Xi_{\kappa,\kappa}^k$, $\Xi_{\mathbf{p},\mathbf{p}}^k$, and $\Xi_{\mathbf{p},\kappa}^k$ are given by

$$\Xi_{\mathbf{p}} \triangleq \mathbb{E}_{\theta}\left\{\left[\frac{\partial}{\partial \mathbf{p}}\ln g_{\mathbf{p}}(\mathbf{p})\right]\cdot\left[\frac{\partial}{\partial \mathbf{p}}\ln g_{\mathbf{p}}(\mathbf{p})\right]^T\right\}, \qquad (3.16)$$

$$\Xi_{\kappa,\kappa}^k \triangleq \mathbb{E}_{\theta}\left\{\left[\frac{\partial}{\partial \kappa_k}\ln g_k(\kappa_k|\mathbf{p})\right]\cdot\left[\frac{\partial}{\partial \kappa_k}\ln g_k(\kappa_k|\mathbf{p})\right]^T\right\}, \qquad (3.17)$$

$$\Xi_{\mathbf{p},\mathbf{p}}^k \triangleq \mathbb{E}_{\theta}\left\{\left[\frac{\partial}{\partial \mathbf{p}}\ln g_k(\kappa_k|\mathbf{p})\right]\cdot\left[\frac{\partial}{\partial \mathbf{p}}\ln g_k(\kappa_k|\mathbf{p})\right]^T\right\}, \qquad (3.18)$$

and

$$\Xi_{\mathbf{p},\kappa}^k \triangleq \mathbb{E}_{\theta}\left\{\left[\frac{\partial}{\partial \mathbf{p}}\ln g_k(\kappa_k|\mathbf{p})\right]\cdot\left[\frac{\partial}{\partial \kappa_k}\ln g_k(\kappa_k|\mathbf{p})\right]^T\right\}, \qquad (3.19)$$

respectively. The FIM $\Xi_{\mathbf{p}}$ describes the FIM from *a priori* knowledge of $\mathbf{p}$, and the FIM's $\Xi_{\kappa,\kappa}^k$, $\Xi_{\mathbf{p},\mathbf{p}}^k$, and $\Xi_{\mathbf{p},\kappa}^k$ characterize the joint *a priori* knowledge of $\mathbf{p}$ and κ_k.

Chapter 4

Evaluation of FIM for SPEB

In the previous chapters, we formulated the localization problem and derived the FIM $\mathbf{J}_\theta$ in (3.9) and (3.12) for deterministic and random parameters, respectively. The SPEB can then be obtained by taking the inverse of $\mathbf{J}_\theta$. However, $\mathbf{J}_\theta$ is a matrix of very high dimension, making it difficult to invert, while only a small submatrix $[\mathbf{J}_\theta^{-1}]_{2\times 2}$ is of interest (see (2.10)). Furthermore, direct matrix inversion provides no insight into the essence of localization problems. To overcome this, we introduce the notion of equivalent Fisher information [10–12].

4.1 Equivalent Fisher Information Matrix

Definition 3. *The equivalent Fisher information matrix (EFIM) of a reduced parameter set is a matrix with a dimension lower than the original FIM, but it retains all the necessary information to derive the Information Inequality of the parameter set of interest.*

Let $\mathbf{J}_e \in \mathbb{R}^{n\times n}$ be

$$\mathbf{J}_e \triangleq \mathbf{A} - \mathbf{B}\mathbf{C}^{-1}\mathbf{B}^T, \tag{4.1}$$

where $\mathbf{A} \in \mathbb{R}^{n\times n}$, $\mathbf{B} \in \mathbb{R}^{n\times(N-n)}$, and $\mathbf{C} \in \mathbb{R}^{(N-n)\times(N-n)}$ are block matrices of the

original FIM $\mathbf{J}_\theta$, such that

$$\mathbf{J}_\theta = \begin{bmatrix} \mathbf{A} & \mathbf{B} \\ \mathbf{B}^T & \mathbf{C} \end{bmatrix}. \tag{4.2}$$

Note that the right hand side of (4.1) is known as the Schur complement of matrix $\mathbf{C}$ [63]. It can be shown that $[\mathbf{J}_\theta^{-1}]_{n \times n} = \mathbf{J}_e^{-1}$, and hence the MSE matrix of the estimates for the first n of N parameters in $\boldsymbol{\theta}$ is bounded below by $\mathbf{J}_e^{-1}$. Therefore, $\mathbf{J}_e$ is the EFIM for these n parameters.

Armed with the notion of EFI, we can reduce the dimension of the original FIM to obtain a $n \times n$ EFIM through one or several steps, where n is the number of parameters of interest. For a two-dimensional localization problem $(n = 2)$, we are interested in the SPEB involving only the 2×2 matrix $[\mathbf{J}_\theta^{-1}]_{2 \times 2}$.

4.2   Analysis without *A Priori* Knowledge

We first focus on the case where *a priori* knowledge of $\boldsymbol{\theta}$ is not available. We apply the notion of EFI to reduce the dimension of the original FIM in (3.9) and to gain insights into the localization problems. The following results present the EFIM for the agent's position.

Proposition 1. *If* a priori *knowledge of the parameters is not available, then the EFIM for the agent's position is*

$$\mathbf{J}_e = \frac{1}{c^2} \mathbf{T}_L \boldsymbol{\Lambda}_L \mathbf{T}_L^T, \tag{4.3}$$

where $\boldsymbol{\Lambda}_L$ *and* $\mathbf{T}_L$ *are given by* (A.4) *and* (A.1), *respectively.*

Proof. Let $\mathbf{A} = \mathbf{T}_{\mathrm{NL}} \boldsymbol{\Lambda}_{\mathrm{NL}} \mathbf{T}_{\mathrm{NL}}^T + \mathbf{T}_L \boldsymbol{\Lambda}_L \mathbf{T}_L^T$, $\mathbf{B} = \mathbf{T}_{\mathrm{NL}} \boldsymbol{\Lambda}_{\mathrm{NL}}$, and $\mathbf{C} = \boldsymbol{\Lambda}_{\mathrm{NL}}$ in (3.9).

32

Applying the notion of EFI in (4.1), we have

$$
\begin{aligned}
\mathbf{J_e} &= \frac{1}{c^2} \left[\left(\mathbf{T}_{NL} \boldsymbol{\Lambda}_{NL} \mathbf{T}_{NL}^T + \mathbf{T}_L \boldsymbol{\Lambda}_L \mathbf{T}_L^T \right) - \mathbf{T}_{NL} \boldsymbol{\Lambda}_{NL} \cdot \boldsymbol{\Lambda}_{NL}^{-1} \cdot \boldsymbol{\Lambda}_{NL} \mathbf{T}_{NL}^T \right] \\
&= \frac{1}{c^2} \mathbf{T}_L \boldsymbol{\Lambda}_L \mathbf{T}_L^T .
\end{aligned}
\tag{4.4}
$$

$\square$

Remark: Proposition 1 shows that if *a priori* knowledge is not available, NLoS signals do not contribute to the EFIM for the agent's position, and hence do not improve the localization accuracy. It implies that we can eliminate these NLoS signals when analyzing the limits of the estimation accuracy. This observation agrees with the results of [37], where the amplitudes of the multipath components are assumed to be known.

Note that the dimension of $\mathbf{J_e}$ in (4.3) is much larger than 2×2, the minimum dimension required for the SPEB. We will apply the notion of EFI again to further reduce the dimension of $\mathbf{J_e}$ in the following theorem, which enables us to investigate the effect of multipath propagation in LoS signals. Before the theorem, we need to define the notion of the first contiguous-cluster.

Definition 4. *In a LoS signal, the first contiguous-cluster is defined to be the set of paths* $\{1, 2, \cdots, j\}$, *such that* $|\tau_i - \tau_{i+1}| < T_s$ *for* $i = 1, 2, \cdots, j-1$, *and* $|\tau_j - \tau_{j+1}| > T_s$, *where* T_s *is the duration of* $s(t)$.

Intuitively, the first contiguous-cluster is the first group of non-disjoint paths (see Fig. 4-1).[1]

Theorem 1. *If a priori knowledge of the parameters is not available, then the EFIM is a 2×2 matrix*

$$
\mathbf{J}_e(\mathbf{p}) = \frac{8\pi^2 \beta^2}{c^2} \sum_{k \in \mathcal{N}_L} (1 - \chi_k) \cdot \mathsf{SNR}_k^{(1)} \cdot \mathbf{q}_k \mathbf{q}_k^T ,
\tag{4.5}
$$

---

[1]Two paths that arrive at time τ_i and τ_j are called non-disjointed if $|\tau_i - \tau_j| < T_s$.
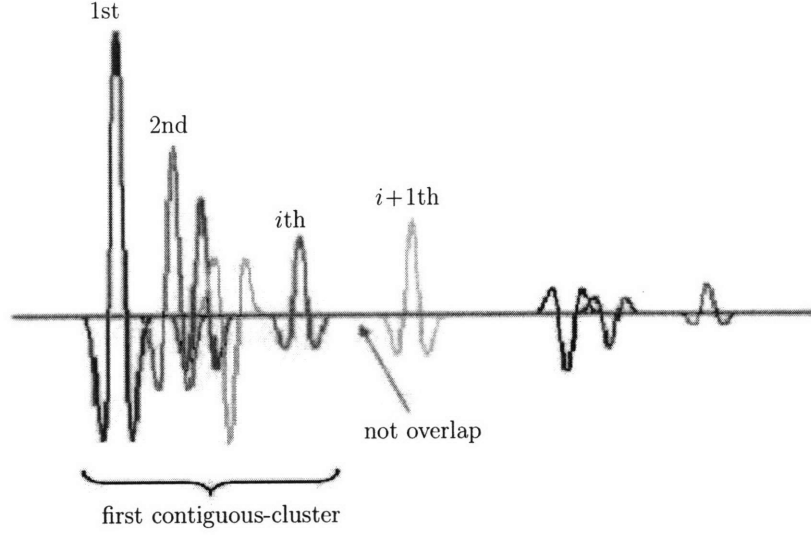
Figure 4-1: Illustration of the first contiguous-cluster in a LoS signal.

where $0 \leq \chi_k \leq 1$ is given by (A.37),

$$\beta \triangleq \left(\frac{\int_{-\infty}^{+\infty} f^2 |S(f)|^2 df}{\int_{-\infty}^{+\infty} |S(f)|^2 df} \right)^{1/2} , \tag{4.6}$$

$$\mathsf{SNR}_k^{(l)} \triangleq \frac{|\alpha_k^{(l)}|^2 \int_{-\infty}^{+\infty} |S(f)|^2 df}{N_0} , \tag{4.7}$$

and $\mathbf{q}_k \triangleq \left[\begin{array}{cc} \cos \phi_k & \sin \phi_k \end{array} \right]^T$ with

$$\phi_k = \arctan \frac{y - y_k}{x - x_k} . \tag{4.8}$$

Furthermore, only the first contiguous-cluster of LoS signals contains information for localization.

Proof. See Appendix A.3.1. □

Before giving the interpretation of above result, we introduce the notion of ranging

34

information.

Definition 5. *Ranging information (RI) is a* 2×2 *matrix of the form*

$$\lambda \cdot \mathbf{J}_r(\phi) \,, \tag{4.9}$$

where λ *is a nonnegative number, and*

$$\mathbf{J}_r(\phi) \triangleq \begin{bmatrix} \cos^2 \phi & \cos \phi \sin \phi \\ \cos \phi \sin \phi & \sin^2 \phi \end{bmatrix} \,, \tag{4.10}$$

with ϕ *denoting the AoA from the anchor to the agent. The number* λ *is called the ranging information intensity (RII), and the matrix* $\mathbf{J}_r(\phi)$ *is called the elementary ranging information.*[2]

With the above definition, (4.5) can be rewritten as

$$\mathbf{J}_e(\mathbf{p}) = \sum_{k \in \mathcal{N}_L} \lambda_k \cdot \mathbf{J}_r(\phi_k) \,, \tag{4.11}$$

where λ_k is the RII from the kth anchor, given by

$$\lambda_k = \frac{8\pi^2 \beta^2}{c^2}(1 - \chi_k) \cdot \mathsf{SNR}_k^{(1)} \,, \tag{4.12}$$

and $\mathbf{J}_r(\phi_k)$ is the elementary ranging information with the angle ϕ_k.

Remark: In Theorem 1, β is known as the effective bandwidth [28, 64], χ_k is called path-overlap coefficient that characterizes the multipath propagation effect, and $\mathsf{SNR}_k^{(l)}$ denotes the SNR of the lth path in $r_k(t)$. We draw the following observations from the Theorem 1:

- The original FIM in (3.9) can be transformed into a simple 2×2 EFIM in a canonical form, given by (4.11), as a weighted sum of the elementary ranging

---

[2]The elementary ranging information is one-dimensional along the direction from the anchor to the agent with unit intensity, i.e., $\mathbf{J}_r(\phi)$ has one (and only one) non-zero eigenvalue equal to 1 with corresponding eigenvector $\mathbf{q} = \begin{bmatrix} \cos \phi & \sin \phi \end{bmatrix}^T$.

information from individual anchors. Each anchor (e.g. the kth anchor) can provide only one-dimensional RI along the direction from the anchor to the agent, given by $\mathbf{q}_k$, with intensity λ_k.[3]

- The RII λ_k depends on the effective bandwidth of $s(t)$, the SNR of the first path, and the path-overlap coefficient. The path-overlap coefficient χ_k is determined by the propagation condition of the first contiguous-cluster in the LoS signal. More precisely, among the parameters in $\boldsymbol{\kappa}_k$, only the amplitudes of the first path $\alpha_k^{(1)}$ and the NLoS biases $b_k^{(l)}$ in the first contiguous-cluster affect the SPEB (refer to (A.37)).

- Path-overlap in the first contiguous-cluster effectively reduces the RII ($0 \leq \chi_k \leq 1$), thus leading to a higher SPEB, unless the signal via the first path does not overlap with others ($\chi_k = 0$).

- The expression of χ_k in (A.37) shows that it is necessary to include $\alpha_k^{(l)}$'s in the parameter vector, unless the first contiguous-cluster contains only the first path.[4] Intuitively, localization information is obtained from the estimates of ToA $\tau_k^{(1)}$'s, and path-overlap would cause interpath interference. Therefore, eliminating multipath parameters would result in a looser performance bound in cluttered environments.

We can specialize the above theorem into a case in which the first path in a LoS signal is completely resolvable, i.e., the first contiguous-cluster contains only a single element.

Corollary 1. *If a priori knowledge of the parameters is not available and the first contiguous-cluster contains only the first path, then the RII from the kth anchor is*

$$\lambda_k = \frac{8\pi^2\beta^2}{c^2} \cdot \mathsf{SNR}_k^{(1)} . \tag{4.13}$$

---

[3]For notational convenience, we suppress the dependence of $\mathbf{q}_k$ and λ_k on the agent's position $\mathbf{p}$ throughout the paper.

[4]The amplitudes of all multipath components are not included in the analysis of [37, 49].

Proof. See Appendix A.3.2. □

Remark: Corollary 1 corresponds to the case when $\chi_k = 0$ in (4.12). In such a case, λ_k attains its maximum value since there is no path-overlap. This result is intuitive and important: the RII depends only on the first path of the LoS signal, if the first path is resolvable. If the signal via the first path overlaps with others, however, these paths will deteriorate the accuracy of the first path's estimate and hence the RII.

The above results give closed-form expressions of the EFIM for localization, which provide insights into the localization problem and facilitate further analysis. For ultrawide bandwidth (UWB) signals, the assumption of non-overlapping is quite reasonable since larger bandwidth signals possess better multipath resolvability.

From Theorem 1, the SPEB can be derived as

$$\mathcal{P}(\mathbf{p}) = \frac{c^2}{8\pi^2\beta^2} \cdot \frac{2 \cdot \sum_{k\in\mathcal{N}_{\mathrm{L}}}(1-\chi_k) \cdot \mathrm{SNR}_k^{(1)}}{\sum_{k\in\mathcal{N}_{\mathrm{L}}} \sum_{m\in\mathcal{N}_{\mathrm{L}}}(1-\chi_k)(1-\chi_m) \cdot \mathrm{SNR}_k^{(1)}\mathrm{SNR}_m^{(1)} \sin^2(\phi_k - \phi_m)} .$$

(4.14)

For the special case in which the first paths are resolvable, by Corollary 1, we have $\chi_k = 0$ and the SPEB in (4.14) becomes

$$\mathcal{P}(\mathbf{p}) = \frac{c^2}{8\pi^2\beta^2} \cdot \frac{2 \cdot \sum_{k\in\mathcal{N}_{\mathrm{L}}} \mathrm{SNR}_k^{(1)}}{\sum_{k\in\mathcal{N}_{\mathrm{L}}} \sum_{m\in\mathcal{N}_{\mathrm{L}}} \mathrm{SNR}_k^{(1)}\mathrm{SNR}_m^{(1)} \sin^2(\phi_k - \phi_m)} .$$

(4.15)

Equation (4.15) is consistent with the results based on single path models in [8, 37], however, those results are not accurate for scenarios in which the first path is not resolvable.

4.3 Analysis with *A Priori* Knowledge of Channel Parameters

We then consider the case where there is *a priori* knowledge of the channel parameters, but not of the agent's position. In such cases, since $\mathbf{p}$ is deterministic but unknown, $g_{\mathbf{p}}(\mathbf{p})$ is eliminated in (3.10) and hence the *a priori* p.d.f. of $\boldsymbol{\theta}$ becomes

$$g(\boldsymbol{\theta}) = \prod_{k \in \mathcal{N}_\circledast} g_k(\boldsymbol{\kappa}_k | \mathbf{p}) \, . \tag{4.16}$$

Similar to the results in the previous section, we can derive the 2×2 EFIM for the corresponding FIM in Sec. 3.2.

Theorem 2. *If a priori knowledge of the channel parameters is available and the sets of channel parameters corresponding to different anchors are mutually independent, then the EFIM is a 2×2 matrix*

$$\mathbf{J}_e(\mathbf{p}) = \sum_{k \in \mathcal{N}_L} \lambda_k \cdot \mathbf{J}_r(\phi_k) + \sum_{k \in \mathcal{N}_{NL}} \lambda_k \cdot \mathbf{J}_r(\phi_k) \, , \tag{4.17}$$

where the RII λ_k is given by (A.52) for LoS signals and (A.53) for NLoS signals, and $\mathbf{J}_r(\phi_k)$ is the elementary ranging information with angle ϕ_k.

Proof. See Appendix A.3.3. □

Remark: Theorem 2 generalizes the result of Theorem 1 from deterministic to hybrid parameter estimation.[5] In this case, the EFIM is still a 2×2 matrix and can be expressed in a canonical form as a weighed sum of elementary ranging information from individual anchors. In addition, the property that every anchor provides only one-dimensional information for localization is retained as in Theorem 1.

In Appendix A.3.4, we show that *a priori* channel knowledge increases the RII, leading to higher localization accuracy, and when *a priori* knowledge goes to zero, the

---

[5]This is the case where the agent's position $\mathbf{p}$ is deterministic and the channel parameters are random.

result of Theorem 2 degenerate to that of Theorem 1 as expected. On the other hand, from the perspective of Bayesian estimation, we show in Appendix A.3.4 that one can consider $b_k^{(1)}$ ($k \in \mathcal{N}_{\mathrm{L}}$) as random parameters with infinite *a priori* Fisher information instead of eliminating them from $\boldsymbol{\theta}$ as in our model in Sec. 2.1. Therefore, it is not necessary to distinguish the RII in (A.52) for LoS signals and that in (A.53) for NLoS signals. As such, we can treat all signals as NLoS signals with appropriate *a priori* Fisher information.

4.4 Analysis with *A Priori* Knowledge of Channel Parameters and Agent's Position

We next consider the case where *a priori* knowledge of the agent's position is available in addition to that of the channel parameters. Unlike the previous two cases, the topology, i.e., the anchors and the agent, changes with the agent's positions, i.e., ϕ_k is different.

The 2×2 EFIM is given in (A.67) in Appendix A.3.6, and it is more intricate than those of the previous two cases. However, if we consider the far-field scenario, where the agent's *a priori* position is concentrated in a small area relative to the distances between the anchors and the agent, ϕ_k is approximately the same for different possible agent's position, and we have the following result.

Proposition 2. *If 1) a priori knowledge of the agent's position and the channel parameters is available, and 2) the sets of channel parameters corresponding to different anchors are mutually independent, then in far-field scenarios, the EFIM is a 2×2 matrix*

$$\mathbf{J}_e = \boldsymbol{\Xi}_{\mathbf{p}} + \sum_{k \in \mathcal{N}_\circledast} \lambda_k(\bar{\mathbf{p}}) \cdot \mathbf{J}_r \left(\bar{\phi}_k\right), \tag{4.18}$$

39

where $\bar{\mathbf{p}}$ is the expected agent's position, given by

$$\bar{\mathbf{p}} = \mathbb{E}_{\mathbf{p}}\{\mathbf{p}\} = \int \mathbf{p} \cdot g_p(\mathbf{p}) \, d\mathbf{p}, \qquad (4.19)$$

$\bar{\phi}_k$ is the AoA from kth anchor to $\bar{\mathbf{p}}$, and the RII $\lambda_k(\bar{\mathbf{p}})$ is given by (A.70), $\mathbf{J}_r\left(\bar{\phi}_k\right)$ is the elementary ranging information with angle $\bar{\phi}_k$, and $\Xi_{\mathbf{p}}$ is the EFIM from the a priori knowledge of the agent's position, given by (3.16).

Proof. See Appendix A.3.6. $\qquad\qquad\qquad\qquad\qquad\qquad\qquad\qquad\square$

Remark: This is the most general case in which we also exploit the *a priori* knowledge of the agent's position, in addition to that of the channel parameters, for localization. The expressions for the EFIM can be involved in general. Fortunately, in far-field scenarios, the EFIM can be simply written as the sum of two parts as shown in (4.18): the first part is the EFIM from the *a priori* knowledge of the agent's position, and the second part is a weighted sum of the elementary ranging information from individual anchors as in the previous two cases. Proposition 2 unifies the contribution from anchors and that from the *a priori* knowledge of the agent's position into the EFIM. The concept of localization with *a priori* knowledge of the agent's position is useful for a wide range of applications such as successive localization or tracking.

4.5 Example: Localization Using UWB Transmissions

We now take localization via UWB transmissions as an example to illustrate the contribution of *a priori* channel knowledge. In such systems, the multipath components tend to be resolvable (not overlapping) due to its wide transmission bandwidth. To gain some insights, we consider a simple scenario in which the channel knowledge is available, and $b_k^{(l)}$ and $\alpha_k^{(l)}$ are mutually independent *a priori*. Hence, the EFIM from

40

the *a priori* channel knowledge can be written as

$$\mathbf{J}_{\mathrm{p}} = \mathrm{diag}\left\{\mathbf{0}, \Xi_1, \Xi_2, \cdots, \Xi_{N_\circledast}\right\}, \tag{4.20}$$

where

$$\Xi_k = \mathrm{diag}\left\{\gamma(b_k^{(1)}),\ \gamma(\alpha_k^{(1)}),\ \cdots,\ \gamma(b_k^{(L_k)}),\ \gamma(\alpha_k^{(L_k)})\right\}, \tag{4.21}$$

and $\gamma(b_k^{(l)})$ and $\gamma(\alpha_k^{(l)})$ are the *a priori* Fisher information of $b_k^{(l)}$ and $\alpha_k^{(l)}$, respectively. Note that $\gamma(b_k^{(1)}) = \infty$ for LoS signals. Using Theorem 2, the EFIM in (4.17) becomes

$$\mathbf{J}_{\mathrm{e}}(\mathbf{p}) = \sum_{k \in \mathcal{N}_\circledast}\left(\sum_{l=1}^{L_k} w_{k,l} \cdot \lambda_k^{(l)}\right) \mathbf{J}_{\mathrm{r}}(\phi_k), \tag{4.22}$$

where

$$w_{k,l} = \frac{\gamma(b_k^{(l)})}{\lambda_k^{(l)} + \gamma(b_k^{(l)})}, \qquad \text{and} \qquad \lambda_k^{(l)} = \frac{8\pi^2\beta^2}{c^2} \cdot \mathbb{E}_\theta\{\mathsf{SNR}_k^{(l)}\}. \tag{4.23}$$

Remark: Coefficient $w_{k,l}$ weighs the RII of the lth path in received waveform $r_k(t)$. It has the maximum value of 1 when $\gamma(b_k^{(l)}) \to \infty$, and the minimum value of 0 when $\gamma(b_k^{(l)}) \to 0$. The expression for $\mathbf{J}_{\mathrm{e}}(\mathbf{p})$ has the following implications:

- The LoS path contributes all of its RI to the EFIM since $\gamma(b_k^{(1)}) = \infty$ and hence $w_{k,1} = 1$.

- The NLoS path with *a priori* knowledge of the bias $b_k^{(l)}$ contributes some RI to the EFIM, since $0 \leq \gamma(b_k^{(l)}) \leq \infty$ and hence $0 \leq w_{k,l} \leq 1$. When the *a priori* knowledge of $b_k^{(l)}$ goes to 0, the path does not contribute any RI to the EFIM since $w_{k,l} = 0$. This result is consistent with Corollary 1. On the other hand, if $b_k^{(l)}$ is known, the path contributes all of its RI as a LoS path since $w_{k,l} = 1$.

- The coefficient $w_{k,l}$ does not depend on $\gamma(\alpha_k^{(l)})$, i.e., the *a priori* knowledge of $\alpha_k^{(l)}$. This is consistent with Theorem 1 and should be expected since multipath components are resolvable.

The coefficients $w_{k,l}$ quantifies the contribution of the multipath components with *a priori* knowledge to the EFIM. These findings are not restricted to specific NLoS bias models as in [65] and provide a more general view of the contribution from the *a priori* channel knowledge.

4.6 Generalization to 3D Localization

All the results obtained thus far can be easily extended to three dimensional case, i.e., $\mathbf{p} = [\, x \ \ y \ \ z \,]^T$ and $\mathbf{q}_k$ becomes

$$\mathbf{q}_k = \left[\ \cos \varphi_k \cos \phi_k \ \ \sin \varphi_k \cos \phi_k \ \ \sin \phi_k \ \right]^T, \tag{4.24}$$

where φ_k and ϕ_k are the angles in the polar coordinates. Similarly, we have a corresponding 3×3 EFIM in the form of (4.17).

Chapter 5

Wideband Localization with Antenna Arrays

In this chapter, we consider localization systems using wideband antenna arrays, which can provide both ToA and AoA metrics. Since orientation of the array may be unknown, we develop a model for jointly estimating the agent's position and orientation, and then derive the SPEB and the squared orientation error bound (SOEB).

5.1   Wideband Antenna Array Model

Consider a network where each agent is equipped with an N_∇-antenna array, which can extract both the ToA and AoA metrics from neighboring anchors. The agents estimate their positions and orientations based on the received waveforms. Without loss of generality, our analysis focuses on a single agent in the network.

Let $\mathcal{N}_\nabla = \{1, 2, \cdots, N_\nabla\}$ denote the set of all antennas, and let $\mathbf{p}_n^{\text{Array}} \triangleq [\, x_n^{\text{Array}} \ y_n^{\text{Array}} \,]^T$ denote the position of the agent's nth antenna, which needs to be estimated. The relative positions of the antennas in the array are usually known, but the orientation of the array may be unknown, depending on the specific system configuration. If we denote $\mathbf{p} = [\, x \ y \,]^T$ as a reference point and φ as the orientation of the array,[1] then

---

[1]Note from geometry that the orientation φ is independent of the specific reference point.

43
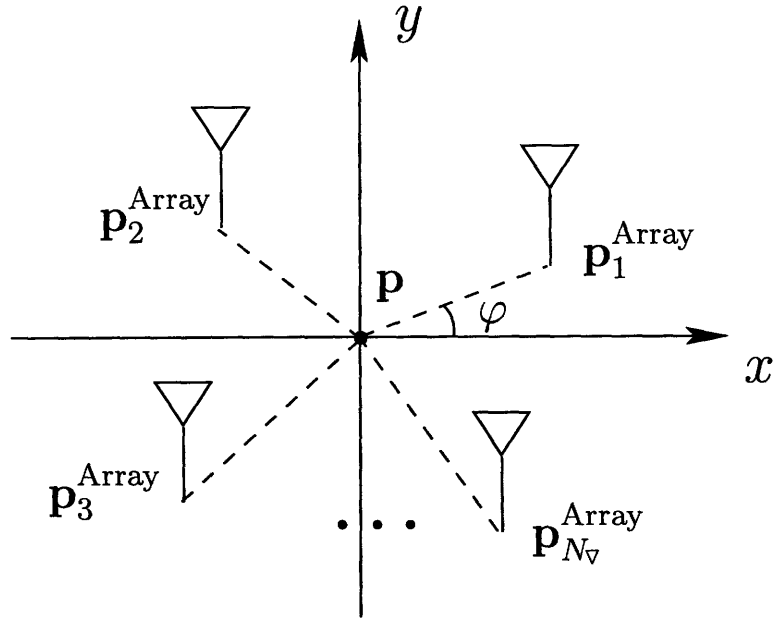
Figure 5-1: Illustration of the reference point $\mathbf{p}$, orientation φ, and the relative positions of the antennas in the array.

the position of the nth antenna in the array can be represented as (Fig. 5-1)

$$\mathbf{p}_n^{\text{Array}} = \mathbf{p} + \left[\begin{array}{c} \Delta x_n(\mathbf{p}, \varphi) \\ \Delta y_n(\mathbf{p}, \varphi) \end{array} \right], \qquad n = 1, 2, \cdots, N_\triangledown, \tag{5.1}$$

where $\Delta x_n(\mathbf{p}, \varphi)$ and $\Delta y_n(\mathbf{p}, \varphi)$ denote the relative distance in x and y direction from the reference point to the nth antenna, respectively. The reference point can be arbitrary, but we will choose the array center defined as follows.[2]

Definition 6. *The array center is defined as the value* $\mathbf{p}_0$, *satisfying*

$$\sum_{n \in \mathcal{N}_\triangledown} \Delta x_n(\mathbf{p}_0, \varphi) = 0 \quad and \quad \sum_{n \in \mathcal{N}_\triangledown} \Delta y_n(\mathbf{p}_0, \varphi) = 0. \tag{5.2}$$

Since the orientation of the array may be unknown, we classify the localization problems into orientation-aware and orientation-unaware cases. In both cases, φ can be thought of as a random parameter with infinite (orientation-aware case) and zero

---

[2]We show later that the array center has the lowest SPEB in far-field scenarios .

44

(orientation-unaware case) *a priori* Fisher information [10].

The received waveform at the agent's nth antenna from the kth anchor can be written as

$$r_{n,k}(t) = \sum_{l=1}^{L_{n,k}} \alpha_{n,k}^{(l)} \cdot s\left(t - \tau_{n,k}^{(l)}\right) + z_{n,k}(t), \qquad t \in [0, T_{\text{ob}}), \tag{5.3}$$

where $s(t)$ is a known wideband waveform, $\alpha_{n,k}^{(l)}$ and $\tau_{n,k}^{(l)}$ are the amplitude and delay, respectively, of the lth path, $L_{n,k}$ is the number of multipath components, $z_{n,k}(t)$ represents the observation noise modeled as additive white Gaussian processes with two-side power spectral density $N_0/2$, and $[0, T_{\text{ob}})$ is the observation interval. The relationship between the nth antenna's position and the delay of the lth path is given by

$$\tau_{n,k}^{(l)} = \frac{1}{c}\left[\left\|\mathbf{p}_n^{\text{Array}} - \mathbf{p}_k\right\| + b_{n,k}^{(l)}\right]. \tag{5.4}$$

Since the parameters to be considered include the position of the reference point, array orientation, and the nuisance multipath parameters, we have

$$\boldsymbol{\theta} = \begin{bmatrix} \mathbf{p}^T & \varphi & \check{\boldsymbol{\kappa}}_1^T & \check{\boldsymbol{\kappa}}_2^T & \cdots & \check{\boldsymbol{\kappa}}_N^T \end{bmatrix}^T, \tag{5.5}$$

where $\check{\boldsymbol{\kappa}}_n$ consists of the multipath parameters associated with the received waveforms from all anchors at the nth antenna,

$$\check{\boldsymbol{\kappa}}_n = \begin{bmatrix} \boldsymbol{\kappa}_{n,1}^T & \boldsymbol{\kappa}_{n,2}^T & \cdots & \boldsymbol{\kappa}_{n,N_\circledast}^T \end{bmatrix}^T, \tag{5.6}$$

and each $\boldsymbol{\kappa}_{n,k}$ consists of the multipath parameters associated with $r_{n,k}(t)$,

$$\boldsymbol{\kappa}_{n,k} = \begin{bmatrix} b_{n,k}^{(1)} & \alpha_{n,k}^{(1)} & \cdots & b_{n,k}^{(L_{n,k})} & \alpha_{n,k}^{(L_{n,k})} \end{bmatrix}^T. \tag{5.7}$$

5.2 Squared Orientation Error Bound

The overall received waveforms at the antenna array can be written as

$$\mathbf{r}(t) = \left[\begin{array}{cccc} \mathbf{r}_1(t) & \mathbf{r}_2(t) & \cdots & \mathbf{r}_{N_{\triangledown}}(t) \end{array}\right]^T, \qquad t \in [0, T_{\mathrm{ob}}), \qquad (5.8)$$

where the received waveforms at the nth antenna is given by

$$\mathbf{r}_n(t) = \left[\begin{array}{cccc} r_{n,1}(t) & r_{n,2}(t) & \cdots & r_{n,N_{\circledast}}(t) \end{array}\right]^T. \qquad (5.9)$$

Similar to Sec. 2.2, $\mathbf{r}(t)$ can be represented by a random vector $\mathbf{r}$ (where $r_{n,k}(t)$ is represented by a random vector $\mathbf{r}_{n,k}$) using the KL expansion.

Definition 7. *The squared orientation error bound (SOEB) is defined to be*

$$\mathcal{P}(\varphi) \triangleq \left[\mathbf{J}_{\boldsymbol{\theta}}^{-1}\right]_{3,3} \qquad (5.10)$$

where $[\cdot]_{3,3}$ denotes the third diagonal element of its argument.

We consider the multipath parameter vectors $\boldsymbol{\kappa}_{n,k}$ for different n's and k's to be independent, and hence the *a priori* p.d.f. of $\boldsymbol{\theta}$ can be written as

$$g(\boldsymbol{\theta}) = g_{\mathrm{p}}(\mathbf{p})\, g_{\varphi}(\varphi) \cdot \prod_{k \in \mathcal{N}_{\circledast}} \prod_{n \in \mathcal{N}_{\triangledown}} g_{n,k}(\boldsymbol{\kappa}_{n,k}|\mathbf{p}, \varphi), \qquad (5.11)$$

where $g_{\mathrm{p}}(\mathbf{p})$ is the p.d.f. of the agent's position, $g_{\varphi}(\varphi)$ is the p.d.f. of the agent's orientation, and $g_{n,k}(\boldsymbol{\kappa}_{n,k}|\mathbf{p}, \varphi)$ is the joint p.d.f. of the multipath parameters conditioned on the agent's position and orientation.

5.3 Analysis with *A Priori* Knowledge of Channel Parameters

We first consider scenarios in which *a priori* knowledge of the channel parameters is available, but there is no *a priori* knowledge of the agent's position nor orientation.

In such cases, $\mathbf{p}$ and φ are deterministic but unknown, and hence $g_{\mathbf{p}}(\mathbf{p})$ and $g_{\varphi}(\varphi)$ are eliminated in (5.11). Following similar steps in Sec. 4.3, we have the following theorems.

Theorem 3. *If a priori knowledge of the channel parameters is available and the sets of channel parameters corresponding to different antennas and anchors are mutually independent, then the EFIM for the position and the EFI for the orientation, using an $N_\triangledown$-antenna array, are given respectively by*

$$\mathbf{J}_e^{Array}(\mathbf{p}) = \sum_{n \in \mathcal{N}_\triangledown} \mathbf{J}_{e,n} - \frac{1}{\sum_{n \in \mathcal{N}_\triangledown} \sum_{k \in \mathcal{N}_\circledast} \lambda_{n,k} h_{n,k}^2 + \Xi} \cdot \mathbf{q}\mathbf{q}^T, \qquad (5.12)$$

and

$$J_e^{Array}(\varphi) = \sum_{n \in \mathcal{N}_\triangledown} \sum_{k \in \mathcal{N}_\circledast} \lambda_{n,k} h_{n,k}^2 - \mathbf{q}^T \left(\sum_{n \in \mathcal{N}_\triangledown} \mathbf{J}_{e,n} \right)^{-1} \mathbf{q}, \qquad (5.13)$$

where $\Xi = \infty$ and $\Xi = 0$ correspond to orientation-aware and orientation-unaware localization, respectively. In the above expressions,

$$\mathbf{J}_{e,n} = \sum_{k \in \mathcal{N}_\circledast} \lambda_{n,k} \cdot \mathbf{J}_r(\phi_{n,k}) \qquad (5.14)$$

is the individual EFIM corresponding to the nth antenna,

$$\mathbf{q} = \sum_{n \in \mathcal{N}_\triangledown} \sum_{k \in \mathcal{N}_\circledast} \lambda_{n,k} h_{n,k} \cdot \mathbf{q}_{n,k} \qquad (5.15)$$

$$h_{n,k} = \frac{d}{d\varphi} \Delta x_n(\mathbf{p}, \varphi) \cdot \cos \phi_{n,k} + \frac{d}{d\varphi} \Delta y_n(\mathbf{p}, \varphi) \cdot \sin \phi_{n,k}, \qquad (5.16)$$

where the RII $\lambda_{n,k}$ is given by (A.87), and $\mathbf{q}_{n,k} = \begin{bmatrix} \cos \phi_{n,k} & \sin \phi_{n,k} \end{bmatrix}^T$ with $\phi_{n,k}$ denoting the AoA from the kth anchor to the nth antenna.

Proof. See Appendix A.4.1. □

Remark: The EFIM for the position in (5.12), when an agent is equipped with an antenna array, consists of two parts: 1) the sum of localization information obtained

47

from individual antennas, and 2) the information reduction due to the uncertainty in the orientation estimate, which is subtracted from the first part.[3] Since $\mathbf{q}\mathbf{q}^T$ in the second part is a positive semi-definite 2×2 matrix and $\sum_{n \in \mathcal{N}_\nabla} \sum_{k \in \mathcal{N}_\circledast} \lambda_{n,k} h_{n,k}^2$ is positive, we always have the following inequality

$$\mathbf{J}_e^{\text{Array}}(\mathbf{p}) \preceq \sum_{n \in \mathcal{N}_\nabla} \mathbf{J}_{e,n}, \tag{5.17}$$

where the equality in (5.17) is achieved for orientation-aware localization (i.e., $\Xi = \infty$), or orientation-independent localization (i.e., $\mathbf{q} = \mathbf{0}$). The inequality in (5.17) is due to the uncertainty in the orientation estimate, which degrades the localization accuracy, except for $\Xi = \infty$ or $\mathbf{q} = \mathbf{0}$. Therefore, the EFIM for the position, using antenna arrays, is bounded above by the sum of all EFIM's corresponding to individual antennas.

Note that the EFIM in (5.12) depends only on the individual RI's between each pair of anchors and antennas through $\lambda_{n,k}$'s and $\phi_{n,k}$'s, and the array geometry through $h_{n,k}$'s. Hence, it is not necessary to jointly consider the received waveforms at the N_∇ antennas, implying that AoA obtained by antenna arrays does not increase localization accuracy. Though counterintuitive at first, this finding should not be too surprising since AoA is obtained indirectly through ToA's by the antenna array, and the ToA information has already been fully exploited for localization by individual antennas.

While the equality in (5.12) is achieved for every reference point in orientation-aware localization, only a unique reference point achieves this equality in orientation-unaware localization. We make this statement precise in the following definition.

Definition 8. *The orientation center is a reference point* $\mathbf{p}^*$ *such that*

$$\mathbf{J}_e^{Array}(\mathbf{p}^*) = \sum_{n \in \mathcal{N}_\nabla} \mathbf{J}_{e,n}. \tag{5.18}$$

---

[3]For notational convenience, we suppress the dependence of $h_{n,k}$, $\lambda_{n,k}$, and $\mathbf{q}$ on the reference position $\mathbf{p}$ throughout the paper.

Note that every reference point is an orientation center in orientation-aware localization. In orientation-unaware localization, we have the following theorem.

Proposition 3. *Orientation center* $\mathbf{p}^*$ *exists and is unique in orientation-unaware localization, and hence for any* $\mathbf{p} \neq \mathbf{p}^*$,

$$\mathbf{J}_e^{Array}(\mathbf{p}) \prec \mathbf{J}_e^{Array}(\mathbf{p}^*) . \tag{5.19}$$

Proof. See Appendix A.4.2. $\square$

Remark: The orientation center $\mathbf{p}^*$ generally depends on the topology of the anchors and the agent, the properties of the received waveforms, the array geometry, and the array orientation. Since $\mathbf{q} = \mathbf{0}$ at the orientation center, the EFIM for the array center and the EFI for the orientation do not depend on each other, and hence the SPEB and the SOEB can be calculated separately. The theorem also implies that the SPEB of reference points other than $\mathbf{p}^*$ will be strictly larger than that of $\mathbf{p}^*$. The SPEB for any reference point is given in the next theorem.

Corollary 2. *The SOEB is independent of the reference point* $\mathbf{p}$, *and the SPEB is*

$$\mathcal{P}(\mathbf{p}) = \mathcal{P}(\mathbf{p}^*) + \frac{\|\mathbf{p} - \mathbf{p}^*\|^2}{J_e(\varphi)} , \tag{5.20}$$

where $J_e(\varphi)$ *is the EFI for the orientation.*

Proof. See Appendix A.4.3. $\square$

Remark: The corollary shows that the SOEB for the orientation does not depend on the specific reference point, which was not apparent in (5.13). This is intuitive since different reference points only introduce different translations, but not rotations. On the other hand, different reference point $\mathbf{p}$ results in different $h_{n,k}$'s and hence different $\mathbf{q}$, which in turn gives different EFIM for position (see (5.12)). We can interpret the relationship in (5.20) as follows: the SPEB of the reference point $\mathbf{p}$ is equal to that of the orientation center $\mathbf{p}^*$ plus the orientation-induced position error,

49

which increases with the squared distance from $\mathbf{p}$ to $\mathbf{p}^*$ and is proportional to the SOEB.

5.4 Analysis with *A Priori* Knowledge of Channel Parameters and Agent's Position

We next consider scenarios in which *a priori* knowledge of the agent's position and orientation is available. Note that the topology, i.e., the anchors and the agent's antennas, changes with the agent's positions and orientations. We focus on far-field scenarios as they provide insights into the contribution of the *a priori* knowledge of the agent's position to localization.

In far-field scenarios, the antennas in the array are closely located such that the received waveforms from each anchor experience statistically similar propagation channels, i.e., $\alpha_{n,k}^{(l)}$'s and $b_{n,k}^{(l)}$'s are i.i.d. respectively for all n. Since $\phi_{n,k} = \phi_k$ for all n, we have $\lambda_{n,k} = \lambda_k$, $\mathbf{q}_{n,k} = \mathbf{q}_k$ and $\mathbf{J}_{e,n} = \mathbf{J}_e$.

Proposition 4. *In far-field scenarios, the array center becomes the orientation center and has the minimum SPEB.*

Proof. See Appendix A.4.4. $\qquad\qquad\qquad\qquad\qquad\qquad\qquad\qquad\qquad$ $\square$

Remark: Since the orientation center has the minimum SPEB, Proposition 4 implies that the array center always achieves the minimum SPEB in far-field scenarios. Hence, the array center should be chosen as the reference point, since its position can be determined from the array geometry alone, without requiring the received waveforms and the knowledge of the anchor's topology.

Corollary 3. *If 1) a priori knowledge of the channel parameters, the agent's position, and the agent's orientation is available, and 2) the sets of channel parameters corresponding to different anchors are mutually independent, then in far-field scenarios, the EFIM for the array center and the EFI for the orientation, using an $N_\triangledown$-antenna*

array, are given respectively by

$$\mathbf{J}_e^{Array}(\mathbf{p}_0) = N_{\nabla} \cdot \mathbf{J}_e + \Xi_{\mathbf{p}} \,, \tag{5.21}$$

and

$$J_e^{Array}(\varphi) = \sum_{n \in \mathcal{N}_{\nabla}} \sum_{k \in \mathcal{N}_{\circledast}} \lambda_k \bar{h}_{n,k}^2 + \Xi_{\varphi} \,, \tag{5.22}$$

where $\mathbf{J}_e$ is the EFIM corresponding to a single antenna, $\bar{h}_{n,k}$ is a function of $\mathbf{p}_0$, $\Xi_{\mathbf{p}}$ is the EFIM from the a priori knowledge of the array center, given by (3.16), and Ξ_{φ} is the EFI from the a priori knowledge of the agent's orientation, given by

$$\Xi_{\varphi} \triangleq \mathbb{E}_{\varphi} \left\{ \left[\frac{\partial}{\partial \varphi} \ln g_{\varphi}(\varphi) \right] \cdot \left[\frac{\partial}{\partial \varphi} \ln g_{\varphi}(\varphi) \right] \right\} \,. \tag{5.23}$$

Proof. See Appendix A.4.5. □

Remark: Corollary 3 shows that in far-field scenarios, the EFIM for the position and the EFI for the orientation can be written as a sum of two parts, respectively: the first part is from the received waveforms, and the second part is from the *a priori* knowledge, which is characterized by $\Xi_{\mathbf{p}}$ or Ξ_{φ}. Since the array center is the orientation center, $\mathbf{J}_e^{Array}(\mathbf{p}_0)$ and $J_e^{Array}(\varphi)$ do not depend on each other, and hence the SPEB and SOEB can be calculated separately. Note that in far-field scenarios, the localization performance of an N_{∇}-antenna array is equivalent to that of a single antenna with N_{∇} measurements, regardless of the array geometry.

We now illustrate an application of the above theorem for AoA estimation using wideband antenna arrays. Consider a far-field scenario in which the agent has determined its center's position $\mathbf{p}_0$, such that ϕ_k is known. Therefore, estimation of the AoA from the kth anchor to the array, i.e., $\tilde{\phi}_k \triangleq \phi_k - \varphi$, is equivalent to the estimation of the array orientation. By applying Corollary 3, we derive the EFI for the AoA to the array using a wideband antenna array in the following corollary.

Corollary 4. *The EFI for the AoA from the kth anchor to the array, $\tilde{\phi}_k$, is*

$$J_e^{Array}(\tilde{\phi}_k) = \lambda_k \cdot \sum_{n \in \mathcal{N}_\triangledown} \bar{h}_{n,k}^2 + \Xi_\varphi \,. \tag{5.24}$$

5.5 Example: Uniform Linear and Circular Array

The above results are valid for arbitrary array geometries. We now illustrate these results for two commonly used arrays, i.e., the uniform linear array (ULA) and the uniform circular array (UCA), in far-field scenarios (see Fig. 5-2). Without loss of generality, we consider the array center as the reference point, and the position of each antenna in the array can be represented in terms of the array center $\mathbf{p}_0$ and the orientation φ.

- Uniform linear array:

$$\mathbf{p}_n^{Array} = \mathbf{p}_0 + \Delta \left(n - \frac{N_\triangledown + 1}{2} \right) \cdot \begin{bmatrix} \cos\varphi \\ \sin\varphi \end{bmatrix}, \tag{5.25}$$

where Δ is the spacing of the antennas.

- Uniform circular array:

$$\mathbf{p}_n^{Array} = \mathbf{p}_0 + R_0 \cdot \begin{bmatrix} \cos(2\pi \cdot \frac{n-1}{N_\triangledown} + \varphi) \\ \sin(2\pi \cdot \frac{n-1}{N_\triangledown} + \varphi) \end{bmatrix}, \tag{5.26}$$

where R_0 is the radius of the array.

5.5.1 Localization and Orientation

For orientation estimation, the EFI for the orientation, by Corollary 3, is

$$J_e^{L}(\varphi) = \frac{N_\triangledown(N_\triangledown - 1)(N_\triangledown + 1)}{12} \Delta^2 \cdot \sum_{k \in \mathcal{N}_\circledast} \lambda_k \sin^2(\phi_k - \varphi) + \Xi_\varphi \tag{5.27}$$

52

for the ULA, and

$$
J_e^C(\varphi) = \begin{cases} 2R_0^2 \cdot \sum_{k \in \mathcal{N}_\circledast} \lambda_k \sin^2(\phi_k - \varphi) + \Xi_\varphi, & N_\triangledown = 2 \\ N_\triangledown R_0^2/2 \cdot \sum_{k \in \mathcal{N}_\circledast} \lambda_k + \Xi_\varphi, & N_\triangledown > 2 \end{cases}, \qquad (5.28)
$$

for the UCA.

For position estimation, by Corollary 3, the SPEB for the array center in far field scenarios is the same for both the ULA and the UCA. However, the SPEB's for other positions are usually different, depending on the orientation accuracy achieved by different array geometries. For example, the SPEB's can be calculated from (5.20) using (5.27) for the ULA and (5.28) for the UCA.

5.5.2 AoA Estimation

From Corollary 4, the EFI for the AoA from the kth anchor to the array can be written as

$$
J_e^L(\tilde{\phi}_k) = \frac{N_\triangledown(N_\triangledown - 1)(N_\triangledown + 1)}{12} \Delta^2 \cdot \lambda_k \sin^2(\tilde{\phi}_k) + \Xi_\varphi, \qquad (5.29)
$$

for the ULA, and

$$
J_e^C(\tilde{\phi}_k) = \begin{cases} 2R_0^2 \cdot \lambda_k \sin^2(\tilde{\phi}_k) + \Xi_\varphi, & N_\triangledown = 2 \\ N_\triangledown R_0^2/2 \cdot \lambda_k + \Xi_\varphi, & N_\triangledown > 2 \end{cases}. \qquad (5.30)
$$

for the UCA.

Note that $J_e^L(\tilde{\phi}_k)$ in (5.29) agrees with $J_e^C(\tilde{\phi}_k)$ in (5.30) when $N_\triangledown = 2$, as it should, since the two array geometries coincide in this case. When $N_\triangledown > 2$, $J_e^L(\tilde{\phi}_k)$ is highly dependent on the specific AoA ϕ_k, while the performance of the UCA is independent of the AoA. For a fair comparison, we consider an example with the same array size, i.e., $R_0 = (N_\triangledown - 1) \cdot \Delta/2$. If *a priori* orientation knowledge is not available, i.e.,

53

$\Xi_\varphi = 0$, then the ratio of EFI's is

$$\frac{J_e^L(\tilde\phi_k)}{J_e^C(\tilde\phi_k)} = \begin{cases} 1, & N_\nabla = 2 \\ \frac{2\cdot(N_\nabla+1)\sin^2(\tilde\phi_k)}{3\cdot(N_\nabla-1)}, & N_\nabla > 2 \end{cases} . \tag{5.31}$$

When $N_\nabla \geq 5$, the above ratio is always less than 1, implying that the UCA outperforms the ULA. When $N_\nabla = 3, 4$, the ratio depends on the AoA from the kth anchor to the array, and on average,

$$\mathbb{E}_{\phi_k}\left\{\frac{J_e^L(\tilde\phi_k)}{J_e^C(\tilde\phi_k)}\right\} = \frac{(N_\nabla+1)}{3\cdot(N_\nabla-1)} < 1\,, \tag{5.32}$$

provided ϕ_k is uniformly distributed on $[\,0, 2\pi)$. Therefore, we conclude that the UCA can provide better AoA estimates in general and its performance is more robust to different AoA's.

5.6 Multiple Antennas at Anchors

The discussion above focused on the case where each anchor is equipped with only one antenna. From the result in (5.12), the gain of using an antenna array at the agent mainly comes from the multiple copies of the waveform received at different antennas.[4] Its performance is equivalent to a single antenna with measurements in N_∇ time slots, and the advantage of using antenna arrays lies in its ability for simultaneous measurements at the agent.

If anchors are equipped with multiple antennas, each antenna can be viewed as an individual anchor, and hence the agent's SPEB goes down with the number of the antennas at each anchor. Note that all the antennas at a given anchor provide RI approximately in the same direction with the same intensity, as they are closely located.

---

[4]In near-field scenarios, there may be additional gain that arises from the spatial diversity of the multiple antennas at the agent.

Uniform linear array   Uniform circular array
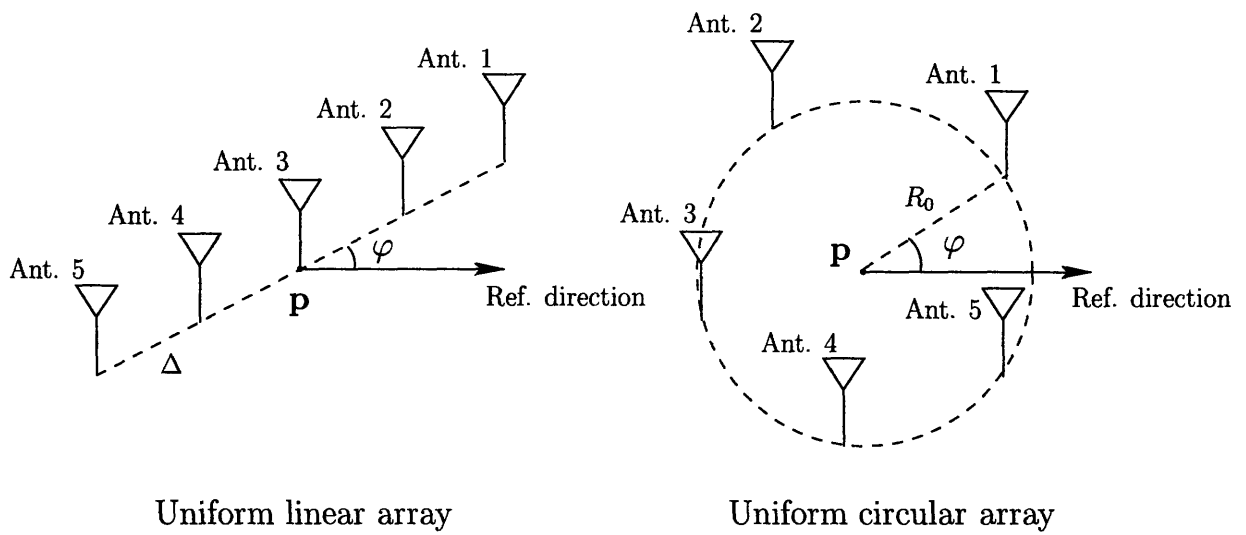
Figure 5-2: Example of the uniform linear and circular array of $N_\nabla = 5$.

Chapter 6

Effect of Clock Asynchronism

In this chapter, we consider a scenario in which the clocks of all anchors are perfectly synchronized but the agent operates asynchronously with the anchors. In such a scenario, the one-way time-of-flight measurement contains a time offset between the agent's clock and the anchors' clock.[1] Here, we investigate the effect of the time offset on the localization accuracy.

6.1 Localization with a Single Antenna

Consider the scenario described in Sec. 2, where each agent is equipped with a single antenna. When the agent operates asynchronously with the anchors, the relationship of (2.2) becomes

$$\tau_k^{(l)} = \frac{1}{c}\Big[\ \|\mathbf{p} - \mathbf{p}_k\| + b_k^{(l)} + B\ \Big],\tag{6.1}$$

where B is a random parameter that characterizes the time offset. In this case, the parameter vector $\boldsymbol{\theta}$ becomes

$$\boldsymbol{\theta} = \Big[\ \mathbf{p}^T\quad B\quad \boldsymbol{\kappa}_1^T\quad \boldsymbol{\kappa}_2^T\quad \cdots\quad \boldsymbol{\kappa}_{N_\circledast}^T\ \Big]^T.\tag{6.2}$$

---

[1]We consider scenarios in which localization time is short relative to clock drifts, such that the time offset is the same for all measurements from the anchors.

Similar to Theorem 2, where $\mathbf{p}$ is deterministic but unknown and the remaining parameters are random, we have the following result.

Theorem 4. *If 1) a priori knowledge of the channel parameters and the time offset is available, and 2) the sets of channel parameters corresponding to different anchors are mutually independent, then the EFIM for the position and the EFI for the time offset are given respectively by*

$$\mathbf{J}_e^B(\mathbf{p}) = \sum_{k \in \mathcal{N}_\circledast} \lambda_k \cdot \mathbf{J}_r(\phi_k) - \frac{1}{\sum_{k \in \mathcal{N}_\circledast} \lambda_k + \Xi_B} \cdot \mathbf{q}_B \mathbf{q}_B^T \tag{6.3}$$

and

$$J_e(B) = \sum_{k \in \mathcal{N}_\circledast} \lambda_k + \Xi_B - \mathbf{q}_B^T \left(\sum_{k \in \mathcal{N}_\circledast} \lambda_k \cdot \mathbf{J}_r(\phi_k) \right)^{-1} \mathbf{q}_B, \tag{6.4}$$

where the RII λ_k is given by (A.53), $\mathbf{J}_r(\phi_k)$ is the elementary ranging information with angle ϕ_k,

$$\mathbf{q}_B = \sum_{k \in \mathcal{N}_\circledast} \lambda_k \cdot \mathbf{q}_k, \tag{6.5}$$

and Ξ_B is the EFI from the a priori knowledge of the time offset B, given by

$$\Xi_B \triangleq \mathbb{E}_B \left\{ \left[\frac{\partial}{\partial B} \ln g_B(B) \right] \cdot \left[\frac{\partial}{\partial B} \ln g_B(B) \right] \right\} \tag{6.6}$$

with $g_B(\cdot)$ denoting the a priori p.d.f. of the time offset B.

Proof. See Appendix A.5.1. $\qquad\qquad\qquad\qquad\qquad\qquad\qquad\qquad\qquad$ $\square$

Remark: Since $\mathbf{q}_B \mathbf{q}_B^T$ is a positive semi-definite matrix and $\sum_{k \in \mathcal{N}_\circledast} \lambda_k$ is positive in (6.3), compare to Theorem 2, we always have the inequality

$$\mathbf{J}_e^B(\mathbf{p}) \preceq \mathbf{J}_e(\mathbf{p}) \tag{6.7}$$

where the equality in (6.7) is achieved for time-offset-known localization (i.e., $\Xi_B =$

58

∞), or time-offset-independent localization (i.e., $\mathbf{q}_B = \mathbf{0}$). The former corresponds to the case where there is accurate knowledge of the time offset, while the latter depends on the RII from each anchor, and the geometry of the anchors and the agent. The inequality of (6.7) results from the uncertainty in the additional parameter B, which degrades the localization accuracy. Hence, the SPEB in the presence of uncertain time offset is always higher than or equal to that without a offset or with a precisely known offset.

We next consider the case where *a priori* knowledge of the agent's position is available, and in far-field scenarios, we have the following theorem.

Corollary 5. *If 1) a priori knowledge of the agent's position, the time-offset and the channel parameters is available, and 2) the sets of channel parameters corresponding to different anchors are mutually independent, then in far-field scenarios, the EFIM for the agent's position and the EFI for the time offset are given respectively by*

$$\mathbf{J}_e^B = \Xi_{\mathbf{p}} + \sum_{k \in \mathcal{N}_\circledast} \lambda_k(\bar{\mathbf{p}}) \cdot \mathbf{J}_r(\bar{\phi}_k) - \frac{1}{\sum_{k \in \mathcal{N}_\circledast} \lambda_k(\bar{\mathbf{p}}) + \Xi_B} \cdot \mathbf{q}_B(\bar{\mathbf{p}}) \mathbf{q}_B(\bar{\mathbf{p}})^T \quad (6.8)$$

and

$$J_e = \Xi_B + \sum_{k \in \mathcal{N}_\circledast} \lambda_k(\bar{\mathbf{p}}) - \mathbf{q}_B(\bar{\mathbf{p}})^T \left(\Xi_{\mathbf{p}} + \sum_{k \in \mathcal{N}_\circledast} \lambda_k(\bar{\mathbf{p}}) \cdot \mathbf{J}_r(\bar{\phi}_k) \right)^{-1} \mathbf{q}_B(\bar{\mathbf{p}}), \quad (6.9)$$

where $\bar{\mathbf{p}}$ is the expected agent's position, $\bar{\phi}_k$ is the AoA from the kth anchor to $\bar{\mathbf{p}}$, and $\Xi_{\mathbf{p}}$ is the EFIM from the a priori knowledge of the agent's position, given by (3.16).

Proof. The proof uses the far-field assumption and it is similar to those of Proposition 2 and Corollary 3. □

6.2 Localization with Antenna Arrays

Consider the scenario describing in Sec. 5 where each agent is equipped with an array of N_∇-antennas. Incorporating the time offset B, (5.4) becomes

$$\tau_{n,k}^{(l)} = \frac{1}{c}\Big[\, \|\mathbf{p}_n^{\text{Array}} - \mathbf{p}_k\| + b_{n,k}^{(l)} + B\,\Big],\tag{6.10}$$

and the corresponding parameter vector $\boldsymbol{\theta}$ becomes

$$\boldsymbol{\theta} = \Big[\; \mathbf{p}^T \quad \varphi \quad B \quad \check{\boldsymbol{\kappa}}_1^T \quad \check{\boldsymbol{\kappa}}_2^T \quad \cdots \quad \check{\boldsymbol{\kappa}}_N^T \;\Big]^T.\tag{6.11}$$

Similar to Theorem 3, where $\mathbf{p}$ and φ are deterministic but unknown and the remaining parameters are random, we have the following theorem.

Theorem 5. *If a priori knowledge of the channel parameters is available and the sets of channel parameters corresponding to different antennas and anchors are mutually independent, then the EFIM for the position, the orientation, and the time offset, using an N_∇-antenna array, is given by*

$$\mathbf{J}_e^{\text{Array-B}} = \begin{bmatrix} \sum_{n\in\mathcal{N}_\nabla}\sum_{k\in\mathcal{N}_\circledast}\lambda_{n,k}\mathbf{q}_{n,k}\mathbf{q}_{n,k}^T & \sum_{n\in\mathcal{N}_\nabla}\sum_{k\in\mathcal{N}_\circledast}h_{n,k}\lambda_{n,k}\mathbf{q}_{n,k} & \sum_{n\in\mathcal{N}_\nabla}\sum_{k\in\mathcal{N}_\circledast}\lambda_{n,k}\mathbf{q}_{n,k} \\ \sum_{n\in\mathcal{N}_\nabla}\sum_{k\in\mathcal{N}_\circledast}h_{n,k}\lambda_{n,k}\mathbf{q}_{n,k}^T & \sum_{n\in\mathcal{N}_\nabla}\sum_{k\in\mathcal{N}_\circledast}h_{n,k}^2\lambda_{n,k} + \Xi & \sum_{n\in\mathcal{N}_\nabla}\sum_{k\in\mathcal{N}_\circledast}h_{n,k}\lambda_{n,k} \\ \sum_{n\in\mathcal{N}_\nabla}\sum_{k\in\mathcal{N}_\circledast}\lambda_{n,k}\mathbf{q}_{n,k}^T & \sum_{n\in\mathcal{N}_\nabla}\sum_{k\in\mathcal{N}_\circledast}h_{n,k}\lambda_{n,k} & \sum_{n\in\mathcal{N}_\nabla}\sum_{k\in\mathcal{N}_\circledast}\lambda_{n,k} + \Xi_B \end{bmatrix},\tag{6.12}$$

where $\Xi = \infty$ and $\Xi = 0$ correspond to orientation-aware and orientation-unaware localization, respectively, and $\lambda_{n,k}$, $\mathbf{q}_{n,k}$, $h_{n,k}$, and Ξ_B are given by (A.87), (5.15), (5.16) and (6.6), respectively.

Proof. The proof is similar to those of Theorem 3 and Theorem 4. $\qquad\qquad\square$

Remark: Theorem 5 gives the complete EFIM for the agent's position, orientation, and time offset. Note that the EFIM is a 4×4 matrix, and we can obtain the individual EFIM for the agent's position, and EFI's for the agent's orientation and time offset by applying the notion of EFI again.

We next consider the case where *a priori* knowledge of the agent's position and orientation is available. In far-field scenarios, we have the following result, which corresponds to Corollary 3.

Corollary 6. *If 1) a priori knowledge of the agent's position, the agent's orientation, and the channel parameters is available, and 2) the sets of channel parameters corresponding to different anchors are mutually independent, then in far-field scenarios, the EFIM for the position, the EFI for the orientation, and the EFI for the time offset, using an $N_\triangledown$-antenna array, are given respectively by*

$$\mathbf{J}_e^{Array\text{-}B}(\mathbf{p}_0) = \Xi_\mathbf{p} + N_\triangledown \left\{ \bar{\mathbf{J}}_e - \frac{1}{\sum_{k\in\mathcal{N}_\circledast} \lambda_k(\bar{\mathbf{p}}_0) + \Xi_B/N_\triangledown} \cdot \mathbf{q}_B(\bar{\mathbf{p}}_0)\,\mathbf{q}_B(\bar{\mathbf{p}}_0)^T \right\}, \quad (6.13)$$

$$J_e^{Array\text{-}B}(\varphi) = \sum_{n\in\mathcal{N}_\triangledown} \sum_{k\in\mathcal{N}_\circledast} \bar{h}_{n,k}^2 \lambda_k(\bar{\mathbf{p}}_0) + \Xi_\varphi, \qquad (6.14)$$

and

$$J_e^{Array\text{-}B}(B) = \Xi_B + N_\triangledown \left\{ \sum_{k\in\mathcal{N}_\circledast} \lambda_k(\bar{\mathbf{p}}_0) - \mathbf{q}_B(\bar{\mathbf{p}}_0)^T \left(\frac{1}{N_\triangledown} \cdot \Xi_\mathbf{p} + \bar{\mathbf{J}}_e \right)^{-1} \mathbf{q}_B(\bar{\mathbf{p}}_0) \right\},$$

$$(6.15)$$

where $\bar{\mathbf{p}}_0$ is the expected position of the agent's array center, and $\bar{h}_{n,k}$ is a function of $\bar{\mathbf{p}}_0$.

Proof. See Appendix A.5.2. ☐

We then investigate the performance of AoA estimation as in Corollary 4 in the presence of a time offset. The EFI for the AoA to the array using wideband antenna arrays is given in the following corollary.

Corollary 7. *In the presence of a time offset, the EFI for the AoA from the kth*

anchor to the array, $\tilde{\phi}_k$, is

$$J_e^{Array\text{-}B}(\tilde{\phi}_k) = \lambda_k \sum_{n \in \mathcal{N}_\nabla} \bar{h}_{n,k}^2 + \Xi_\varphi. \tag{6.16}$$

Remark: Despite the presence of the time offset, the above result is the same as that in Corollary 4, which implies that the accuracy of AoA estimation does not depend on the knowledge of the time offset. Intuitively, since the AoA is estimated from the difference between the ToA's of the received waveforms at the antennas, and thus the time offset is eliminated from the relative ToA's.

Chapter 7

Numerical Results

In this chapter, we illustrate applications of our analytical results using numerical examples. We deliberately restrict our attention to a simple network to gain insights, although our analytical results are valid for arbitrary topology with any number of anchors and any number of multipath components in the received waveforms.

7.1 Effect of Path-Overlap

We investigate the effect of path-overlap on the SPEB when *a priori* knowledge of parameters is not available. In particular, we compare the SPEB obtained by the full-parameter model proposed in this paper and that obtained by the partial-parameter model proposed in [36].

Without loss of generality, we consider a simple topology with four anchors ($N_\circledast = 4$) equally spaced on a circle and an agent at the center receiving all LoS waveforms (see Fig. 7-1). Each waveform consists of two paths: one LoS path ($\mathsf{SNR}_k^{(1)} = 0\mathrm{dB}$) and one NLoS path ($\mathsf{SNR}_k^{(2)} = -3\mathrm{dB}$), and the separations of the two paths $\tau_k^{(2)} - \tau_k^{(1)}$ are identical for $k \in \{1, 2, 3, 4\}$. In addition, the transmitted wideband waveform is a second derivative of Gaussian pulse with width approximately equal to 4ns.

Two models are used for comparison as follows:

- Model I (Full-Parameter Model): both the amplitudes and the NLoS biases

are considered as parameters, i.e., $\boldsymbol{\theta} = \begin{bmatrix} \mathbf{p}^T & \boldsymbol{\kappa}_1^T & \cdots & \boldsymbol{\kappa}_4^T \end{bmatrix}^T$ where $\boldsymbol{\kappa}_k = \begin{bmatrix} \alpha_k^{(1)} & b_k^{(2)} & \alpha_k^{(2)} \end{bmatrix}^T$.

- Model II (Partial-Parameter Model [36]): the amplitudes are assumed to be precisely known and only the NLoS biases are considered as parameters, i.e., $\boldsymbol{\theta} = \begin{bmatrix} \mathbf{p}^T & b_1^{(2)} & \cdots & b_4^{(2)} \end{bmatrix}^T$.

Figure 7-2 shows the SPEB as a function of path separation $\tau_k^{(2)} - \tau_k^{(1)}$ according to Theorem 1. The following observations can be made:

- First, path-overlap increases the SPEB in both models, since the overlap interferes with the ability to estimate the first path and hence reduces the RII. Note that the shape of the curves depends on the autocorrelation function of the waveform $s(t)$.

- Second, when the path separation exceeds the pulse width (approximately 4ns), the two models give the same SPEB, which equals the non-overlapping case. In such cases, the two paths do not overlap in time, and the RII is determined by only the first path. This agrees with the analysis in Sec. 4. Mathematically, this corresponds to a diagonal $\mathbf{J}_\eta$ in (3.7).

- Third, excluding the amplitudes in the parameter vector in Model II incorrectly provides more RI, and hence results in a loose bound when the two paths overlap. This demonstrates the importance of using the complete parameter model.

7.2   Improvement from *A Priori* Channel Knowledge

In this section, we quantify the contribution of *a priori* knowledge of the channel parameters $\boldsymbol{\alpha}$ and $\mathbf{b}$ to the SPEB using the same setting as in Sec. 7.1, except a
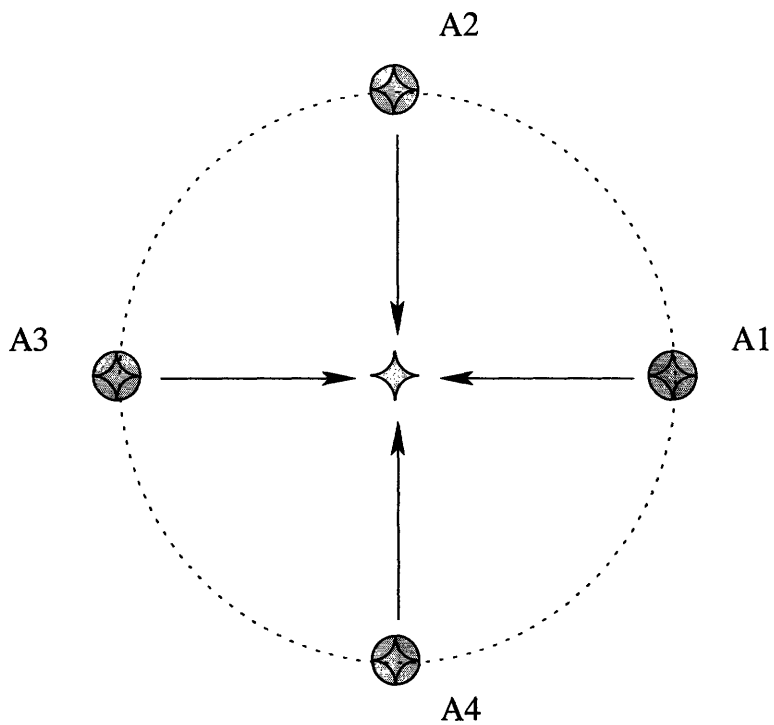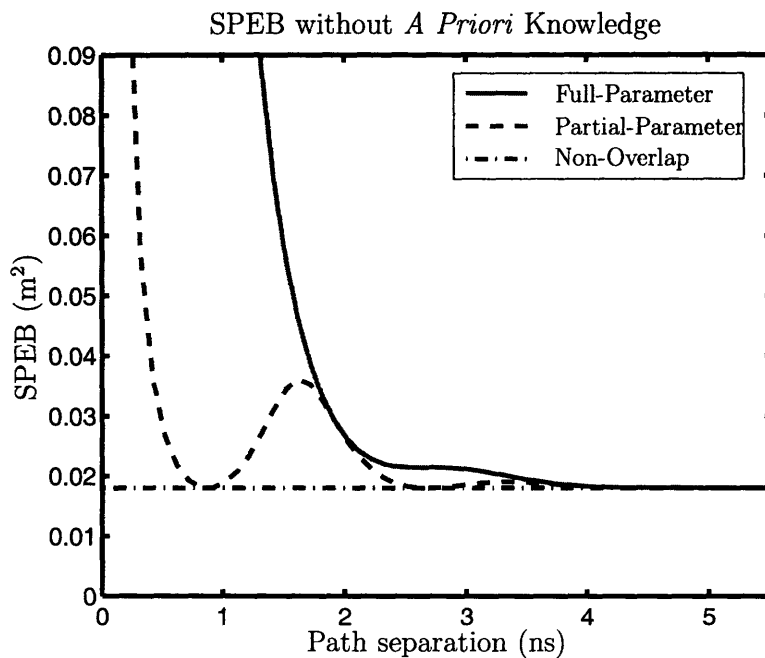
Figure 7-1: Network topology.

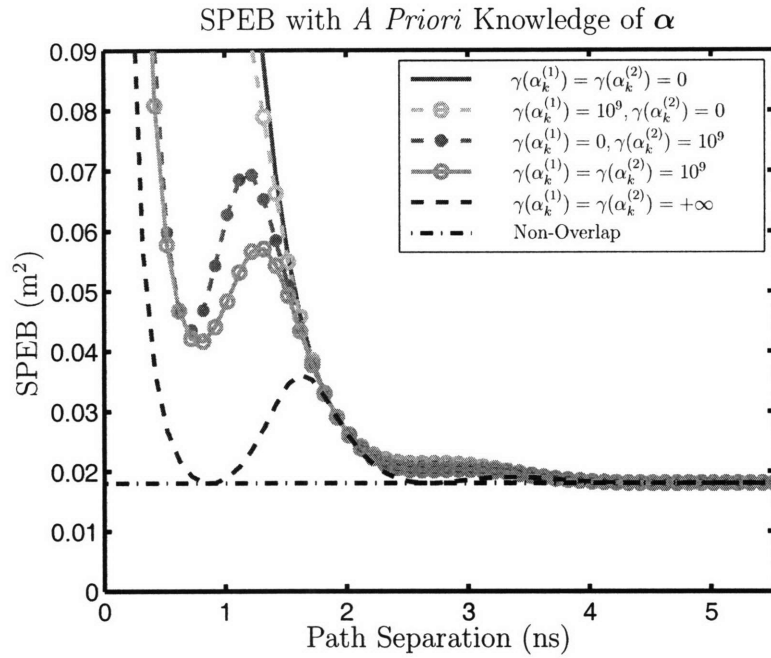Figure 7-2: SPEB as a function of path separation for different parameter models.

priori knowledge of $\alpha_k^{(1)}$, $\alpha_k^{(2)}$ and $b_k^{(2)}$ is now added. For simplicity, we consider these parameters to be independent *a priori*. In Fig. 7-3(a), the SPEB's are plotted as functions of the path separation for different *a priori* knowledge of $\alpha_k^{(1)}$ and $\alpha_k^{(2)}$ (no *a priori* knowledge of $b_k^{(2)}$); while in Fig. 7-3(b), the SPEB's are plotted for different *a priori* knowledge of $b_k^{(2)}$ (no *a priori* knowledge of $\alpha_k^{(1)}$ and $\alpha_k^{(2)}$).[1] Several observations can be made from the results.

- First, in both figures, an increase in the *a priori* knowledge either of the amplitude $\boldsymbol{\alpha}$ or of the NLoS bias $\mathbf{b}$ decreases the SPEB.[2] This should be expected since *a priori* channel knowledge increases the RII, as indicated in Appendix A.3.4, and thereby the localization accuracy.

- Second, in Fig. 7-3(a), as the *a priori* knowledge of $\alpha_k^{(1)}$ and $\alpha_k^{(2)}$ approaches infinity, the SPEB obtained using our full parameter model converges to that in Fig. 7-2 obtained using the partial parameter model. This can be explained by the fact that the partial parameter model excludes $\boldsymbol{\alpha}$ from the parameter vector, which is equivalent to assuming known $\boldsymbol{\alpha}$ and hence infinite Fisher information from their *a priori* knowledge $(\gamma(\alpha_k^{(1)}) = \gamma(\alpha_k^{(2)}) = \infty)$.

- Third, Fig. 7-3(b) shows that the SPEB decreases with increasing *a priori* knowledge of $\mathbf{b}$. This is because NLoS paths, in addition to the first path, can be exploited for ranging, when the *a priori* knowledge of the NLoS biases is available. Thus, NLoS signals can be beneficial for localization, as shown analytically in Sec. 4.3.

- Fourth, it is surprising to observe that, when *a priori* knowledge of $\mathbf{b}$ is available, path-overlap can result in lower SPEB compared to non-overlapping scenarios. This happens at certain path separations that depend on the autocorrelation function of $s(t)$. Intuitively, path-overlap can lead to a higher SNR and hence a lower SPEB, compared to non-overlapping cases, when *a priori* knowledge of the bias vector $\mathbf{b}$ is available.

---

[1]The *a priori* knowledge is characterized by Fisher information $\gamma(\cdot)$.

[2]The amplitude vector $\boldsymbol{\alpha}$ contains all the $\alpha_k^{(l)}$'s, while the NLoS bias $\mathbf{b}$ contains all the $b_k^{(l)}$'s.

(a) SPEB as a function of path separation with *a priori* knowledge of $\boldsymbol{\alpha}$, while $\gamma(b_k^{(2)}) = 0$.
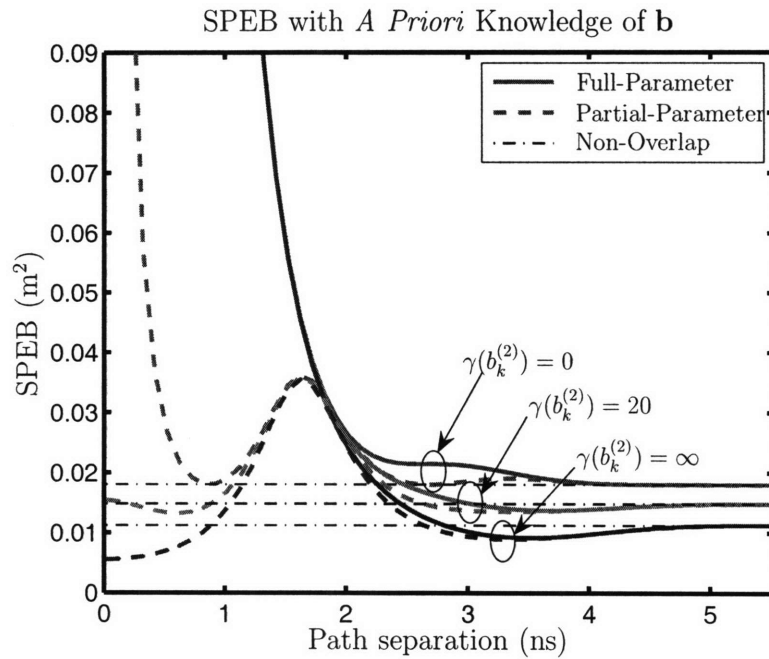
(b) SPEB as a function of path separation with *a priori* knowledge of $\mathbf{b}$, while $\gamma(\alpha_k^{(1)}) = \gamma(\alpha_k^{(2)}) = 0$.

Figure 7-3: SPEB as a function of path separation with *a priori* knowledge of the amplitudes $\boldsymbol{\alpha}$ and the NLoS biases $\mathbf{b}$.

7.3 Path-Overlap Coefficient for Different Transmitted Waveforms

We here investigate the path-overlap coefficient for different shapes of transmitted waveform $s(t)$. Fig. 7-4(a) shows the six waveforms for our numerical results: they are a Gaussian pulse, the first through third derivatives of a Gaussian pulse, a triangular pulse, and a rectangular pulse, with a pulse width of approximately 4ns.

We consider a simply case where the received waveform has only two multipath components, i.e., $L = 2$, to gain insights into the effect of path-overlap on localization. The path-overlap coefficients for these six waveforms as functions of the path inter-arrival time are plotted in Fig. 7-4(b). First, path-overlap coefficient χ decreases from 1 to 0 in general as the path inter-arrival time increases. This can be explained as follows: larger path inter-arrival time causes less overlap of the signals via the two paths, and hence less interference from the second path to the estimation of the first path. As can be expected, when the path inter-arrival time exceeds 4ns, approximately the width of the transmitted waveform, χ goes to 0, the minimum, since there is no overlap and hence no interference. Second, the performance of the rectangular waveform for ranging is remarkably better than others except for the point where inter-arrival time equals 4ns. The path-overlap coefficient depends on the autocorrelation function of the transmitted waveform according to (A.37). The second derivative of the autocorrelation function of the rectangular waveform has a very sharp peak at the origin, which results in small path-overlap coefficients, and another peak at 4ns, which results in a throb in the curve of the path-overlap coefficient at 4ns. This is also true for all other curves: the fluctuations of these curves are determined by the autocorrelation function of the corresponding transmitted waveforms.
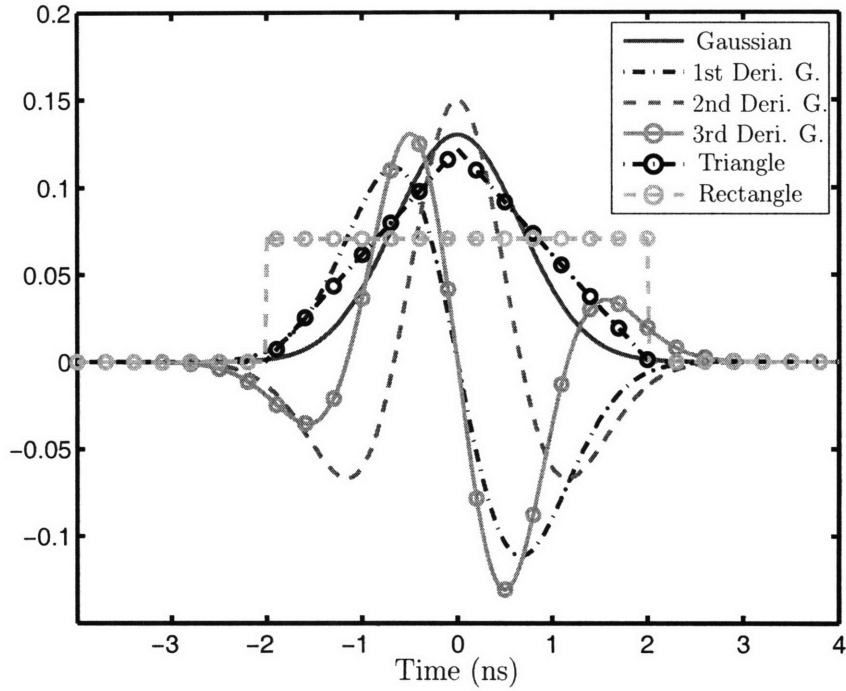
(a) Different waveform $s(t)$ for numerical results: a Gaussian pulse, the first through third derivatives of a Gaussian pulse, a triangular pulse, and a rectangular pulse.
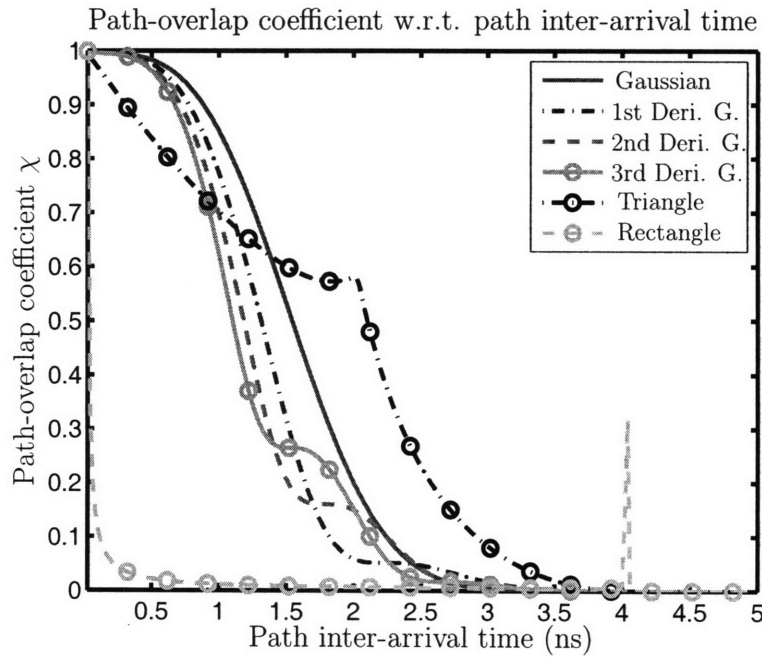
(b) Path-overlap coefficient as a function of path inter-arrival time.

Figure 7-4: Path-overlap coefficient as a function of path inter-arrival time for different transmitted waveforms in the case $L = 2$.

7.4 Path-Overlap Coefficient for Different Propagation Channels

We now investigate the dependence of path-overlap coefficient χ on path arrival rate for different number of multipath components. We first generate channels with L multipath components according to a simple Poisson model with a fixed arrival rate ν, and then calculate χ according to (A.37). Figure 7-5 shows the average path-overlap coefficient as a function of path inter-arrival rate $(1/\nu)$ for different L, where the averaging is obtained by Monte-Carlo simulations. Several observations can be made from the results.

- First, the path-overlap coefficient χ is monotonically decreasing from 1 to 0 with $1/\nu$. This agrees with our intuition that denser multipath propagation causes more interference between the first path and other multipath components, and hence the received waveform provides less RII.

- Second, for a fixed ν, the path-overlap coefficient increases with L. This should be expected as additional multipath components may interfere with earlier paths, degrading the estimation accuracy of the first path and hence reducing the RII.

- Third, the performance difference between a channel with five and that with fifty multipath components is insignificant. This indicates that the effect of additional multipath beyond the fifth path can be neglected, implying that the first five paths is sufficient for calculating the RII.

7.5 Outage in Ranging Ability

We have observed that the channel quality for ranging is characterized by the path-overlap coefficient. If the multipath propagation has a high path-overlap coefficient (close to 1), we may consider the channel in outage for ranging. We define the ranging
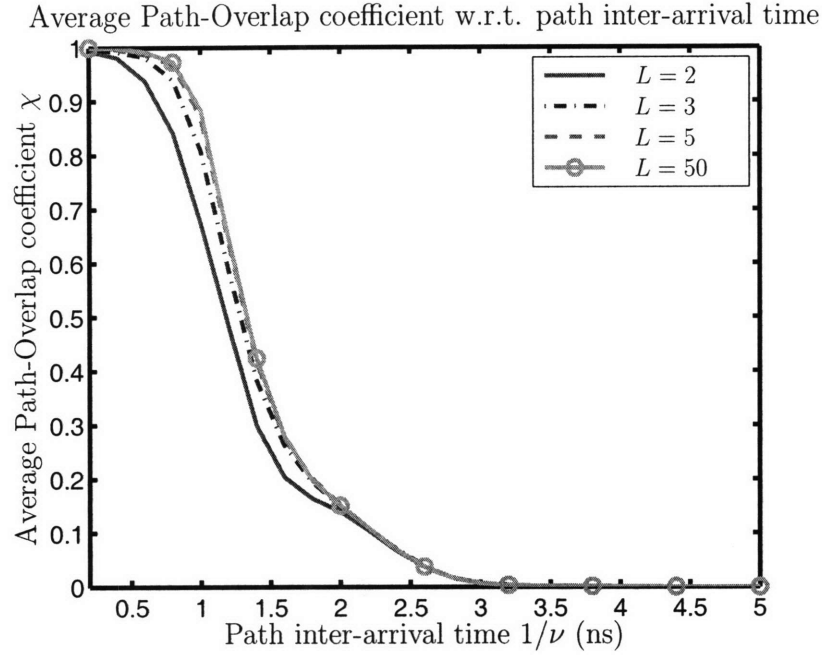
Figure 7-5: Path-overlap coefficient as a function of path inter-arrival time for different number of multipath components.

ability outage (RAO) as

$$p_{\text{out}}(\chi_{\text{th}}) \triangleq \mathbb{P}\{\chi > \chi_{\text{th}}\}, \tag{7.1}$$

where χ_{th} is the threshold for the path-overlap coefficient. The RAO tells us that with probability $p_{\text{out}}(\chi_{\text{th}})$, the path-overlap coefficient will exceed χ_{th} so that the propagation channel is unsatisfactory for ranging.

The RAO's as a function of χ_{th} for different Poisson arrival rate are plotted in Fig. 7-6 for a channel with $L = 50$. The RAO's decrease from 1 to 0, as the threshold χ_{th} increases or the path arrival rate ν decreases. This should be expected because the probability of path-overlap decreases with the path arrival rate, and consequently decreases the RAO. The RAO can be used as a measure to quantify the channel quality for ranging and to guide the design of the optimal transmitted waveform for ranging.
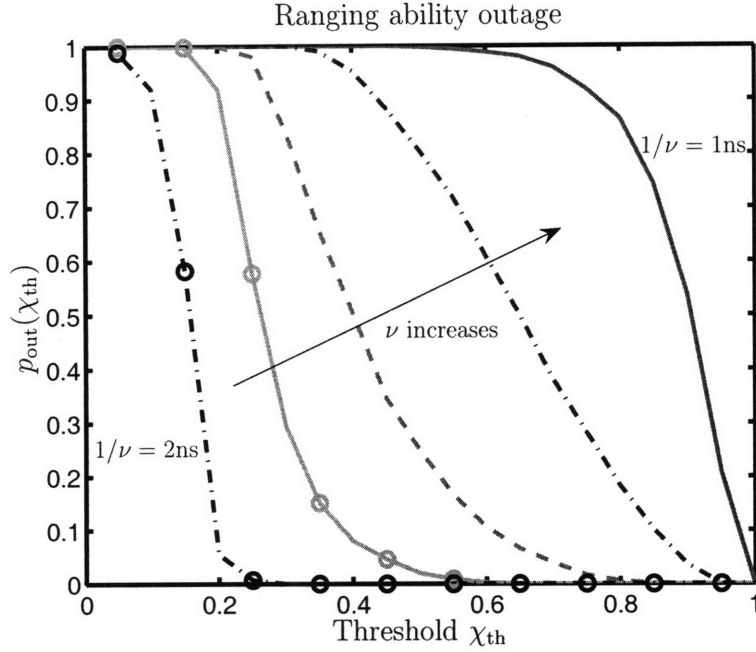
Figure 7-6: RAO as a function of the threshold χ_{th} for different path inter-arrival time $1/\nu$ with $L = 50$.

7.6 SPEB for Different Reference Positions with *A Priori* Knowledge of Channel and Orientation

We consider the SPEB for different reference points of a ULA when a priori knowledge of the orientation is available. The numerical results are based on a network with six equally spaced anchor nodes ($N_{\circledast} = 6$) located on a circle with an agent in the center. The agent is equipped with a 5-antenna array ($N_{\triangledown} = 5$) whose spacing is 0.5m ($\Delta = 0.5$). In far-field scenarios, $\lambda_{n,k} = \lambda_k = 10$ and $\phi_{n,k} = \phi_k$.

The SPEB as a function of different reference points along the ULA is plotted in Fig. 7-7 for different *a priori* knowledge of the orientation, Ξ_{φ}. First, we see that *a priori* knowledge of the orientation improves the localization accuracy since the SPEB decreases with increasing Ξ_{φ}. The curve of $\Xi_{\varphi} = 0$ corresponds to orientation-unaware case and the one of $\Xi_{\varphi} = \infty$ corresponds to orientation-aware case. Second, the array center has the best localization accuracy, and its SPEB does not depend on Ξ_{φ}, which agrees with Corollary 3. Third, the SPEB increases with both the distance

72
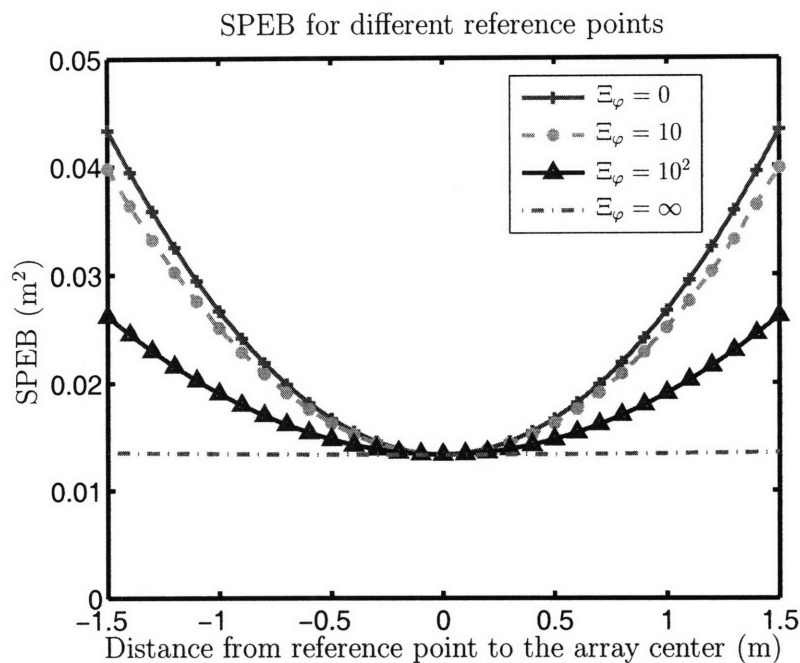
Figure 7-7: SPEB as a function of the distance from the reference point to the array center for different *a priori* knowledge of the orientation Ξ_φ.

from the reference point to the array center and the error in the orientation estimate, as predicted by Corollary 2. Fourth, the SPEB is independent of the specific reference point if $\Xi_\varphi = \infty$, as referred to orientation-aware localization.

7.7   SOEB for Different Reference Positions with *A Priori* Knowledge of Channel and Position

We investigate the SOEB for different reference points of a ULA when *a priori* knowledge of the reference point is available. The parameters are the same as those of the previous example except that *a priori* knowledge of the reference point is available instead.

The SOEB as a function of different reference points along the ULA is plotted in Fig. 7-8 for different *a priori* knowledge of the reference point, $\Xi_\mathbf{p}$. The results are counterparts of those in Fig. 7-7. First, *a priori* knowledge of the reference point

73
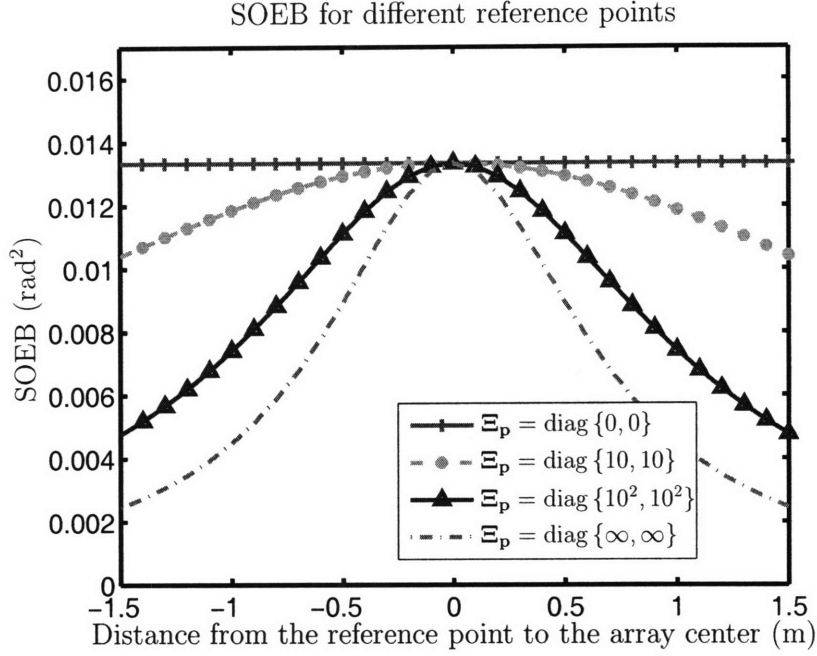
Figure 7-8: SOEB as a function of the distance from the reference point to the array center for different *a priori* knowledge of the reference point $\Xi_{\mathbf{p}}$.

improves the orientation accuracy since the SOEB decreases with increasing $\Xi_{\mathbf{p}}$. This agrees with both intuition and Corollary 3. Second, the array center has the worst orientation accuracy, and its SOEB does not depend on $\Xi_{\mathbf{p}}$. This should be expected since the knowledge for the array center tells nothing about the array orientation. Third, the SOEB decreases as a function of the distance from the reference point to the array center if *a priori* knowledge of the reference point is available. This observation can be verified by Theorem 3. Fourth, the SOEB is independent of the specific reference point if $\Xi_{\mathbf{p}} = \mathbf{0}$, as shown in Corollary 2.

7.8   Performance Comparison of ULA and UCA

We compare the performance of the ULA and the UCA for AoA estimation as a function of the number of antennas in the array. We consider a case where the *a priori* knowledge of the orientation is not available, i.e., $\Xi_{\varphi} = 0$, and Fig. 7-9 shows the ratio of SOEB's corresponding to the UCA and the ULA for different AoA,

74
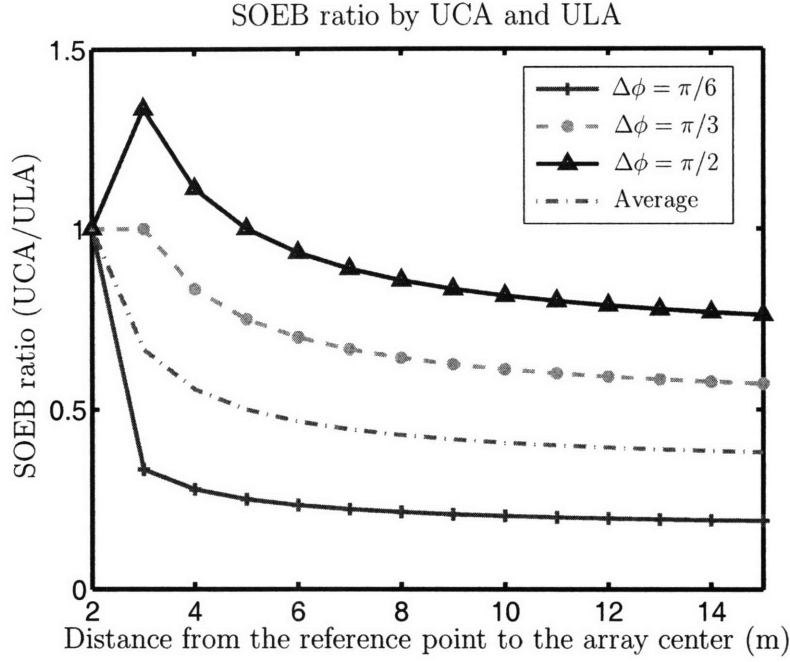
Figure 7-9: The ratio of SOEB's for the ULA and the UCA as a function of different number of antennas in the array. The four curves correspond to $\Delta\phi = \pi/6, \pi/3, \pi/2$, and average over uniform $\Delta\phi \in [0, 2\pi)$.

$\tilde{\phi} \triangleq \phi - \varphi$. First, the performance of the ULA and the UCA is always the same for $N_\nabla = 2$, since they have actually the same array geometry in this case. Second, the ratio highly depends on $\tilde{\phi}$ for $N_\nabla = 3, 4$, while it is less than 1 for $N_\nabla \geq 5$. But the average ratio over uniform $\phi \in [0, 2\pi)$ is always less than 1, implying that the UCA outperforms the ULA. This can be explained by (5.31). Finally, the asymptotical ratio as $N_\nabla \to \infty$ can be found as

$$\lim_{N_\nabla \to \infty} \frac{\mathcal{P}_C(\tilde{\phi})}{\mathcal{P}_L(\tilde{\phi})} = \lim_{N_\nabla \to \infty} \frac{J_e^L(\tilde{\phi})}{J_e^C(\tilde{\phi})} = \frac{2}{3}\sin^2(\tilde{\phi}). \tag{7.2}$$

7.9 SPEB with Time Offset and Squared Error Bound for Time Offset

We investigate the effect of time offset on the SPEB and the squared error bound for the time offset, using the network illustrated in Fig. 7-1. The received waveform from each anchor provides the agent with RII $\lambda_k = 10$ ($k = 1, 2, 3, 4$). Initially, four anchors are fixed with $\phi_1 = 0$, $\phi_2 = \pi/2$, $\phi_3 = \pi$, and $\phi_4 = 3\pi/2$, respectively. We now vary the position of Anchor A1 counter-clockwise along the circle. Figure 7-10(a) and 7-10(b) shows the SPEB and the squared error bound for the time offset, respectively, as functions of ϕ_1 for different *a priori* knowledge of the time offset. We have the following observations.

- First, the SPEB decreases as *a priori* knowledge of the time offset increases. The curve of $\Xi_B = \infty$ in Fig. 7-10(a), corresponding to the case where the time offset is precisely known, is equivalent to systems without the time offset. Similarly, the squared error bound for the time offset also decreases as Ξ_B increases. The curve of $\Xi_B = \infty$ in Fig. 7-10(b) always equals zero since the bias is precisely known. These observations agree with Theorem 4.

- Second, all of the four curves have the same value at $\phi_1 = 0$ in Fig. 7-10(a), which implies that the time offset has no effect on the SPEB at this point. This phenomenon is due to the fact that $\mathbf{q}_B = \mathbf{0}$ for $\phi_1 = 0$, which we refer to as time-offset-independent localization. In this case, the squared error bound for the time offset also achieves the minimum. These observations agree with Theorem 4.

- Third, as ϕ_1 increases from 0 to π, all curves in Fig. 7-10(a) first increases and then decreases, while all curves in Fig. 7-10(b) increase monotonically. We give the following interpretations: all the anchors tend to gather on one side of agent, as ϕ_1 increases from 0 to π, and hence the error of the time offset estimate becomes larger (to see this more intuitively, consider only anchor A1 and anchor A3). In Fig. 7-10(a), the SPEB first increases because localization

information is decreasing and uncertainty in B is increasing, which corresponds to the two parts in (6.3). Then, the SPEB drops due to the fact that localization information begins to increase (when $\phi_1 > \pi/2$), while the error of the time offset estimate increases much slower.
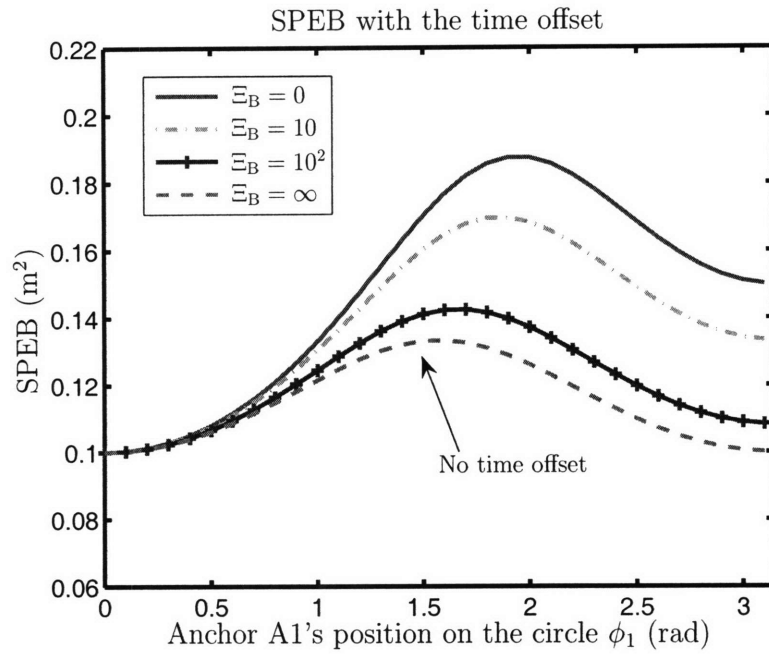
(a) SPEB as a function of Anchor A1's position
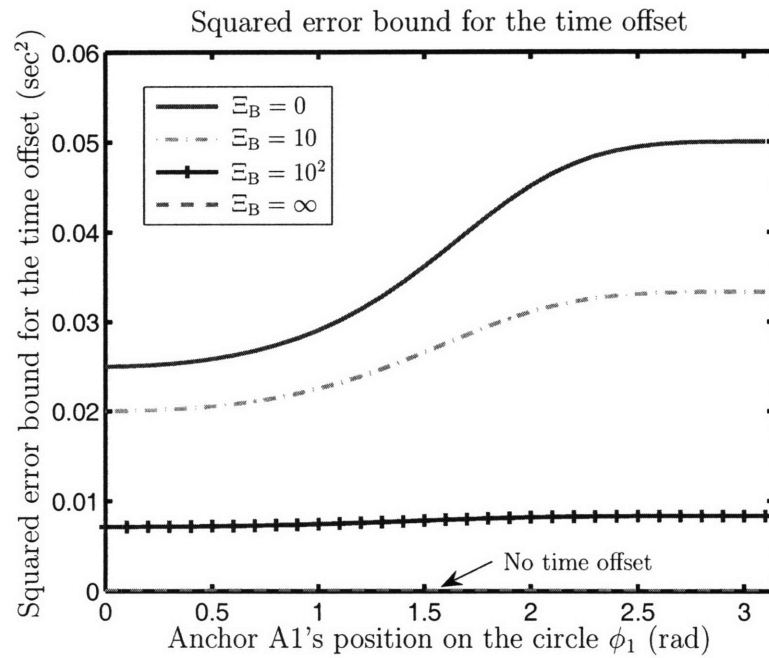
(b) Squared error bound for the time offset as a function of Anchor A1's position

Figure 7-10: SPEB and the squared error bound for the time offset with different *a priori* knowledge of the time offset, and $\Xi_B = 0, 10, 10^2, \infty$ respectively.

Chapter 8

Conclusion

Analysis of localization performance in the literature mainly employs specific signal metrics, such as ToA, AoA, RSS, and TDoA, rather than utilizing the entire received waveforms [8]. Our analysis is based on the entire received waveforms and exploits all the localization information inherent in these signal metrics, implicitly or explicitly. In particular, ToA and joint ToA/AoA metrics were incorporated in our analysis in Sec. 4 and 5, respectively. Similarly, TDoA and joint TDoA/AoA metrics were included in the analysis of Sec. 6, and the RSS metric has been implicitly exploited from *a priori* channel knowledge in (A.17), since RSS can be approximated as

$$\int |r_k(t)|^2 dt \simeq \sum_{l=1}^{L_k} |\alpha_k^{(l)}|^2 \cdot \int s^2(t) dt. \tag{8.1}$$

From the achievability point of view, maximum likelihood (ML) and maximum a posterior (MAP) estimates respectively achieve the CRB asymptotically in the high SNR regimes for the cases without and with *a priori* knowledge [28]. High SNR can be attained using sequences with good correlation properties [66–68], or simply repeated transmissions. Therefore, the SPEB is achievable.

In this thesis, we investigated the fundamental limits of localization accuracy for wideband wireless location-aware systems. We proposed the measure called the squared position error bound (SPEB) to characterize the limits, and derived the SPEB succinctly by using equivalent Fisher information analysis. Our results showed that

the localization information can be decomposed into contribution from the *a priori* knowledge of the agent's position and that from anchors, which incorporates both the measurements and the *a priori* channel knowledge. In particular, the contribution from anchors can be written in a canonical form as a weighted sum of the elementary ranging information. We also investigated the use of wideband antenna arrays and the effect of unknown time offset in terms of the SPEB. Our result provides fundamental limits for localization accuracy, because the limits are derived based on received signals rather than the specific signal metrics and hence accounts for all the potential localization information inherent in the signals. Our methodology gives insights into localization problems, and the results can serve as benchmarks for localization algorithms as well as facilitate algorithm development for applications, such as anchor deployment for accurate localization.

Appendix A

Proofs

A.1 Block Matrices for Fisher Information Matrix

This appendix lists the block matrices used in the Fisher information matrix in (3.9).

- The following block matrices appear in $\mathbf{T}$ in (3.8):

$$
\mathbf{T_L} = \begin{bmatrix} \mathbf{G}_1 & \mathbf{G}_2 & \cdots & \mathbf{G}_M \\ \mathbf{D}_1 & & & \\ & \mathbf{D}_2 & & \\ & & \ddots & \\ & & & \mathbf{D}_M \end{bmatrix} \quad \text{and} \quad \mathbf{T_{NL}} = \begin{bmatrix} \mathbf{G}_{M+1} & \mathbf{G}_{M+2} & \cdots & \mathbf{G}_{N_\circledast} \\ \mathbf{0} & & & \\ & \mathbf{0} & & \\ & & \ddots & \\ & & & \mathbf{0} \end{bmatrix},
$$

(A.1)

where

$$
\mathbf{D}_k = \begin{bmatrix} \mathbf{0} & \mathbf{I}_{2L_k-1} \end{bmatrix} \quad \text{and} \quad \mathbf{G}_k = \mathbf{q}_k \cdot \mathbf{l}_k^T \tag{A.2}
$$

with

$$
\mathbf{l}_k = \underbrace{\begin{bmatrix} 1 & 0 & \cdots & 1 & 0 \end{bmatrix}}_{2L_k}^T. \tag{A.3}
$$

- The following block matrices appear for $\mathbf{J}_\eta$ in (3.7):

$$\mathbf{\Lambda}_{\mathrm{L}} = \mathrm{diag}\left\{\mathbf{\Psi}_1, \mathbf{\Psi}_2, \cdots, \mathbf{\Psi}_M\right\}, \qquad \mathbf{\Lambda}_{\mathrm{NL}} = \mathrm{diag}\left\{\mathbf{\Psi}_{M+1}, \mathbf{\Psi}_{M+2}, \cdots, \mathbf{\Psi}_{N_\oplus}\right\},$$

$$\text{(A.4)}$$

where $\mathbf{\Psi}_k \in \mathbb{R}^{2L_k \times 2L_k}$ whose elements

$$[\mathbf{\Psi}_k]_{ij} = \mathbb{E}_{\mathbf{r}}\left\{-\frac{\partial^2 \ln f(\mathbf{r}|\boldsymbol{\theta})}{\partial \eta_k^{(i)} \partial \eta_k^{(j)}}\right\} \qquad \text{for} \quad i,j = 1, 2, \cdots, 2L_k. \qquad \text{(A.5)}$$

In particular, every element in $\mathbf{\Psi}_k$ can be expressed as

$$\mathbb{E}_{\mathbf{r}}\left\{-\frac{\partial^2 \ln f(\mathbf{r}|\boldsymbol{\theta})}{\partial \tau_k^{(i)} \partial \tau_k^{(j)}}\right\} = \frac{2\,\alpha_k^{(i)}\alpha_k^{(j)}}{N_0} \int \frac{\partial}{\partial \tau_k^{(i)}} s\left(t - \tau_k^{(i)}\right) \cdot \frac{\partial}{\partial \tau_k^{(j)}} s\left(t - \tau_k^{(j)}\right) dt$$

$$= \frac{2\,\alpha_k^{(i)}\alpha_k^{(j)}}{N_0} \int \left|2\pi f S(f)\right|^2 \exp\left(-j2\pi f \cdot (\tau_k^{(i)} - \tau_k^{(j)})\right) df$$

$$= \frac{2\,\alpha_k^{(i)}\alpha_k^{(j)}}{N_0} \frac{\partial^2}{\partial \tau_k^{(i)} \partial \tau_k^{(j)}} R_s\left(\tau_k^{(i)} - \tau_k^{(j)}\right), \qquad \text{(A.6a)}$$

$$\mathbb{E}_{\mathbf{r}}\left\{-\frac{\partial^2 \ln f(\mathbf{r}|\boldsymbol{\theta})}{\partial \tau_k^{(i)} \partial \tilde{\alpha}_k^{(j)}}\right\} = \frac{2\,\alpha_k^{(i)} \cdot c}{N_0} \int \frac{\partial}{\partial \tau_k^{(i)}} s\left(t - \tau_k^{(i)}\right) \cdot s\left(t - \tau_k^{(j)}\right) dt$$

$$= \frac{2\,\alpha_k^{(i)} \cdot c}{N_0} \int j \cdot f \left|S(f)\right|^2 \exp\left(-j2\pi f \cdot (\tau_k^{(i)} - \tau_k^{(j)})\right) df$$

$$= \frac{2\,\alpha_k^{(i)} \cdot c}{N_0} \frac{\partial}{\partial \tau_k^{(i)}} R_s\left(\tau_k^{(i)} - \tau_k^{(j)}\right), \qquad \text{(A.6b)}$$

$$\mathbb{E}_{\mathbf{r}}\left\{-\frac{\partial^2 \ln f(\mathbf{r}|\boldsymbol{\theta})}{\partial \tilde{\alpha}_k^{(i)} \partial \tilde{\alpha}_k^{(j)}}\right\} = \frac{2\,c^2}{N_0} \int s\left(t - \tau_k^{(i)}\right) \cdot s\left(t - \tau_k^{(j)}\right) dt$$

$$= \frac{2\,c^2}{N_0} \int \left|S(f)\right|^2 \exp\left(-j2\pi f \cdot (\tau_k^{(i)} - \tau_k^{(j)})\right) df$$

$$= \frac{2\,c^2}{N_0} R_s\left(\tau_k^{(i)} - \tau_k^{(j)}\right), \qquad \text{(A.6c)}$$

where $R_s(\tau) = \int s(t)s(t-\tau)dt$. Note that

$$\mathbb{E}_{\mathbf{r}}\left\{-\frac{\partial^2 \ln f(\mathbf{r}|\boldsymbol{\theta})}{\partial \tau_k^{(i)\,2}}\right\} = 8\pi^2 \beta^2 \cdot \mathrm{SNR}_k^{(i)}, \qquad \text{(A.7)}$$

where β and $\mathsf{SNR}_k^{(i)}$ are given by (4.6) and (4.7), respectively.

A.2 Wideband Channel Model and *A Priori* Channel Knowledge

Wideband channel measurements have shown that the multipath components follow random arrival and their amplitudes are subject to path loss, large and small-scale fading. While our discussion is valid for any wideband channels that can be described by (2.1), we consider the model of IEEE 802.15.4a standard for exposition. Specifically, this standard uses Poisson arrivals, log-normal shadowing, Nakagami small-scale fading with exponential power dispersion profile (PDP) [17].

A.2.1 Path Arrival Time

The arrival time of multipath components is commonly modeled by a Poisson process [17,61], and we have

$$g_{\tau_k}(\tau_k^{(l)}|\tau_k^{(l-1)}) = \nu \cdot \exp\left[-\nu\left(\tau_k^{(l)} - \tau_k^{(l-1)}\right)\right], \qquad \tau_k^{(l)} \geq \tau_k^{(l-1)} \text{ and } l \geq 2, \quad \text{(A.8)}$$

where ν is the path arrival rate. Using (2.2), we obtain

$$g_{b_k}(b_k^{(l)}|b_k^{(l-1)}) = \frac{\nu}{c} \cdot \exp\left[-\frac{\nu}{c} \cdot \left(b_k^{(l)} - b_k^{(l-1)}\right)\right], \qquad b_k^{(l)} \geq b_k^{(l-1)} \text{ and } l \geq 1. \quad \text{(A.9)}$$

Note that $b_k^{(0)} = 0$ for consistency.

A.2.2 Path Loss and Large-Scale Fading

The received signal strength (RSS) in dB at the distance d_k can be written as [17]

$$P_k = P_0 - 10\beta \log_{10}\left(\frac{d_k}{d_0}\right) + w, \qquad \text{(A.10)}$$

where P_0 is the expected RSS at the reference distance d_0, β is the propagation (path gain) exponent, and w is a random variable (r.v.) that accounts for large-scale fading, or shadowing. Shadowing is usually modeled with a log-normal distribution, such that w is a Gaussian r.v. with zero-mean and variance σ_S^2, i.e., $w \sim N(0, \sigma_S^2)$.[1] The p.d.f. of the RSS of $r_k(t)$ can then be written as

$$g_{\mathrm{P}}(P_k|d_k) \propto \exp\left\{-\frac{1}{2\sigma_S^2}\left[P_k - P_0 + 10\beta\log_{10}\left(\frac{d_k}{d_0}\right)\right]^2\right\}, \qquad (A.11)$$

where $d_k = \|\mathbf{p} - \mathbf{p}_k\|$, and P_k is given by

$$P_k = 10\log_{10}\left[\sum_{l=1}^{L_k}\mathbb{E}_s\left\{|\alpha_k^{(l)}|^2\right\}\right], \qquad (A.12)$$

with $\mathbb{E}_s\{\cdot\}$ denoting the average over small-scale fading.

A.2.3   Power Dispersion Profile and Small-Scale Fading

As in [16, 17], we consider an exponential PDP given by,[2]

$$\mathbb{E}_s\left\{|\alpha_k^{(l)}|^2\right\} = Q_k \exp(-\tau_k^{(l)}/\gamma_k) \triangleq Q_k^{(l)} \qquad (A.13)$$

where γ_k is the decay constant, and Q_k is a normalization coefficient such that

$$Q_k = \frac{10^{P_k/10}}{\sum_{l=0}^{L_k}\exp(-\tau_k^{(l)}/\gamma_k)}. \qquad (A.14)$$

---

[1] The standard deviation is typically 1-2 dB (LoS) and 2-6 dB (NLoS) [18] around the path gain.

[2] Note that the first component of LoS signals can exhibit a stronger strength than (A.13) in some UWB measurement [16]. In such cases, (A.13) and (A.14) need to be modified, accordingly.

In addition, $\alpha_k^{(l)}$ is a Nakagami r.v. with second moment given by (A.13). Specifically, we have

$$
\begin{aligned}
g_{\alpha_k}(\alpha_k^{(l)}|\mathbf{b}_k, d_k, P_k) &= g_{\alpha_k}(\alpha_k^{(l)}|\boldsymbol{\tau}_k, P_k) \\
&= \frac{2}{\Gamma(m_l)} \left(\frac{m_l}{Q_k^{(l)}}\right)^{m_l} |\alpha_k^{(l)}|^{2m_l-1} \exp\left(-\frac{m_l}{Q_k^{(l)}} \cdot |\alpha_k^{(l)}|^2\right), \quad \text{(A.15)}
\end{aligned}
$$

where $\Gamma(m_l)$ is the gamma function and $m_l \geq 1/2$ is the Nakagami m-factor, which is a function of $\boldsymbol{\tau}_k$ [17].

A.2.4   *A Priori* PDF for Multipath Parameters

The joint p.d.f. of the multipath parameters and the RSS, conditioned on the distance from the kth anchor to the agent, can be derived as

$$
g_k(\boldsymbol{\alpha}_k, \mathbf{b}_k, P_k|d_k) = g_\mathrm{P}(P_k|d_k) \cdot \prod_{l=1}^{L_k} g_{\alpha_k}\left(\alpha_k^{(l)}|\mathbf{b}_k, d_k, P_k\right) \cdot \prod_{l=1}^{L_k} g_{\mathbf{b}_k}\left(b_k^{(l)}|b_k^{(l-1)}\right). \quad \text{(A.16)}
$$

By integrating over P_k, we obtain the p.d.f. of the multipath parameters of $r_k(t)$ as follows

$$
g_k(\boldsymbol{\kappa}_k|d_k) = g_k(\boldsymbol{\alpha}_k, \mathbf{b}_k|d_k) = \int_{-\infty}^{\infty} g_k(\boldsymbol{\alpha}_k, \mathbf{b}_k, P_k|d_k) \, dP_k. \quad \text{(A.17)}
$$

Equation (A.17) characterizes the *a priori* knowledge of channel parameters, and can be obtained, for IEEE 802.15.4a standard, by substituting (A.9), (A.11) and (A.15) into (A.16) and (A.17). Note that d_k is a function of $\mathbf{p}$ and since $\mathbf{p}_k$ is known, we have the following relationship

$$
g_k(\boldsymbol{\kappa}_k|\mathbf{p}) = g_k(\boldsymbol{\kappa}_k|d_k). \quad \text{(A.18)}
$$

A.3   Proofs of the Theorems in Chapter 4

A.3.1   Proof of Theorem 1

Proof. We first prove that $\mathbf{J}_e(\mathbf{p})$ is given by (4.5). Following the notations in Appendix A.1, we write $\mathbf{G}_k$ in (A.2) as

$$\mathbf{G}_k \triangleq \left[\begin{array}{c|c} \mathbf{q}_k & \check{\mathbf{G}}_k \end{array}\right] \tag{A.19}$$

where

$$\check{\mathbf{G}}_k = \mathbf{q}_k \cdot \check{\mathbf{l}}_k^T, \quad \text{and} \quad \check{\mathbf{l}}_k = \underbrace{\left[\begin{array}{cccccc} 0 & 1 & 0 & \cdots & 1 & 0 \end{array}\right]}_{2L_k-1}^T. \tag{A.20}$$

Recall that in (A.7)

$$\mathbb{E}_\mathbf{r}\left\{-\frac{\partial^2 \ln f(\mathbf{r}|\boldsymbol{\theta})}{\partial \tau_k^{(1)\,2}}\right\} = 8\pi^2\beta^2 \cdot \text{SNR}_k^{(1)}, \tag{A.21}$$

we now define $\mathbf{k}_k \in \mathbb{R}^{2L_k-1}$ and matrix $\check{\boldsymbol{\Psi}}_k \in \mathbb{R}^{(2L_k-1)\times(2L_k-1)}$ such that

$$\boldsymbol{\Psi}_k = \left[\begin{array}{cc} 8\pi^2\beta^2 \cdot \text{SNR}_k^{(1)} & \mathbf{k}_k^T \\ \mathbf{k}_k & \check{\boldsymbol{\Psi}}_k \end{array}\right]. \tag{A.22}$$

It follows from Theorem 1 that $\mathbf{J}_e = \mathbf{T}_L \boldsymbol{\Lambda}_L \mathbf{T}_L^T / c^2$, which can be written as

$$\mathbf{J}_e = \frac{1}{c^2}\left[\begin{array}{cc} \mathbf{A} & \mathbf{B} \\ \mathbf{B}^T & \mathbf{C} \end{array}\right], \tag{A.23}$$

86

where

$$A \triangleq \sum_{k \in \mathcal{N}_L} G_k \Psi_k G_k^T$$

$$= R + \sum_{k \in \mathcal{N}_L} \left\{ \breve{G}_k k_k q_k^T + q_k k_k^T \breve{G}_k^T + \breve{G}_k \breve{\Psi}_k \breve{G}_k^T \right\}, \tag{A.24a}$$

$$B \triangleq \left[\begin{array}{cccc} G_1 \Psi_1 D_1^T & G_2 \Psi_2 D_2^T & \cdots & G_M \Psi_M D_M^T \end{array} \right]$$

$$= \left[\begin{array}{cccc} q_1 k_1^T + \breve{G}_1 \breve{\Psi}_1 & q_2 k_2^T + \breve{G}_2 \breve{\Psi}_2 & \cdots & q_M k_M^T + \breve{G}_M \breve{\Psi}_M \end{array} \right], \tag{A.24b}$$

$$C \triangleq \mathrm{diag} \left\{ D_1 \Psi_1 D_1^T, D_2 \Psi_2 D_2^T, \cdots, D_M \Psi_M D_M^T \right\}$$

$$= \mathrm{diag} \left\{ \breve{\Psi}_1, \breve{\Psi}_2, \cdots, \breve{\Psi}_M \right\}, \tag{A.24c}$$

and

$$R \triangleq 8\pi^2 \beta^2 \sum_{k \in \mathcal{N}_L} \mathrm{SNR}_k^{(1)} \cdot q_k q_k^T. \tag{A.25}$$

Since A is a 2×2 matrix, we can obtain a 2×2 EFIM

$$J_e(p) = \frac{1}{c^2} \left\{ A - BC^{-1}B^T \right\}. \tag{A.26}$$

Substituting (A.24) into (A.26), we obtain $J_e(p)$, after some algebra, as

$$J_e(p) = \frac{1}{c^2} \left\{ R - \sum_{k \in \mathcal{N}_L} q_k k_k^T \breve{\Psi}_k^{-1} k_k q_k^T \right\}$$

$$= \frac{8\pi^2 \beta^2}{c^2} \sum_{k \in \mathcal{N}_L} (1 - \chi_k) \cdot \mathrm{SNR}_k^{(1)} \cdot q_k q_k^T, \tag{A.27}$$

where χ_k is a scalar, given by

$$\chi_k \triangleq \frac{k_k^T \breve{\Psi}_k^{-1} k_k}{8\pi^2 \beta^2 \cdot \mathrm{SNR}_k^{(1)}}. \tag{A.28}$$

This completes the proof of (4.5).

Next, we show that only the first contiguous-cluster contains information for lo-

calization. Let us focus on χ_k and first define the following notations for convenience:

$$R_s(i,j) \triangleq R_s(t)|_{t=\tau_k^{(i)}-\tau_k^{(j)}}, \qquad \ddot{R}_s(i,j) \triangleq -\frac{\partial^2}{\partial t^2}R_s(t)|_{t=\tau_k^{(i)}-\tau_k^{(j)}},$$

$$\dot{R}_s(i,j) \triangleq \frac{\partial}{\partial t}R_s(t)|_{t=\tau_k^{(i)}-\tau_k^{(j)}} = -\dot{R}_s(j,i), \tag{A.29}$$

$$\boldsymbol{\Upsilon}_k \triangleq \begin{bmatrix} R_s(1,1) & -\dot{R}_s(1,2) & R_s(1,2) & -\dot{R}_s(1,3) & R_s(1,3) & \cdots & R_s(1,L_k) \\ -\dot{R}_s(1,2) & \ddot{R}_s(2,2) & \dot{R}_s(2,2) & \ddot{R}_s(2,3) & \dot{R}_s(2,3) & \cdots & \dot{R}_s(2,L_k) \\ R_s(1,2) & \dot{R}_s(2,2) & R_s(2,2) & -\dot{R}_s(2,3) & R_s(2,3) & \cdots & R_s(2,L_k) \\ \vdots & \vdots & & & & & \vdots \\ -\dot{R}_s(1,L_k) & \ddot{R}_s(2,L_k) & \cdots & & & & \dot{R}_s(L_k,L_k) \\ R_s(1,L_k) & \dot{R}_s(2,L_k) & \cdots & & & & R_s(L_k,L_k) \end{bmatrix},$$

$$\tag{A.30}$$

$$\mathbf{t}_k \triangleq \begin{bmatrix} \dot{R}_s(1,1) & \ddot{R}_s(1,2) & \dot{R}_s(1,2) & \cdots & \ddot{R}_s(1,L_k) & \dot{R}_s(1,L_k) \end{bmatrix}^T. \tag{A.31}$$

Then, we can express $\breve{\boldsymbol{\Psi}}_k$ and $\mathbf{t}_k$ as

$$\breve{\boldsymbol{\Psi}}_k = \frac{2}{N_0} \text{diag}\left\{c, \alpha_k^{(2)}, c, \cdots, \alpha_k^{(L_k)}, c\right\} \cdot \boldsymbol{\Upsilon}_k \cdot \text{diag}\left\{c, \alpha_k^{(2)}, c, \cdots, \alpha_k^{(L_k)}, c\right\}, \tag{A.32}$$

and

$$\mathbf{k}_k = \frac{2\alpha_k^{(1)}}{N_0}\text{diag}\left\{c, \alpha_k^{(2)}, c, \cdots, \alpha_k^{(L_k)}, c\right\} \cdot \mathbf{t}_k. \tag{A.33}$$

Substituting (A.32) and (A.33) into (A.28), we obtain

$$\chi_k = \frac{1}{4\pi^2\beta^2} \cdot \mathbf{t}_k^T \boldsymbol{\Upsilon}_k^{-1} \mathbf{t}_k. \tag{A.34}$$

If the length of the first contiguous-cluster in the received waveform is $L_k'(\leq L_k)$,

χ_k in (A.34) can be further simplified. In such cases,

$$\ddot{R}_s(i,j) = \dot{R}_s(i,j) = R_s(i,j) = 0 \tag{A.35}$$

for $i \in \{1, 2, \cdots, L_k'\}$ and $j \in \{L_k' + 1, L_k' + 2, \cdots, L_k\}$, and[3]

$$\mathbf{t}_k \triangleq \begin{bmatrix} \breve{\mathbf{t}}_k^T & \mathbf{0}^T \end{bmatrix}^T \quad \text{and} \quad \boldsymbol{\Upsilon}_k \triangleq \begin{bmatrix} \breve{\boldsymbol{\Upsilon}}_k & \mathbf{0} \\ \mathbf{0} & \boxtimes \end{bmatrix} \tag{A.36}$$

where $\breve{\mathbf{t}}_k \in \mathbb{R}^{2L_k'-1}$ and $\breve{\boldsymbol{\Upsilon}}_k \in \mathbb{R}^{(2L_k'-1)\times(2L_k'-1)}$. Therefore, (A.34) becomes

$$\chi_k = \frac{1}{4\pi^2\beta^2} \cdot \breve{\mathbf{t}}_k^T \breve{\boldsymbol{\Upsilon}}_k^{-1} \breve{\mathbf{t}}_k, \tag{A.37}$$

which depends only on the first L_k' paths. As a result, we can see that only the first contiguous-cluster of LoS signals contains information for localization.

Note that $0 \le \chi_k \le 1$. χ_k is nonnegative since it is a quadratic form and $\breve{\boldsymbol{\Upsilon}}_k$ is a positive semi-definite FIM (hence is $\breve{\boldsymbol{\Upsilon}}_k^{-1}$); and $\chi_k \le 1$ since the contribution from each anchor to the EFIM in (A.27) is nonnegative.

$\square$

A.3.2 Proof of Corollary 1

Proof. If the signal via the first path do not overlap with others, then this scenario can be thought of as a special case of Theorem 1 with $L_k' = 1$, i.e., the first contiguous-cluster contains only one path. In this case, (A.37) becomes

$$\chi_k = \frac{1}{4\pi^2\beta^2} \cdot \breve{\mathbf{t}}_k^T \breve{\boldsymbol{\Upsilon}}_k^{-1} \breve{\mathbf{t}}_k = \frac{1}{4\pi^2\beta^2} \cdot \frac{\dot{R}_s^2(1,1)}{R_s(1,1)}. \tag{A.38}$$

Since signal waveform $s(t)$ is continuous and time-limited in realistic cases, we have

$$\dot{R}_s(1,1) = \frac{\partial}{\partial\tau} R_s(\tau) \bigg|_{\tau=0} = 0, \tag{A.39}$$

---

[3]$\boxtimes$ is a block matrix that is irrelevant to the rest of the derivation.

implying that $\chi_k = 0$. Hence, the RII becomes

$$\lambda_k = \frac{8\pi^2\beta^2}{c^2}\, \mathsf{SNR}_k^{(1)}. \tag{A.40}$$

$\square$

A.3.3 Proof of Theorem 2

Proof. If *a priori* knowledge of the channel parameters are available and the sets of channel parameters from different anchors are independent, then the FIM is

$$\mathbf{J}_\theta = \frac{1}{c^2} \begin{bmatrix} \mathbf{T}_{\mathrm{NL}}\bar{\boldsymbol{\Lambda}}_{\mathrm{NL}}\mathbf{T}_{\mathrm{NL}}^T + \mathbf{T}_{\mathrm{L}}\bar{\boldsymbol{\Lambda}}_{\mathrm{L}}\mathbf{T}_{\mathrm{L}}^T & \mathbf{T}_{\mathrm{NL}}\bar{\boldsymbol{\Lambda}}_{\mathrm{NL}} \\ \bar{\boldsymbol{\Lambda}}_{\mathrm{NL}}\mathbf{T}_{\mathrm{NL}}^T & \bar{\boldsymbol{\Lambda}}_{\mathrm{NL}} \end{bmatrix} + \mathbf{J}_{\mathrm{p}}, \tag{A.41}$$

where

$$\bar{\boldsymbol{\Lambda}}_{\mathrm{NL}} = \mathbb{E}_\theta\left\{\boldsymbol{\Lambda}_{\mathrm{NL}}\right\} \triangleq \mathrm{diag}\left\{\bar{\boldsymbol{\Psi}}_1, \bar{\boldsymbol{\Psi}}_2, \cdots, \bar{\boldsymbol{\Psi}}_M\right\} \tag{A.42}$$

$$\bar{\boldsymbol{\Lambda}}_{\mathrm{L}} = \mathbb{E}_\theta\left\{\boldsymbol{\Lambda}_{\mathrm{L}}\right\} \triangleq \mathrm{diag}\left\{\bar{\boldsymbol{\Psi}}_{M+1}, \bar{\boldsymbol{\Psi}}_{M+2}, \cdots, \bar{\boldsymbol{\Psi}}_{N_\circledast}\right\}. \tag{A.43}$$

The FIM $\mathbf{J}_\theta$ can be then written as

$$\mathbf{J}_\theta = \frac{1}{c^2}\begin{bmatrix} \mathbf{A} & \mathbf{B} \\ \mathbf{B}^T & \mathbf{C} \end{bmatrix}, \tag{A.44}$$

where

$$\mathbf{A} \triangleq \begin{bmatrix} \sum_{k\in\mathcal{N}_\circledast}\mathbf{G}_k\bar{\boldsymbol{\Psi}}_k\mathbf{G}_k^T + c^2\boldsymbol{\Xi}_{\mathrm{p,p}}^k & \mathbf{G}_1\bar{\boldsymbol{\Psi}}_1\mathbf{D}_1^T + c^2\boldsymbol{\Xi}_{\mathrm{p},\kappa}^1 & \cdots & \mathbf{G}_M\bar{\boldsymbol{\Psi}}_M\mathbf{D}_M^T + c^2\boldsymbol{\Xi}_{\mathrm{p},\kappa}^M \\ \left(\mathbf{G}_1\bar{\boldsymbol{\Psi}}_1\mathbf{D}_1^T + c^2\boldsymbol{\Xi}_{\mathrm{p},\kappa}^1\right)^T & \mathbf{D}_1\bar{\boldsymbol{\Psi}}_1\mathbf{D}_1^T + c^2\boldsymbol{\Xi}_{\kappa,\kappa}^1 & & \\ \vdots & & \ddots & \\ \left(\mathbf{G}_M\bar{\boldsymbol{\Psi}}_M\mathbf{D}_M^T + c^2\boldsymbol{\Xi}_{\mathrm{p},\kappa}^M\right)^T & & & \mathbf{D}_M\bar{\boldsymbol{\Psi}}_M\mathbf{D}_M^T + c^2\boldsymbol{\Xi}_{\kappa,\kappa}^M \end{bmatrix}$$

$$\mathbf{B} \triangleq \begin{bmatrix} \mathbf{G}_{M+1}\bar{\boldsymbol{\Psi}}_{M+1} + c^2\boldsymbol{\Xi}_{\mathrm{p},\kappa}^{M+1} & \mathbf{G}_{M+2}\bar{\boldsymbol{\Psi}}_{M+2} + c^2\boldsymbol{\Xi}_{\mathrm{p},\kappa}^{M+2} & \cdots & \mathbf{G}_{N_\circledast}\bar{\boldsymbol{\Psi}}_{N_\circledast} + c^2\boldsymbol{\Xi}_{\mathrm{p},\kappa}^{N_\circledast} \\ \mathbf{0} & \mathbf{0} & \cdots & \mathbf{0} \end{bmatrix}$$

$$\mathbf{C} \triangleq \mathrm{diag}\left\{\bar{\boldsymbol{\Psi}}_{M+1} + c^2\boldsymbol{\Xi}_{\kappa,\kappa}^{M+1}, \bar{\boldsymbol{\Psi}}_{M+2} + c^2\boldsymbol{\Xi}_{\kappa,\kappa}^{M+2}, \cdots, \bar{\boldsymbol{\Psi}}_{N_\circledast} + c^2\boldsymbol{\Xi}_{\kappa,\kappa}^{N_\circledast}\right\}. \tag{A.45}$$

Apply the notion of EFI, and we have the the 2×2 EFIM as

$$
\begin{aligned}
\mathbf{J}_{\mathrm{e}}(\mathbf{p}) = \frac{1}{c^2} \Bigg\{ & \sum_{k \in \mathcal{N}_\circledast} \left(\mathbf{G}_k \bar{\mathbf{\Psi}}_k \mathbf{G}_k^T + c^2 \mathbf{\Xi}_{\mathbf{p},\mathbf{p}}^k \right) \\
& - \sum_{k \in \mathcal{N}_{\mathrm{L}}} \left(\mathbf{G}_k \bar{\mathbf{\Psi}}_k \mathbf{D}_k^T + c^2 \mathbf{\Xi}_{\mathbf{p},\kappa}^k \right) \left(\mathbf{D}_k \bar{\mathbf{\Psi}}_k \mathbf{D}_k^T + c^2 \mathbf{\Xi}_{\kappa,\kappa}^k \right)^{-1} \left(\mathbf{G}_k \bar{\mathbf{\Psi}}_k \mathbf{D}_k^T + c^2 \mathbf{\Xi}_{\mathbf{p},\kappa}^k \right)^T \\
& - \sum_{k \in \mathcal{N}_{\mathrm{NL}}} \left(\mathbf{G}_k \bar{\mathbf{\Psi}}_k + c^2 \mathbf{\Xi}_{\mathbf{p},\kappa}^k \right) \left(\bar{\mathbf{\Psi}}_k + c^2 \mathbf{\Xi}_{\kappa,\kappa}^k \right)^{-1} \left(\mathbf{G}_k \bar{\mathbf{\Psi}}_k + c^2 \mathbf{\Xi}_{\mathbf{p},\kappa}^k \right)^T \Bigg\}.
\end{aligned}
$$

$$(A.46)$$

From (A.18), we have $g_k(\boldsymbol{\kappa}_k | \mathbf{p}) = g_k(\boldsymbol{\kappa}_k | d_k)$, and

$$
\mathbf{\Xi}_{\mathbf{p},\mathbf{p}}^k = \mathbb{E}_{\boldsymbol{\theta}} \left\{ \left[\frac{\partial}{\partial \mathbf{p}} \ln g_k(\boldsymbol{\kappa}_k | \mathbf{p}) \right] \cdot \left[\frac{\partial}{\partial \mathbf{p}} \ln g_k(\boldsymbol{\kappa}_k | \mathbf{p}) \right]^T \right\} = \mathbf{q}_k \cdot \tilde{\mathbf{\Xi}}_{\mathbf{p},\mathbf{p}}^k \cdot \mathbf{q}_k^T \qquad (A.47)
$$

$$
\mathbf{\Xi}_{\mathbf{p},\kappa}^k = \mathbb{E}_{\boldsymbol{\theta}} \left\{ \left[\frac{\partial}{\partial \mathbf{p}} \ln g_k(\boldsymbol{\kappa}_k | \mathbf{p}) \right] \cdot \left[\frac{\partial}{\partial \boldsymbol{\kappa}_k} \ln g_k(\boldsymbol{\kappa}_k | \mathbf{p}) \right]^T \right\} = \mathbf{q}_k \cdot \tilde{\mathbf{\Xi}}_{\mathbf{p},\kappa}^k , \qquad (A.48)
$$

where

$$
\tilde{\mathbf{\Xi}}_{\mathbf{p},\mathbf{p}}^k \triangleq \mathbb{E}_{\boldsymbol{\theta}} \left\{ \left[\frac{\partial}{\partial d_k} \ln g_k(\boldsymbol{\kappa}_k | d_k) \right] \cdot \left[\frac{\partial}{\partial d_k} \ln g_k(\boldsymbol{\kappa}_k | d_k) \right] \right\} \qquad (A.49)
$$

$$
\tilde{\mathbf{\Xi}}_{\mathbf{p},\kappa}^k \triangleq \mathbb{E}_{\boldsymbol{\theta}} \left\{ \left[\frac{\partial}{\partial d_k} \ln g_k(\boldsymbol{\kappa}_k | d_k) \right] \cdot \left[\frac{\partial}{\partial \boldsymbol{\kappa}_k} \ln g_k(\boldsymbol{\kappa}_k | d_k) \right]^T \right\} . \qquad (A.50)
$$

Substituting (A.47) and (A.48) into (A.46), the EFIM can be further simplified as

$$
\mathbf{J}_{\mathrm{e}}(\mathbf{p}) = \sum_{k \in \mathcal{N}_{\mathrm{L}}} \lambda_k \cdot \mathbf{J}_{\mathrm{r}}(\phi_k) + \sum_{k \in \mathcal{N}_{\mathrm{NL}}} \lambda_k \cdot \mathbf{J}_{\mathrm{r}}(\phi_k) \qquad (A.51)
$$

where λ_k is the RII of the received signal from the kth anchor

$$\lambda_k = \frac{1}{c^2} \left\{ \mathbf{l}_k^T \bar{\boldsymbol{\Psi}}_k \mathbf{l}_k + c^2 \tilde{\boldsymbol{\Xi}}_{\mathbf{p},\mathbf{p}}^k - \left(\mathbf{l}_k^T \bar{\boldsymbol{\Psi}}_k \mathbf{D}_k^T + c^2 \tilde{\boldsymbol{\Xi}}_{\mathbf{p},\kappa}^k \right) \left(\mathbf{D}_k \bar{\boldsymbol{\Psi}}_k \mathbf{D}_k^T + c^2 \boldsymbol{\Xi}_{\kappa,\kappa}^k \right)^{-1} \left(\mathbf{l}_k^T \bar{\boldsymbol{\Psi}}_k \mathbf{D}_k^T + c^2 \tilde{\boldsymbol{\Xi}}_{\mathbf{p},\kappa}^k \right)^T \right\}$$

$$\text{for} \quad k \in \mathcal{N}_{\mathrm{L}} , \tag{A.52}$$

$$\lambda_k = \frac{1}{c^2} \left\{ \mathbf{l}_k^T \bar{\boldsymbol{\Psi}}_k \mathbf{l}_k + c^2 \tilde{\boldsymbol{\Xi}}_{\mathbf{p},\mathbf{p}}^k - \left(\mathbf{l}_k^T \bar{\boldsymbol{\Psi}}_k + c^2 \tilde{\boldsymbol{\Xi}}_{\mathbf{p},\kappa}^k \right) \left(\bar{\boldsymbol{\Psi}}_k + c^2 \boldsymbol{\Xi}_{\kappa,\kappa}^k \right)^{-1} \left(\mathbf{l}_k^T \bar{\boldsymbol{\Psi}}_k + c^2 \tilde{\boldsymbol{\Xi}}_{\mathbf{p},\kappa}^k \right)^T \right\}$$

$$\text{for} \quad k \in \mathcal{N}_{\mathrm{NL}} . \tag{A.53}$$

$\square$

A.3.4 Consistency of RII's for LoS and NLoS Signals

This section is to show that 1) the results in Theorem 2 degenerates to that of Theorem 1 when *a priori* knowledge is not available, and 2) *a priori* knowledge improves to localization accuracy in terms of RII.

- When *a priori* knowledge is not available, $\boldsymbol{\Xi}_{\kappa,\kappa}^k$, $\boldsymbol{\Xi}_{\mathbf{p},\kappa}^k$, and $\boldsymbol{\Xi}_{\mathbf{p},\mathbf{p}}^k$ in Theorem 2 are all equal to zero, and the corresponding RII λ_k in (A.52) and (A.53) reduce to

$$\begin{aligned} \lambda_k &= \frac{1}{c^2} \left\{ \mathbf{l}_k^T \boldsymbol{\Psi}_k \mathbf{l}_k - \left(\mathbf{l}_k^T \boldsymbol{\Psi}_k \mathbf{D}_k^T \right) \left(\mathbf{D}_k \boldsymbol{\Psi}_k \mathbf{D}_k^T \right)^{-1} \left(\mathbf{D}_k \boldsymbol{\Psi}_k \mathbf{l}_k \right) \right\} \\ &= \frac{1}{c^2} \cdot \mathbf{l}_k^T \left\{ \begin{bmatrix} 8\pi^2 \beta^2 \cdot \mathrm{SNR}_k^{(1)} & \mathbf{k}_k^T \\ \mathbf{k}_k & \breve{\boldsymbol{\Psi}}_k \end{bmatrix} - \begin{bmatrix} \mathbf{k}_k^T \\ \breve{\boldsymbol{\Psi}}_k \end{bmatrix} \breve{\boldsymbol{\Psi}}_k^{-1} \begin{bmatrix} \mathbf{k}_k & \breve{\boldsymbol{\Psi}}_k \end{bmatrix} \right\} \mathbf{l}_k \\ &= \frac{1}{c^2} \left\{ 8\pi^2 \beta^2 \cdot \mathrm{SNR}_k^{(1)} - \mathbf{k}_k^T \breve{\boldsymbol{\Psi}}_k^{-1} \mathbf{k}_k \right\} \\ &= \frac{8\pi^2 \beta^2}{c^2} (1 - \chi_k) \cdot \mathrm{SNR}_k^{(1)} \end{aligned} \tag{A.54}$$

for $k \in \mathcal{N}_{\mathrm{L}}$, and

$$\lambda_k = \frac{1}{c^2} \left\{ \mathbf{l}_k^T \boldsymbol{\Psi}_k \mathbf{l}_k - \mathbf{l}_k^T \boldsymbol{\Psi}_k \cdot \boldsymbol{\Psi}_k^{-1} \cdot \boldsymbol{\Psi}_k \mathbf{l}_k \right\} = 0 \tag{A.55}$$

for $k \in \mathcal{N}_{\mathrm{NL}}$.

- To show that *a priori* knowledge increases the ranging information intensity, we consider λ_k in (A.52). Note that $1/\lambda_k$ equals the upper-left element of $\mathbf{F}_k^{-1}$, where

$$
\begin{aligned}
\mathbf{F}_k &\triangleq \frac{1}{c^2}
\begin{bmatrix}
\mathbf{l}_k^T \bar{\boldsymbol{\Psi}}_k \mathbf{l}_k + c^2 \tilde{\Xi}_{\mathbf{p},\mathbf{p}}^k & \mathbf{l}_k^T \bar{\boldsymbol{\Psi}}_k \mathbf{D}_k^T + c^2 \tilde{\Xi}_{\mathbf{p},\kappa}^k \\
\mathbf{D}_k \bar{\boldsymbol{\Psi}}_k \mathbf{l}_k + c^2 \tilde{\boldsymbol{\Gamma}}_{\mathbf{p},\kappa}^{k\,T} & \mathbf{D}_k \bar{\boldsymbol{\Psi}}_k \mathbf{D}_k^T + c^2 \Xi_{\kappa,\kappa}^k
\end{bmatrix} \\[2mm]
&= \frac{1}{c^2}
\begin{bmatrix}
\mathbf{l}_k^T \bar{\boldsymbol{\Psi}}_k \mathbf{l}_k & \mathbf{l}_k^T \bar{\boldsymbol{\Psi}}_k \mathbf{D}_k^T \\
\mathbf{D}_k \bar{\boldsymbol{\Psi}}_k \mathbf{l}_k & \mathbf{D}_k \bar{\boldsymbol{\Psi}}_k \mathbf{D}_k^T
\end{bmatrix} +
\begin{bmatrix}
\tilde{\Xi}_{\mathbf{p},\mathbf{p}}^k & \tilde{\Xi}_{\mathbf{p},\kappa}^k \\
\tilde{\boldsymbol{\Gamma}}_{\mathbf{p},\kappa}^{k\,T} & \Xi_{\kappa,\kappa}^k
\end{bmatrix} \\[2mm]
&\succeq \frac{1}{c^2}
\begin{bmatrix}
\mathbf{l}_k^T \bar{\boldsymbol{\Psi}}_k \mathbf{l}_k & \mathbf{l}_k^T \bar{\boldsymbol{\Psi}}_k \mathbf{D}_k^T \\
\mathbf{D}_k \bar{\boldsymbol{\Psi}}_k \mathbf{l}_k & \mathbf{D}_k \bar{\boldsymbol{\Psi}}_k \mathbf{D}_k^T
\end{bmatrix} \triangleq \mathbf{F}_k^0.
\end{aligned}
\tag{A.56}
$$

The inequality in (A.56) is due to the fact that

$$
\begin{bmatrix}
\tilde{\Xi}_{\mathbf{p},\mathbf{p}}^k & \tilde{\Xi}_{\mathbf{p},\kappa}^k \\
\tilde{\boldsymbol{\Gamma}}_{\mathbf{p},\kappa}^{k\,T} & \Xi_{\kappa,\kappa}^k
\end{bmatrix}
= \mathbb{E}_\theta \left\{ \left[\frac{\partial}{\partial \tilde{\boldsymbol{\theta}}_k} \ln g_k(\boldsymbol{\kappa}_k | d_k) \right] \cdot \left[\frac{\partial}{\partial \tilde{\boldsymbol{\theta}}_k} \ln g_k(\boldsymbol{\kappa}_k | d_k) \right]^T \right\} \succeq \mathbf{0},
\tag{A.57}
$$

where $\tilde{\boldsymbol{\theta}}_k = \begin{bmatrix} d_k & \boldsymbol{\kappa}_k^T \end{bmatrix}^T$. Hence, we have $\mathbf{F}_k^{-1} \preceq \mathbf{F}_k^{0\,-1}$. Since the upper-left element of $\mathbf{F}_k^{0\,-1}$ equals the inverse of the (4.12), (A.56) implies that *a priori* knowledge increases the RII.

A.3.5 Consistency of EFIM's for LoS and NLoS Signals

We now show that (A.52) and (A.53) are equivalent when the EFI for $b_k^{(1)}$ from *a priori* knowledge goes to infinity. In other words, the contribution of NLoS signals to localization is as important as that of LoS signals when the bias of the first path in NLoS signals is precisely known.

The block matrices $\Xi_{\kappa,\kappa}^k$ in (3.17) and $\tilde{\Xi}_{\mathbf{p},\kappa}^k$ in (A.48) for NLoS signals can be

93

written as

$$\Xi^k_{\kappa,\kappa} = \begin{bmatrix} t^2 & \mathbf{v}^T_k \\ \mathbf{v}_k & \breve{\Xi}^k_{\kappa,\kappa} \end{bmatrix} \quad \text{and} \quad \tilde{\Xi}^k_{\mathbf{p},\kappa} = \begin{bmatrix} w & \breve{\tilde{\Xi}}^k_{\mathbf{p},\kappa} \end{bmatrix}, \tag{A.58}$$

where $\mathbf{v}_k, \breve{\tilde{\Xi}}^k_{\mathbf{p},\kappa} \in \mathbb{R}^{2L_k-1}$, and $\breve{\Xi}^k_{\kappa,\kappa} \in \mathbb{R}^{(2L_k-1)\times(2L_k-1)}$. Note that t^2 corresponds to the Fisher information of $b^{(1)}_k$. When the *a priori* knowledge of $b^{(1)}_k$ goes to ∞, i.e., $g_{\mathbf{b}}(b^{(1)}_k) \rightarrow \delta(b^{(1)}_k)$, we claim that

$$\lim_{t^2\to\infty} \left[\bar{\Psi}_k + c^2\Xi^k_{\kappa,\kappa}\right]^{-1} = \begin{bmatrix} 0 & \mathbf{0}^T \\ \mathbf{0} & \left(\mathbf{D}_k\bar{\Psi}_k\mathbf{D}^T_k + c^2\breve{\Xi}^k_{\kappa,\kappa}\right)^{-1} \end{bmatrix}. \tag{A.59}$$

Proof. Similar to (A.22), we can partition $\bar{\Psi}_k$ as

$$\bar{\Psi}_k = \begin{bmatrix} u^2_k & \mathbf{k}^T_k \\ \mathbf{k}_k & \breve{\Psi}_k \end{bmatrix}. \tag{A.60}$$

Then, the left-hand-side of (A.59) becomes

$$\text{LHS} = \lim_{t^2\to\infty} \begin{bmatrix} u^2_k + c^2t^2 & \mathbf{k}^T_k + c^2\mathbf{v}^T_k \\ \mathbf{k}_k + c^2\mathbf{v}_k & \breve{\Psi}'_k + c^2\breve{\Xi}^k_{\kappa,\kappa} \end{bmatrix}^{-1} = \lim_{t^2\to\infty} \begin{bmatrix} A & \mathbf{B} \\ \mathbf{B}^T & \mathbf{C} \end{bmatrix}, \tag{A.61}$$

where

$$A \triangleq \left[u^2_k + c^2t^2 - \left(\mathbf{k}_k + c^2\mathbf{v}_k\right)^T \left(\breve{\Psi}_k + c^2\breve{\Xi}^k_{\kappa,\kappa}\right)^{-1} \left(\mathbf{k}_k + c^2\mathbf{v}_k\right)\right]^{-1}, \tag{A.62}$$

$$\mathbf{B} \triangleq -\frac{1}{u^2_k + c^2t^2}\left(\mathbf{k}_k + c^2\mathbf{v}_k\right) \cdot \mathbf{C}^{-1}, \tag{A.63}$$

$$\mathbf{C} \triangleq \left[\breve{\Psi}_k + c^2\breve{\Xi}^k_{\kappa,\kappa} - \frac{1}{u^2_k + c^2t^2}\left(\mathbf{k}_k + c^2\mathbf{v}_k\right)\left(\mathbf{k}_k + c^2\mathbf{v}_k\right)^T\right]^{-1}. \tag{A.64}$$

When $b^{(1)}_k$ is precisely known, we have $t^2 \rightarrow \infty$, and hence

$$\lim_{t^2\to\infty} A = 0, \quad \lim_{t^2\to\infty} \mathbf{B} = \mathbf{0}, \quad \text{and} \quad \lim_{t^2\to\infty} \mathbf{C} = \left[\breve{\Psi}_k + c^2\breve{\Xi}^k_{\kappa,\kappa}\right]^{-1}. \tag{A.65}$$

Notice that $\breve{\bar{\Psi}}_k = \mathbf{D}_k \bar{\Psi}_k \mathbf{D}_k^T$. Hence, we proved our claim in (A.59). $\qquad\square$

Substituting (A.59) into (A.53), we have

$$
\lim_{t^2 \to \infty} \lambda_k = \frac{1}{c^2} \Bigg\{ \mathbf{l}_k^T \bar{\Psi}_k \mathbf{l}_k + c^2 \tilde{\Xi}_{\mathbf{p},\mathbf{p}}^k
$$
$$
- \left(\mathbf{l}_k^T \bar{\Psi}_k \mathbf{D}_k^T + c^2 \breve{\tilde{\Xi}}_{\mathbf{p},\kappa}^k \right) \left(\mathbf{D}_k \bar{\Psi}_k \mathbf{D}_k^T + c^2 \breve{\tilde{\Xi}}_{\kappa,\kappa}^k \right)^{-1} \left(\mathbf{l}_k^T \bar{\Psi}_k \mathbf{D}_k^T + c^2 \breve{\tilde{\Xi}}_{\mathbf{p},\kappa}^k \right)^T \Bigg\}
$$

(A.66)

for $k \in \mathcal{N}_{\mathrm{NL}}$. We then see that the right-hand-side of (A.66) equals that of (A.52), i.e., the RII of LoS signals.[4]

This result implies that LoS signals are the same for localization as NLoS with infinite *a priori* knowledge of $b_k^{(1)}$, i.e., $b_k^{(1)}$ is precisely known.

A.3.6 Proof of Proposition 2

Proof. For each of the possible agent's positions, ϕ_k and d_k are different, and hence $\mathbf{q}_k$, $\bar{\Psi}_k$, $\Xi_{\mathbf{p},\mathbf{p}}^k$, $\Xi_{\kappa,\kappa}^k$, and $\Xi_{\mathbf{p},\kappa}^k$ all become functions of $\mathbf{p}$. Note that in this case, we need to take expectation over $\mathbf{p}$ in (3.13) and (3.14). When the *a priori* knowledge of both the channel parameters and the agent's position is available, the EFIM for the agent's position is given by

$$
\mathbf{J}_{\mathbf{e}} = \Xi_{\mathbf{p}} + \sum_{k \in \mathcal{N}_{\circledast}} \Bigg\{ \mathbb{E}_{\mathbf{p}} \left\{ \mathbf{q}_k(\mathbf{p}) \cdot \tilde{\Xi}_{\mathbf{p},\mathbf{p}}^k(\mathbf{p}) \cdot \mathbf{q}_k(\mathbf{p})^T \right\} + \frac{1}{c^2} \cdot \mathbb{E}_{\mathbf{p}} \left\{ \mathbf{q}_k(\mathbf{p}) \cdot \mathbf{l}_k^T \bar{\Psi}_k(\mathbf{p}) \mathbf{l}_k \cdot \mathbf{q}_k(\mathbf{p})^T \right\}
$$
$$
- \frac{1}{c^2} \cdot \mathbb{E}_{\mathbf{p}} \left\{ \mathbf{q}_k(\mathbf{p}) \left(\mathbf{l}_k^T \bar{\Psi}_k(\mathbf{p}) + c^2 \cdot \tilde{\Xi}_{\mathbf{p},\kappa}^k(\mathbf{p}) \right) \right\} \cdot \mathbb{E}_{\mathbf{p}} \left\{ \bar{\Psi}_k(\mathbf{p}) + \Xi_{\kappa,\kappa}^k(\mathbf{p}) \right\}^{-1}
$$
$$
\cdot \mathbb{E}_{\mathbf{p}} \left\{ \left(\mathbf{l}_k^T \bar{\Psi}_k(\mathbf{p}) + c^2 \cdot \tilde{\Xi}_{\mathbf{p},\kappa}^k(\mathbf{p}) \right)^T \mathbf{q}_k(\mathbf{p})^T \right\} \Bigg\} .
$$

(A.67)

In far-field scenarios, where ϕ_k and d_k are approximately the same for all possible

---

[4]Note that the size of $\Xi_{\kappa,\kappa}^k$ and $\tilde{\Xi}_{\mathbf{p},\kappa}^k$ for LoS signals and NLoS signals are different for the same L_k. Indeed, $\breve{\Xi}_{\kappa,\kappa}^k$ and $\breve{\tilde{\Xi}}_{\mathbf{p},\kappa}^k$ are not associated with $b_k^{(1)}$, and hence they are in the same form as $\Xi_{\kappa,\kappa}^k$ and $\tilde{\Xi}_{\mathbf{p},\kappa}^k$ for LoS signals in (A.52).

agent's positions, we can approximate $\mathbf{p} = \bar{\mathbf{p}} = \mathbb{E}_{\mathbf{p}}\{\mathbf{p}\}$ and

$$\mathbb{E}_{\mathbf{p}}\{\mathbf{q}_k(\mathbf{p})\} \approx \mathbf{q}_k(\bar{\mathbf{p}}), \qquad \mathbb{E}_{\mathbf{p}}\{\bar{\boldsymbol{\Psi}}_k(\mathbf{p})\} \approx \bar{\boldsymbol{\Psi}}_k(\bar{\mathbf{p}}), \qquad \mathbb{E}_{\mathbf{p}}\{\boldsymbol{\Xi}^k_{\boldsymbol{\kappa},\boldsymbol{\kappa}}(\mathbf{p})\} \approx \boldsymbol{\Xi}^k_{\boldsymbol{\kappa},\boldsymbol{\kappa}}(\bar{\mathbf{p}}),$$

$$\mathbb{E}_{\mathbf{p}}\left\{\tilde{\boldsymbol{\Xi}}^k_{\mathbf{p},\boldsymbol{\kappa}}(\mathbf{p})\right\} \approx \tilde{\boldsymbol{\Xi}}^k_{\mathbf{p},\boldsymbol{\kappa}}(\bar{\mathbf{p}}), \qquad \mathbb{E}_{\mathbf{p}}\left\{\tilde{\tilde{\boldsymbol{\Xi}}}^k_{\mathbf{p},\mathbf{p}}(\mathbf{p})\right\} \approx \tilde{\tilde{\boldsymbol{\Xi}}}^k_{\mathbf{p},\mathbf{p}}(\bar{\mathbf{p}}). \tag{A.68}$$

Therefore, the EFIM in (A.67) can be approximated as

$$\mathbf{J}_{\mathbf{p}} \approx \boldsymbol{\Xi}_{\mathbf{p}} + \frac{1}{c^2} \sum_{k \in \mathcal{N}_\circledast} \left\{ \mathbf{q}_k(\bar{\mathbf{p}}) \cdot \left(\mathbf{l}_k^T \bar{\boldsymbol{\Psi}}_k(\bar{\mathbf{p}})\mathbf{l}_k + c^2 \cdot \tilde{\Gamma}^k_{\mathbf{p},\mathbf{p}}(\bar{\mathbf{p}})\right) \cdot \mathbf{q}_k(\bar{\mathbf{p}})^T \right.$$

$$\left. - \mathbf{q}_k(\bar{\mathbf{p}}) \left(\mathbf{l}_k^T \bar{\boldsymbol{\Psi}}_k(\bar{\mathbf{p}}) + c^2 \cdot \tilde{\boldsymbol{\Xi}}^k_{\mathbf{p},\boldsymbol{\kappa}}(\bar{\mathbf{p}})\right) \cdot \left(\bar{\boldsymbol{\Psi}}_k(\bar{\mathbf{p}}) + \boldsymbol{\Xi}^k_{\boldsymbol{\kappa},\boldsymbol{\kappa}}(\bar{\mathbf{p}})\right)^{-1} \left(\mathbf{l}_k^T \bar{\boldsymbol{\Psi}}_k(\bar{\mathbf{p}}) + c^2 \cdot \tilde{\boldsymbol{\Xi}}^k_{\mathbf{p},\boldsymbol{\kappa}}(\bar{\mathbf{p}})\right)^T \mathbf{q}_k(\bar{\mathbf{p}})^T \right\}$$

$$= \boldsymbol{\Xi}_{\mathbf{p}} + \sum_{k \in \mathcal{N}_\circledast} \lambda_k(\bar{\mathbf{p}}) \cdot \mathbf{J}_{\mathrm{r}}(\bar{\phi}_k) \tag{A.69}$$

where the RII and the elementary ranging information are, respectively, given by

$$\lambda_k(\bar{\mathbf{p}}) \triangleq \frac{1}{c^2} \left\{ \mathbf{l}_k^T \bar{\boldsymbol{\Psi}}_k(\bar{\mathbf{p}})\mathbf{l}_k + c^2 \tilde{\boldsymbol{\Xi}}^k_{\mathbf{p},\mathbf{p}}(\bar{\mathbf{p}}) \right.$$

$$\left. - \left(\mathbf{l}_k^T \bar{\boldsymbol{\Psi}}_k(\bar{\mathbf{p}}) + c^2 \tilde{\boldsymbol{\Xi}}^k_{\mathbf{p},\boldsymbol{\kappa}}(\bar{\mathbf{p}})\right) \left(\bar{\boldsymbol{\Psi}}_k(\bar{\mathbf{p}}) + c^2 \boldsymbol{\Xi}^k_{\boldsymbol{\kappa},\boldsymbol{\kappa}}(\bar{\mathbf{p}})\right)^{-1} \cdot \left(\mathbf{l}_k^T \bar{\boldsymbol{\Psi}}_k(\bar{\mathbf{p}}) + c^2 \tilde{\boldsymbol{\Xi}}^k_{\mathbf{p},\boldsymbol{\kappa}}(\bar{\mathbf{p}})\right)^T \right\}, \tag{A.70}$$

and

$$\mathbf{J}_{\mathrm{r}}(\bar{\phi}_k) = \mathbf{q}_k(\bar{\mathbf{p}})\, \mathbf{q}_k(\bar{\mathbf{p}})^T. \tag{A.71}$$

$\square$

A.4 Proofs of the Theorems in Chapter 5

A.4.1 Proof of Theorem 3

Since $\mathbf{p}$ and φ are deterministic but unknown, the joint likelihood function of the random vectors $\mathbf{r}$ and $\boldsymbol{\theta}$ can be written as

$$f(\mathbf{r}, \boldsymbol{\theta}) = f(\mathbf{r}|\boldsymbol{\theta}) \cdot g(\boldsymbol{\theta}) = \prod_{n \in \mathcal{N}_\nabla} \prod_{k \in \mathcal{N}_\circledcirc} f(\mathbf{r}_{n,k}|\boldsymbol{\theta}) \, g_{n,k}(\boldsymbol{\kappa}_{n,k}|\mathbf{p}, \varphi). \tag{A.72}$$

Note that $g_{n,k}(\boldsymbol{\kappa}_{n,k}|\mathbf{p}, \varphi) = g_{n,k}(\boldsymbol{\kappa}_{n,k}|d_{n,k})$, and the FIM $\mathbf{J}_\mathbf{p}$ from *a priori* knowledge can be expressed as

$$\mathbf{J}_\mathbf{p} = \begin{bmatrix} \sum_{n \in \mathcal{N}_\nabla} \sum_{k \in \mathcal{N}_\circledcirc} \Xi_{\mathbf{p},\mathbf{p}}^{n,k} & \sum_{n \in \mathcal{N}_\nabla} \sum_{k \in \mathcal{N}_\circledcirc} \Xi_{\mathbf{p},\varphi}^{n,k} & \Xi_{\mathbf{p},1} & \cdots & \Xi_{\mathbf{p},N_\nabla} \\ \sum_{n \in \mathcal{N}_\nabla} \sum_{k \in \mathcal{N}_\circledcirc} \Xi_{\mathbf{p},\varphi}^{n,k\,T} & \sum_{n \in \mathcal{N}_\nabla} \sum_{k \in \mathcal{N}_\circledcirc} \Xi_{\varphi,\varphi}^{n,k} & \Xi_{\varphi,1} & \cdots & \Xi_{\varphi,N_\nabla} \\ \Xi_{\mathbf{p},1}^T & \Xi_{\varphi,1}^T & \Xi_1 & & \\ \vdots & \vdots & & \ddots & \\ \Xi_{\mathbf{p},N_\nabla}^T & \Xi_{\varphi,N_\nabla}^T & & & \Xi_{N_\nabla} \end{bmatrix}, \tag{A.73}$$

where

$$\Xi_{\mathbf{p},\mathbf{p}}^{n,k} = \mathbf{q}_{n,k} \cdot \tilde{\Xi}_{\mathbf{p},\mathbf{p}}^{n,k} \cdot \mathbf{q}_{n,k}^T, \qquad \Xi_{\mathbf{p},\varphi}^{n,k} = \mathbf{q}_{n,k} \cdot \tilde{\Xi}_{\mathbf{p},\mathbf{p}}^{n,k} \cdot h_{n,k}, \qquad \Xi_{\varphi,\varphi}^{n,k} = h_{n,k}^2 \cdot \tilde{\Xi}_{\mathbf{p},\mathbf{p}}^{n,k}, \tag{A.74}$$

and

$$h_{n,k} \triangleq \frac{d}{d\varphi}\Delta x_n(\mathbf{p}, \varphi) \cdot \cos\phi_{n,k} + \frac{d}{d\varphi}\Delta y_n(\mathbf{p}, \varphi) \cdot \sin\phi_{n,k}. \tag{A.75}$$

Block matrices $\Xi_{\mathbf{p},n}$, $\Xi_{\varphi,n}$, and Ξ_n correspond to the nth antenna in the array, and they can further decomposed into block matrices corresponding to each anchor:

$$\Xi_{\mathbf{p},n} = \begin{bmatrix} \Xi_{\mathbf{p},\kappa}^{n,1} & \Xi_{\mathbf{p},\kappa}^{n,2} & \cdots & \Xi_{\mathbf{p},\kappa}^{n,N_\circledcirc} \end{bmatrix} \tag{A.76}$$

$$\Xi_{\varphi,n} = \begin{bmatrix} \Xi_{\varphi,\kappa}^{n,1} & \Xi_{\varphi,\kappa}^{n,2} & \cdots & \Xi_{\varphi,\kappa}^{n,N_\circledcirc} \end{bmatrix} \tag{A.77}$$

$$\Xi_n = \text{diag}\left\{ \Xi_{\kappa,\kappa}^{n,1}, \Xi_{\kappa,\kappa}^{n,2}, \cdots, \Xi_{\kappa,\kappa}^{n,N_\circledcirc} \right\}, \tag{A.78}$$

where for each k

$$\Xi_{\mathbf{p},\kappa}^{n,k} = \mathbf{q}_{n,k} \cdot \tilde{\Xi}_{\mathbf{p},\kappa}^{n,k}, \quad \text{and} \quad \Xi_{\varphi,\kappa}^{n,k} = h_{n,k} \cdot \tilde{\Xi}_{\mathbf{p},\kappa}^{n,k}. \tag{A.79}$$

Note that $\tilde{\Xi}_{\mathbf{p},\mathbf{p}}^{n,k}$, $\tilde{\Xi}_{\mathbf{p},\kappa}^{n,k}$, and $\Xi_{\kappa,\kappa}^{n,k}$ are defined similarly as (A.49), (A.50), and (3.17), except that the subscript $\{k\}$ is replaced with $\{n, k\}$. The transformation matrix can be written as

$$\mathbf{T} = \frac{1}{c} \begin{bmatrix} \mathbf{G}_1 & \mathbf{G}_2 & \cdots & \mathbf{G}_{N_{\bar{v}}} \\ \mathbf{h}_1 & \mathbf{h}_2 & \cdots & \mathbf{h}_{N_{\bar{v}}} \\ & & \mathbf{I} & \end{bmatrix}, \tag{A.80}$$

where each

$$\begin{aligned} \mathbf{G}_n &= \begin{bmatrix} \mathbf{q}_{n,1} \mathbf{1}_{n,1}^T & \mathbf{q}_{n,2} \mathbf{1}_{n,2}^T & \cdots & \mathbf{q}_{n,N_{\circledast}} \mathbf{1}_{n,N_{\circledast}}^T \end{bmatrix}, \\ \mathbf{h}_n &= \begin{bmatrix} h_{n,1} \mathbf{1}_{n,1}^T & h_{n,2} \mathbf{1}_{n,2}^T & \cdots & h_{n,N_{\circledast}} \mathbf{1}_{n,N_{\circledast}}^T \end{bmatrix}. \end{aligned} \tag{A.81}$$

Note that the FIM for $\boldsymbol{\theta}$ is

$$\mathbf{J}_{\boldsymbol{\theta}} = \mathbf{T} \cdot \mathbf{J}_{\boldsymbol{\eta}} \cdot \mathbf{T}^T + \mathbf{J}_{\mathbf{p}} \tag{A.82}$$

where

$$\mathbf{J}_{\boldsymbol{\eta}} = \text{diag} \left\{ \bar{\boldsymbol{\Lambda}}_1, \bar{\boldsymbol{\Lambda}}_2, \cdots, \bar{\boldsymbol{\Lambda}}_{N_{\bar{v}}} \right\} \tag{A.83}$$

and $\bar{\boldsymbol{\Lambda}}_n$ corresponds to the nth antenna as defined in (A.5)

$$\bar{\boldsymbol{\Lambda}}_n = \text{diag} \left\{ \bar{\boldsymbol{\Psi}}_{n,1}, \bar{\boldsymbol{\Psi}}_{n,2}, \cdots, \bar{\boldsymbol{\Psi}}_{n,N_{\circledast}} \right\}. \tag{A.84}$$

We then have the FIM,

$$\mathbf{J}_\theta = \mathbf{T} \cdot \mathbf{J}_\eta \cdot \mathbf{T}^T + \mathbf{J}_p$$

$$= \frac{1}{c^2} \begin{bmatrix} \sum_{n\in\mathcal{N}_\nabla} \mathbf{G}_n \bar{\mathbf{\Lambda}}_n \mathbf{G}_n^T & \sum_{n\in\mathcal{N}_\nabla} \mathbf{G}_n \bar{\mathbf{\Lambda}}_n \mathbf{h}_n^T & \mathbf{G}_1 \bar{\mathbf{\Lambda}}_1 & \cdots & \mathbf{G}_{N_\nabla} \bar{\mathbf{\Lambda}}_{N_\nabla} \\ \sum_{n\in\mathcal{N}_\nabla} \mathbf{h}_n \bar{\mathbf{\Lambda}}_n \mathbf{G}_n^T & \sum_{n\in\mathcal{N}_\nabla} \mathbf{h}_n \bar{\mathbf{\Lambda}}_n \mathbf{h}_n^T & \mathbf{h}_1 \bar{\mathbf{\Lambda}}_1 & \cdots & \mathbf{h}_{N_\nabla} \bar{\mathbf{\Lambda}}_{N_\nabla} \\ \bar{\mathbf{\Lambda}}_1 \mathbf{G}_1^T & \bar{\mathbf{\Lambda}}_1 \mathbf{h}_1^T & \bar{\mathbf{\Lambda}}_1 & & \\ \vdots & \vdots & & \ddots & \\ \bar{\mathbf{\Lambda}}_{N_\nabla} \mathbf{G}_{N_\nabla}^T & \bar{\mathbf{\Lambda}}_{N_\nabla} \mathbf{h}_{N_\nabla}^T & & & \bar{\mathbf{\Lambda}}_{N_\nabla} \end{bmatrix} + \mathbf{J}_p \,.$$

$$(A.85)$$

Substituting (A.73) in (A.85) and applying the notion of EFI, we obtain the 3×3 EFIM for the position and orientation

$$\mathbf{J}_e = \begin{bmatrix} \sum_{n\in\mathcal{N}_\nabla} \sum_{k\in\mathcal{N}_\circledast} \lambda_{n,k} \cdot \mathbf{q}_{n,k} \mathbf{q}_{n,k}^T & \sum_{n\in\mathcal{N}_\nabla} \sum_{k\in\mathcal{N}_\circledast} \lambda_{n,k} h_{n,k} \cdot \mathbf{q}_{n,k} \\ \sum_{n\in\mathcal{N}_\nabla} \sum_{k\in\mathcal{N}_\circledast} \lambda_{n,k} h_{n,k} \cdot \mathbf{q}_{n,k}^T & \sum_{n\in\mathcal{N}_\nabla} \sum_{k\in\mathcal{N}_\circledast} \lambda_{n,k} h_{n,k}^2 \end{bmatrix}, \quad (A.86)$$

where $\lambda_{n,k}$ is the RII from the kth anchor at the nth antenna

$$\lambda_{n,k} \triangleq \frac{1}{c^2} \left\{ \mathbf{l}_{n,k}^T \bar{\mathbf{\Psi}}_{n,k} \mathbf{l}_{n,k} + c^2 \tilde{\Xi}_{p,p}^{n,k} - \left(\mathbf{l}_{n,k}^T \bar{\mathbf{\Psi}}_{n,k} + c^2 \tilde{\Xi}_{p,\kappa}^{n,k} \right) \left(\bar{\mathbf{\Psi}}_{n,k} + c^2 \Xi_{\kappa,\kappa}^{n,k} \right)^{-1} \left(\mathbf{l}_{n,k}^T \bar{\mathbf{\Psi}}_{n,k} + c^2 \tilde{\Xi}_{p,\kappa}^{n,k} \right)^T \right\}.$$

$$(A.87)$$

Therefore, the 2×2 EFIM for the position is

$$\mathbf{J}_e^{\text{Array}}(\mathbf{p}) = \sum_{n\in\mathcal{N}_\nabla} \sum_{k\in\mathcal{N}_\circledast} \lambda_{n,k} \cdot \mathbf{q}_{n,k} \mathbf{q}_{n,k}^T - \frac{1}{\sum_{n\in\mathcal{N}_\nabla} \sum_{k\in\mathcal{N}_\circledast} \lambda_{n,k} h_{n,k}^2} \cdot \mathbf{q}\mathbf{q}^T$$

$$= \sum_{n\in\mathcal{N}_\nabla} \mathbf{J}_{e,n} - \frac{1}{\sum_{n\in\mathcal{N}_\nabla} \sum_{k\in\mathcal{N}_\circledast} \lambda_{n,k} h_{n,k}^2} \cdot \mathbf{q}\mathbf{q}^T \qquad (A.88)$$

where $\mathbf{J}_{e,n}$ is the EFIM for antenna n,

$$\mathbf{J}_{e,n} = \sum_{k\in\mathcal{N}_\circledast} \lambda_{n,k} \cdot \mathbf{J}_r(\phi_{n,k}) \qquad (A.89)$$

99

and

$$\mathbf{q} = \sum_{n \in \mathcal{N}_\triangledown} \sum_{k \in \mathcal{N}_\circledast} \lambda_{n,k} h_{n,k} \cdot \mathbf{q}_{n,k}. \tag{A.90}$$

In addition, the EFI for the orientation is

$$J_{\mathrm{e}}(\varphi) = \sum_{n \in \mathcal{N}_\triangledown} \sum_{k \in \mathcal{N}_\circledast} \lambda_{n,k} h_{n,k}^2 - \mathbf{q}^T \left(\sum_{n \in \mathcal{N}_\triangledown} \mathbf{J}_{\mathrm{e,n}} \right)^{-1} \mathbf{q}. \tag{A.91}$$

A.4.2 Proof of Proposition 3

Since $\mathbf{q}\mathbf{q}^T$ is always positive semi-definite, we need to simply prove that there exists a unique $\mathbf{p}^*$ such that $\mathbf{q}^* = \mathbf{0}$.

Proof. Let $\mathbf{p}$ be an arbitrary reference point, and

$$\mathbf{p}^* = \mathbf{p} + \mathbf{g}(\varphi), \tag{A.92}$$

where $\mathbf{g}(\varphi) = [\, g_x(\varphi), \ g_y(\varphi)\,]^T$, and $g_x(\varphi)$ and $g_y(\varphi)$ denote the relative distance in x and y directions, respectively. Then, $h_{n,k}$ corresponding to $\mathbf{p}$ can be written as a sum of two parts

$$h_{n,k} = h_{n,k}^* + \tilde{h}_{n,k} \tag{A.93}$$

where $h_{n,k}^*$ corresponds to $\mathbf{p}^*$

$$h_{n,k}^* = \frac{d}{d\varphi} \Delta x_n(\mathbf{p}^*, \varphi) \cdot \cos \phi_{n,k} + \frac{d}{d\varphi} \Delta y_n(\mathbf{p}^*, \varphi) \cdot \sin \phi_{n,k}, \tag{A.94}$$

and

$$\begin{aligned}
\tilde{h}_{n,k} &= \frac{d}{d\varphi} g_x(\varphi) \cdot \cos \phi_{n,k} + \frac{d}{d\varphi} g_y(\varphi) \cdot \sin \phi_{n,k} \\
&\triangleq \dot{g}_x \cdot \cos \phi_{n,k} + \dot{g}_y \cdot \sin \phi_{n,k} = \dot{\mathbf{g}}^T \cdot \mathbf{q}_{n,k}.
\end{aligned} \tag{A.95}$$

100

Hence, $\mathbf{q}$ corresponding to the reference position $\mathbf{p}$ is given by

$$\mathbf{q} = \underbrace{\sum_{n \in \mathcal{N}_\nabla} \sum_{k \in \mathcal{N}_\circledast} \lambda_{n,k} h^*_{n,k} \cdot \mathbf{q}_{n,k}}_{\triangleq \mathbf{q}^*} + \underbrace{\sum_{n \in \mathcal{N}_\nabla} \sum_{k \in \mathcal{N}_\circledast} \lambda_{n,k} \tilde{h}_{n,k} \cdot \mathbf{q}_{n,k}}_{\triangleq \tilde{\mathbf{q}}}, \tag{A.96}$$

and $\tilde{\mathbf{q}}$ can be written as

$$\tilde{\mathbf{q}} = \sum_{n \in \mathcal{N}_\nabla} \sum_{k \in \mathcal{N}_\circledast} \mathbf{q}^T_{n,k} \dot{\mathbf{g}} \cdot \lambda_{n,k} \cdot \mathbf{q}_{n,k} = \sum_{n \in \mathcal{N}_\nabla} \sum_{k \in \mathcal{N}_\circledast} \lambda_{n,k} \cdot \mathbf{q}_{n,k} \mathbf{q}^T_{n,k} \cdot \dot{\mathbf{g}} = \sum_{n \in \mathcal{N}_\nabla} \mathbf{J}_{e,n} \cdot \dot{\mathbf{g}}. \tag{A.97}$$

Since $\sum_{n \in \mathcal{N}_\nabla} \mathbf{J}_{e,n} \succ 0$, we have $\mathbf{q}^* = 0$ if and only if

$$\dot{\mathbf{g}} = \left(\sum_{n \in \mathcal{N}_\nabla} \mathbf{J}_{e,n} \right)^{-1} \cdot \mathbf{q}, \tag{A.98}$$

implying that there exists only one $\dot{\mathbf{g}}$, and hence only one $\mathbf{g}(\varphi)$, such that $\mathbf{q}^* = 0$. Therefore, the orientation center $\mathbf{p}^*$ is unique. □

A.4.3   Proof of Corollary 2

We first prove that the SOEB is independent of the reference point $\mathbf{p}$.

Proof. Using the notations in Appendix A.4.2, we show that the EFI for the orientation based on any referent point $\mathbf{p}$

$$J_e(\varphi) = \sum_{n \in \mathcal{N}_\nabla} \sum_{k \in \mathcal{N}_\circledast} \lambda_{n,k} h^2_{n,k} - \mathbf{q}^T \left(\sum_{n \in \mathcal{N}_\nabla} \mathbf{J}_{e,n} \right)^{-1} \mathbf{q} \tag{A.99}$$

equals the EFI for the orientation based on the orientation center $\mathbf{p}^*$

$$J^*_e(\varphi) = \sum_{n \in \mathcal{N}_\nabla} \sum_{k \in \mathcal{N}_\circledast} \lambda_{n,k} h^{*2}_{n,k}. \tag{A.100}$$

101

Let $\mathbf{J} = \sum_{n \in \mathcal{N}_\nabla} \mathbf{J}_{\mathrm{e},n}$. From (A.96) and (A.97), we have

$$\mathbf{q} = \tilde{\mathbf{q}} = \mathbf{J} \cdot \dot{\mathbf{g}}, \tag{A.101}$$

and hence

$$\mathbf{q}^T \mathbf{J}^{-1} \mathbf{q} = \tilde{\mathbf{q}}^T \mathbf{J}^{-1} \tilde{\mathbf{q}} = \tilde{\mathbf{q}}^T \cdot \dot{\mathbf{g}} = \sum_{n \in \mathcal{N}_\nabla} \sum_{k \in \mathcal{N}_\oplus} \lambda_{n,k} \tilde{h}_{n,k}^2 \,. \tag{A.102}$$

On the other hand, we also have

$$\sum_{n \in \mathcal{N}_\nabla} \sum_{k \in \mathcal{N}_\oplus} \lambda_{n,k} h_{n,k}^* \tilde{h}_{n,k} = \mathbf{q}^* \cdot \dot{\mathbf{g}} = 0 \,. \tag{A.103}$$

Therefore, we can verify that the EFI for the orientation in (A.99)

$$
\begin{aligned}
J_{\mathrm{e}}(\varphi) &= \sum_{n \in \mathcal{N}_\nabla} \sum_{k \in \mathcal{N}_\oplus} \lambda_{n,k} (h_{n,k}^* + \tilde{h}_{n,k})^2 - \tilde{\mathbf{q}}^T \mathbf{J}^{-1} \tilde{\mathbf{q}} \\
&= \sum_{n \in \mathcal{N}_\nabla} \sum_{k \in \mathcal{N}_\oplus} \lambda_{n,k} h_{n,k}^{*2} + 2 \sum_{n \in \mathcal{N}_\nabla} \sum_{k \in \mathcal{N}_\oplus} \lambda_{n,k} h_{n,k}^* \tilde{h}_{n,k} = J_{\mathrm{e}}^*(\varphi) \,.
\end{aligned} \tag{A.104}
$$

This shows that the EFI for the orientation is independent of the reference point, and thus is the SOEB. $\qquad\square$

The SPEB achieves the minimum at the orientation center by Proposition 3. We now derive the SPEB for any reference point and relate that to the SPEB at the orientation center. The 3×3 EFIM in (A.86) can be written, using (A.96) and (A.104), as

$$\mathbf{J}_{\mathrm{e}} = \begin{bmatrix} \mathbf{J} & \tilde{\mathbf{q}} \\ \tilde{\mathbf{q}}^T & J_{\mathrm{e}}(\varphi) + \tilde{\mathbf{q}}^T \mathbf{J}^{-1} \tilde{\mathbf{q}} \end{bmatrix} \,. \tag{A.105}$$

Using the equation of Shur's complement [63], we have

$$\mathbf{J}_{\mathrm{e}}^{-1}(\mathbf{p}) = \mathbf{J}^{-1} + \frac{1}{J_{\mathrm{e}}(\varphi)} \cdot \left(\mathbf{J}^{-1} \tilde{\mathbf{q}}\right) \left(\mathbf{J}^{-1} \tilde{\mathbf{q}}\right)^T = \mathbf{J}^{-1} + \frac{1}{J_{\mathrm{e}}(\varphi)} \cdot \dot{\mathbf{g}} \dot{\mathbf{g}}^T \,. \tag{A.106}$$

102

Since translation $\mathbf{g}(\varphi)$ can be represented as

$$\mathbf{g}(\varphi) = \|\mathbf{p} - \mathbf{p}^*\| \cdot \begin{bmatrix} \cos(\varphi + \varphi_0) \\ \sin(\varphi + \varphi_0) \end{bmatrix}, \tag{A.107}$$

where φ_0 is a constant angle, we have

$$\|\dot{\mathbf{g}}\| = \|\mathbf{p} - \mathbf{p}^*\|. \tag{A.108}$$

Then, by taking the trace of both sides of (A.106), we obtain

$$\mathcal{P}(\mathbf{p}) = \mathcal{P}(\mathbf{p}^*) + \frac{\dot{\mathbf{g}}^T \dot{\mathbf{g}}}{J_e(\varphi)} = \mathcal{P}(\mathbf{p}^*) + \frac{\|\mathbf{p} - \mathbf{p}^*\|^2}{J_e(\varphi)}. \tag{A.109}$$

This completes the proof.

A.4.4   Proof of Proposition 4

Proof. Take the array center $\mathbf{p}_0$ as the reference point, and we have

$$\begin{aligned}
\sum_{n \in \mathcal{N}_\triangledown} h_{n,k} &= \sum_{n \in \mathcal{N}_\triangledown} \frac{d}{d\varphi} \Delta x_n(\mathbf{p}_0, \varphi) \cdot \cos \phi_{n,k} + \frac{d}{d\varphi} \Delta y_n(\mathbf{p}_0, \varphi) \cdot \sin \phi_{n,k} \\
&= \frac{d}{d\varphi} \left(\sum_{n \in \mathcal{N}_\triangledown} \Delta x_n(\mathbf{p}_0, \varphi) \right) \cdot \cos \phi_{n,k} + \frac{d}{d\varphi} \left(\sum_{n \in \mathcal{N}_\triangledown} \Delta y_n(\mathbf{p}_0, \varphi) \right) \cdot \sin \phi_{n,k} \\
&= 0. \tag{A.110}
\end{aligned}$$

Consequently,

$$\mathbf{q} = \sum_{n \in \mathcal{N}_\triangledown} \sum_{k \in \mathcal{N}_\oplus} \lambda_k h_{n,k} \cdot \mathbf{q}_k = \sum_{k \in \mathcal{N}_\oplus} \left(\sum_{n \in \mathcal{N}_\triangledown} h_{n,k} \right) \lambda_k \cdot \mathbf{q}_k = 0, \tag{A.111}$$

implying $\mathbf{p}_0 = \mathbf{p}^*$, i.e., the array center is the orientation center. $\square$

A.4.5 Proof of Corollary 3

In far-field scenarios, $\phi_{n,k}$ and $d_{n,k}$ are approximately the same for all possible agent's positions and for all n. When *a priori* knowledge of the agent's position and orientation is available, following the steps of the proof in Appendix A.3.6 and using the fact that the array center is the orientation center, we can obtain the 3×3 EFIM for the array center and orientation as

$$
\mathbf{J}_e(\mathbf{p}_0, \varphi) = \begin{bmatrix} N \cdot \mathbf{J}_e + \Xi_{\mathbf{p}} & \mathbf{0} \\ \mathbf{0}^T & \sum_{n \in \mathcal{N}_{\nabla}} \sum_{k \in \mathcal{N}_{\circledast}} \lambda_k(\bar{\mathbf{p}}_0) \bar{h}_{n,k}^2 + \Xi_{\varphi} \end{bmatrix}, \tag{A.112}
$$

where $\bar{h}_{n,k}$ is a function of $\mathbf{p}_0$, $\mathbf{J}_e$ is the EFIM for each antenna

$$
\mathbf{J}_e = \sum_{k \in \mathcal{N}_{\circledast}} \lambda_k(\bar{\mathbf{p}}_0) \cdot \mathbf{q}_k(\bar{\mathbf{p}}_0) \, \mathbf{q}_k^T(\bar{\mathbf{p}}_0). \tag{A.113}
$$

Note that the non-diagonal elements are zero since $\mathbf{p}_0 = \mathbf{p}^*$.

A.5 Proofs of the Theorems in Chapter 6

A.5.1 Proof of Theorem 4

In the scenario in which there is a time offset, we use the notations in Appendix A.3.3 and can write the FIM as

$$
\mathbf{J}_\theta = \frac{1}{c^2} \begin{bmatrix} \sum_{k \in \mathcal{N}_{\circledast}} \mathbf{G}_k \bar{\Psi}_k \mathbf{G}_k^T & \sum_{k \in \mathcal{N}_{\circledast}} \mathbf{G}_k \bar{\Psi}_k l_k & \mathbf{G}_1 \bar{\Psi}_1 & \cdots & \mathbf{G}_{N_{\circledast}} \bar{\Psi}_{N_{\circledast}} \\ \sum_{k \in \mathcal{N}_{\circledast}} l_k^T \bar{\Psi}_k \mathbf{G}_k & \sum_{k \in \mathcal{N}_{\circledast}} l_k^T \bar{\Psi}_k l_k & l_1^T \bar{\Psi}_1 & \cdots & l_{N_{\circledast}}^T \bar{\Psi}_{N_{\circledast}} \\ \bar{\Psi}_1 \mathbf{G}_1^T & \bar{\Psi}_1 l_1 & \bar{\Psi}_1 & & \\ \vdots & \vdots & & \ddots & \\ \bar{\Psi}_{N_{\circledast}} \mathbf{G}_{N_{\circledast}}^T & \bar{\Psi}_{N_{\circledast}} l_{N_{\circledast}} & & & \bar{\Psi}_{N_{\circledast}} \end{bmatrix} + \mathbf{J}_{\mathrm{p}},
$$

$$
\tag{A.114}
$$

where

$$
\mathbf{J_p} = \begin{bmatrix} \sum_{k \in \mathcal{N}_\circledast} \Xi^k_{\mathbf{p},\mathbf{p}} & 0 & \Xi^1_{\mathbf{p},\kappa} & \cdots & \Xi^{N_\circledast}_{\mathbf{p},\kappa} \\ 0^T & \Xi_\mathrm{B} & 0^T & \cdots & 0^T \\ \Xi^{1\ T}_{\mathbf{p},\kappa} & 0 & \Xi^1_{\kappa,\kappa} & & \\ \vdots & \vdots & & \ddots & \\ \Xi^{N_\circledast\ T}_{\mathbf{p},\kappa} & 0 & & & \Xi^{N_\circledast}_{\kappa,\kappa} \end{bmatrix} . \tag{A.115}
$$

Applying the notion of EFI, we obtain the 3×3 EFIM for the position and the time offset

$$
\mathbf{J_e} = \begin{bmatrix} \sum_{k \in \mathcal{N}_\circledast} \lambda_k \cdot \mathbf{q}_k \mathbf{q}_k^T & \sum_{k \in \mathcal{N}_\circledast} \lambda_k \cdot \mathbf{q}_k \\ \sum_{k \in \mathcal{N}_\circledast} \lambda_k \cdot \mathbf{q}_k^T & \sum_{k \in \mathcal{N}_\circledast} \lambda_k + \Xi_\mathrm{B} \end{bmatrix} , \tag{A.116}
$$

where the RII λ_k is defined as (A.53). Therefore, the 2×2 EFIM for the position $\mathbf{p}$ in the presence of the time offset B becomes

$$
\mathbf{J}^\mathrm{B}_\mathbf{e}(\mathbf{p}) = \sum_{k \in \mathcal{N}_\circledast} \lambda_k \cdot \mathbf{q}_k \mathbf{q}_k^T - \frac{1}{\sum_{k \in \mathcal{N}_\circledast} \lambda_k + \Xi_\mathrm{B}} \cdot \mathbf{q}_\mathrm{B} \mathbf{q}_\mathrm{B}^T , \tag{A.117}
$$

and the EFI for the time offset can be written as

$$
J_\mathrm{e}(B) = \sum_{k \in \mathcal{N}_\circledast} \lambda_k + \Xi_\mathrm{B} - \mathbf{q}_\mathrm{B}^T \left(\sum_{k \in \mathcal{N}_\circledast} \lambda_k \cdot \mathbf{q}_k \mathbf{q}_k^T \right)^{-1} \mathbf{q}_\mathrm{B}, \tag{A.118}
$$

where $\mathbf{q}_\mathrm{B} \triangleq \sum_{k \in \mathcal{N}_\circledast} \lambda_k \cdot \mathbf{q}_k$.

A.5.2 Proof of Corollary 6

Similar to the proof in Appendix A.4.5, we can incorporate the *a priori* knowledge of the array center and orientation into (6.12), and obtain the approximate EFIM in

105

far-field scenarios as

$$\mathbf{J}_e^{\text{Array-B}} = \begin{bmatrix} \sum_{n\in\mathcal{N}_\nabla} \sum_{k\in\mathcal{N}_\circledast} \lambda_{n,k} \mathbf{q}_{n,k} \mathbf{q}_{n,k}^T + \mathbf{\Xi}_{\mathbf{p}} & \sum_{n\in\mathcal{N}_\nabla} \sum_{k\in\mathcal{N}_\circledast} \lambda_{n,k} h_{n,k} \mathbf{q}_{n,k} & \sum_{n\in\mathcal{N}_\nabla} \sum_{k\in\mathcal{N}_\circledast} \lambda_{n,k} \mathbf{q}_{n,k} \\ \sum_{n\in\mathcal{N}_\nabla} \sum_{k\in\mathcal{N}_\circledast} \lambda_{n,k} h_{n,k} \mathbf{q}_{n,k}^T & \sum_{n\in\mathcal{N}_\nabla} \sum_{k\in\mathcal{N}_\circledast} \lambda_{n,k} h_{n,k}^2 + \Xi_\varphi & \sum_{n\in\mathcal{N}_\nabla} \sum_{k\in\mathcal{N}_\circledast} \lambda_{n,k} h_{n,k} \\ \sum_{n\in\mathcal{N}_\nabla} \sum_{k\in\mathcal{N}_\circledast} \lambda_{n,k} \mathbf{q}_{n,k}^T & \sum_{n\in\mathcal{N}_\nabla} \sum_{k\in\mathcal{N}_\circledast} \lambda_{n,k} h_{n,k} & \sum_{n\in\mathcal{N}_\nabla} \sum_{k\in\mathcal{N}_\circledast} \lambda_{n,k} + \Xi_{\text{B}} \end{bmatrix}.$$

$$\text{(A.119)}$$

Recall that in far-field scenarios, $\mathbf{p} = \mathbf{p}^*$, implying that $\sum_{n\in\mathcal{N}_\nabla} \sum_{k\in\mathcal{N}_\circledast} \lambda_{n,k} h_{n,k} \mathbf{q}_{n,k} = \mathbf{0}$ and $\sum_{n\in\mathcal{N}_\nabla} \sum_{k\in\mathcal{N}_\circledast} \lambda_{n,k} h_{n,k} = 0$, and hence

$$\mathbf{J}_e^{\text{Array-B}} = \begin{bmatrix} N_\nabla \cdot \bar{\mathbf{J}}_e + \mathbf{\Xi}_{\mathbf{p}} & \mathbf{0} & N_\nabla \sum_{k\in\mathcal{N}_\circledast} \lambda_k \mathbf{q}_k \\ \mathbf{0}^T & \sum_{n\in\mathcal{N}_\nabla} \sum_{k\in\mathcal{N}_\circledast} \lambda_k \bar{h}_{n,k}^2 + \Xi_\varphi & 0 \\ N_\nabla \sum_{k\in\mathcal{N}_\circledast} \lambda_k \mathbf{q}_k^T & 0 & N_\nabla \sum_{k\in\mathcal{N}_\circledast} \lambda_k + \Xi_{\text{B}} \end{bmatrix}.$$

$$\text{(A.120)}$$

Bibliography

[1] A. Sayed, A. Tarighat, and N. Khajehnouri, "Network-based wireless location: challenges faced in developing techniques for accurate wireless location information," *IEEE Signal Processing Mag.*, vol. 22, no. 4, pp. 24–40, 2005.

[2] K. Pahlavan, X. Li, and J. P. Makela, "Indoor geolocation science and technology," *IEEE Commun. Mag.*, vol. 40, no. 2, pp. 112–118, Feb. 2002.

[3] J. J. Caffery and G. L. Stuber, "Overview of radiolocation in CDMA cellular systems," *IEEE Commun. Mag.*, vol. 36, no. 4, pp. 38–45, Apr. 1998.

[4] N. Patwari, J. N. Ash, S. Kyperountas, A. O. I. Hero, R. L. Moses, and N. S. Correal, "Locating the nodes: cooperative localization in wireless sensor networks," *IEEE Signal Processing Mag.*, vol. 22, no. 4, pp. 54–69, July 2005.

[5] C.-Y. Chong and S. P. Kumar, "Sensor networks: evolution, opportunities, and challenges," *Proc. IEEE*, vol. 91, no. 8, pp. 1247–1256, Aug. 2003.

[6] J. J. Spilker, Jr., "GPS signal structure and performance characteristics," *Journal of the Institute of Navigation*, vol. 25, no. 2, pp. 121–146, Summer 1978.

[7] D. B. Jourdan, D. Dardari, and M. Z. Win, "Position error bound for UWB localization in dense cluttered environments," *IEEE Trans. Aerosp. Electron. Syst.*, vol. 44, 2008, to be published.

[8] S. Gezici, Z. Tian, G. B. Giannakis, H. Kobayashi, A. F. Molisch, H. V. Poor, and Z. Sahinoglu, "Localization via ultra-wideband radios: a look at positioning aspects for future sensor networks," *IEEE Signal Processing Mag.*, vol. 22, pp. 70–84, July 2005.

[9] C. Falsi, D. Dardari, L. Mucchi, and M. Z. Win, "Time of arrival estimation for UWB localizers in realistic environments," *EURASIP J. Appl. Signal Processing (Special Issue on Wireless Location Technologies and Applications)*, vol. 2006, pp. Article ID 32082, 1–13, 2006.

[10] Y. Shen and M. Z. Win, "Fundamental limits of wideband localization accuracy via Fisher information," in *Proc. IEEE Wireless Commun. and Networking Conf.*, HONG KONG, Mar. 2007, pp. 3046–3051.

[11] Y. Shen, H. Wymeersch, and M. Z. Win, "Fundamental limits of wideband cooperative localization via Fisher information," in *Proc. IEEE Wireless Commun. and Networking Conf.*, HONG KONG, Mar. 2007, pp. 3951–3955.

[12] Y. Shen and M. Z. Win, "Performance of localization and orientation using wideband antenna arrays," in *Proc. of IEEE International Conference on Ultra Wideband (ICUWB)*, SINGAPORE, Sept. 2007.

[13] M. Z. Win and R. A. Scholtz, "Impulse radio: How it works," *IEEE Commun. Lett.*, vol. 2, no. 2, pp. 36–38, Feb. 1998.

[14] ——, "Ultra-wide bandwidth time-hopping spread-spectrum impulse radio for wireless multiple-access communications," *IEEE Trans. Commun.*, vol. 48, no. 4, pp. 679–691, Apr. 2000.

[15] ——, "Characterization of ultra-wide bandwidth wireless indoor communications channel: A communication theoretic view," *IEEE J. Select. Areas Commun.*, vol. 20, no. 9, pp. 1613–1627, Dec. 2002.

[16] D. Cassioli, M. Z. Win, and A. F. Molisch, "The ultra-wide bandwidth indoor channel: from statistical model to simulations," *IEEE J. Select. Areas Commun.*, vol. 20, no. 6, pp. 1247–1257, Aug. 2002.

[17] A. F. Molisch, D. Cassioli, C.-C. Chong, S. Emami, A. Fort, B. Kannan, J. Karedal, J. Kunisch, H. Schantz, K. Siwiak, and M. Z. Win, "A comprehensive standardized model for ultrawideband propagation channels," *IEEE Trans. Antennas Propagat.*, vol. 54, no. 11, pp. 3151–3166, Nov. 2006, Special Issue on Wireless Communications.

[18] A. F. Molisch, "Ultrawideband propagation channels-theory, measurements, and modeling," *IEEE Trans. Veh. Technol.*, vol. 54, no. 5, pp. 1528–1545, Sept. 2005.

[19] A. Ridolfi and M. Z. Win, "Ultrawide bandwidth signals as shot-noise: a unifying approach," *IEEE J. Select. Areas Commun.*, vol. 24, no. 4, pp. 899–905, Apr. 2006.

[20] J.-Y. Lee and R. A. Scholtz, "Ranging in a dense multipath environment using an UWB radio link," *IEEE J. Select. Areas Commun.*, vol. 20, no. 9, pp. 1677–1683, Dec. 2002.

[21] W. Suwansantisuk, M. Z. Win, and L. A. Shepp, "On the performance of wide-bandwidth signal acquisition in dense multipath channels," *IEEE Trans. Veh. Technol.*, vol. 54, no. 5, pp. 1584–1594, Sept. 2005, special section on *Ultra-Wideband Wireless Communications-A New Horizon*.

[22] W. Suwansantisuk and M. Z. Win, "Multipath aided rapid acquisition: Optimal search strategies," *IEEE Trans. Inform. Theory*, vol. 52, no. 1, pp. 174–193, Jan. 2007.

[23] Z. N. Low, J. H. Cheong, C. L. Law, W. T. Ng, and Y. J. Lee, "Pulse detection algorithm for Line-of-Sight (LOS) UWB ranging applications," *IEEE Antennas Wireless Propagat. Lett.*, vol. 4, pp. 63–67, 2005.

[24] D. Dardari, C.-C. Chong, and M. Z. Win, "Threshold-based time-of-arrival estimators in UWB dense multipath channels," *IEEE Trans. Commun.*, vol. 56, 2008, to be published.

[25] Z. Zhang, C. L. Law, and Y. L. Guan, "BA-POC-Based ranging method with multipath mitigation," *IEEE Antennas Wireless Propagat. Lett.*, vol. 4, pp. 492–495, 2005.

[26] M. Spirito, "On the accuracy of cellular mobile station location estimation," *IEEE Trans. Veh. Technol.*, vol. 50, no. 3, pp. 674–685, 2001.

[27] R. Yarlagadda, I. Ali, N. Al-Dhahir, and J. E. Hershey, "GPS GDOP metric," *IEE Proceedings-Radar, Sonar Navigation*, vol. 147, no. 5, pp. 259–264, May 2000.

[28] H. L. Van Trees, *Detection, Estimation and Modulation Theory*. New York, NY: Wiley, 1968, vol. 1.

[29] H. V. Poor, *An Introduction to Signal Detection and Estimation*, 2nd ed. New York: Springer-Verlag, 1994.

[30] J. Chaffee and J. Abel, "GDOP and the Cramer-Rao bound," in *Proceedings of the Position, Location and Navigation Symposium (PLANS)*, Las Vegas, NV, Apr. 1994, pp. 663–668.

[31] J. Caffery, Ed., *Wireless Location in CDMA Cellular Radio Systems*. Boston, MA: Kluwer, 2000.

[32] T. Rappaport, J. Reed, and B. Woerner, "Position location using wireless communications on highways of the future," *IEEE Communications Magazine*, vol. 34, no. 10, pp. 33–41, 1996.

[33] D. Niculescu and B. Nath, "Ad hoc positioning system (APS) using AOA," *Proc. IEEE Joint Conf. of the IEEE Computer and Commun. Societies*, vol. 3, pp. 1734–1743, Mar./Apr. 2003.

[34] N. Patwari and A. Hero III, "Using Proximity and Quantized RSS for Sensor Localization in Wireless Networks," *IEEE/ACM 2nd Workshop on Wireless Sensor Nets. & Applications*, pp. 20–29, 2003.

[35] T. Pavani, G. Costa, M. Mazzotti, A. Conti, and D. Dardari, "Experimental results on indoor localization techniques through wireless sensors network," in *IEEE Proc. of Vehicular Technology Conference (VTC 2006-Spring).*, vol. 2, May 2006, pp. 663–667.

[36] Y. Qi and H. Kobayashi, "Cramér-Rao lower bound for geolocation in non-line-of-sight environment," in *Proceedings of the International Conference on Acoustics, Speech, and Signal Processing*, Orlando, FL, May 2002, pp. 2473–2476.

[37] Y. Qi, H. Suda, and H. Kobayashi, "On time-of-arrival positioning in a multipath environment," in *Proc. IEEE Semiannual Veh. Technol. Conf.*, Los Angeles, CA, Sept. 2004, pp. 3540–3544.

[38] A. F. Molisch, *Wireless Communications*, 1st ed. Piscataway, New Jersey, 08855-1331: IEEE Press, J. Wiley and Sons, 2005.

[39] M. Silventoinen and T. Rantalainen, "Mobile station emergency locating in GSM," in *Proc. of IEEE Int. Conf. on Personal Wireless Commun.*, New Delhi, 1996, pp. 232–238.

[40] J. Caffery and G. Stuber, "Radio location in urban CDMA microcells," in *Proc. IEEE Int. Symp. on Personal, Indoor and Mobile Radio Commun.*, vol. 2, Toronto, Ont., 1995, pp. 858–862.

[41] M. Gavish and E. Fogel, "Effect of bias on bearing-only target location," *IEEE Trans. Aerosp. Electron. Syst.*, vol. 26, no. 1, pp. 22–26, Jan. 1990.

[42] M. Wylie and J. Holtzman, "The non-line of sight problem in mobile location estimation," in *Universal Personal Communications, 1996. Record., 1996 5th IEEE International Conference on*, vol. 2, Cambridge, MA, 1996, pp. 827–831.

[43] S.-S. Woo, H.-R. You, and J.-S. Koh, "The NLOS mitigation technique for position location using IS-95CDMA networks," in *Proc. IEEE Semiannual Veh. Technol. Conf.*, vol. 6, Boston, MA, 2000, pp. 2556–2560.

[44] S. Al-Jazzar, J. Caffery, J., and H.-R. You, "A scattering model based approach to NLOS mitigation in TOA location systems," in *Proc. IEEE Semiannual Veh. Technol. Conf.*, vol. 2, 2002, pp. 861–865.

[45] P.-C. Chen, "A non-line-of-sight error mitigation algorithm in location estimation," in *Proc. IEEE Wireless Commun. and Networking Conf.*, vol. 1, Sept. 1999, pp. 316–320.

[46] L. Xiong, "A selective model to suppress NLOS signals in angle-of-arrival (AOA) location estimation," in *Proc. 9th IEEE Int. Symp. on Personal, Indoor and Mobile Radio Communications*, vol. 1, Boston, MA, 1998, pp. 461–465.

[47] H. Wang, L. Yip, K. Yao, and D. Estrin, "Lower bounds of localization uncertainty in sensor networks," in *Proc. IEEE Int. Conf. Acoustics, Speech, and Signal Processing*, Montreal, QC, May 2004, pp. 917–920.

[48] M. Wax and A. Leshem, "Joint estimation of time delays and directions of arrival of multiple reflections of a known signal," *IEEE Trans. Signal Processing*, vol. 45, no. 10, pp. 2477–2484, Oct. 1997.

[49] Y. Qi, H. Kobayashi, and H. Suda, "Analysis of wireless geolocation in a non-line-of-sight environment," *IEEE Trans. Wireless Commun.*, vol. 5, no. 3, pp. 672–681, 2006.

[50] C. Botteron, A. Host-Madsen, and M. Fattouche, "Cramer-Rao bounds for the estimation of multipath parameters and mobiles' positions in asynchronous DS-CDMA systems," *IEEE Trans. Signal Processing*, vol. 52, no. 4, pp. 862–875, 2004.

[51] H. Koorapaty, H. Grubeck, and M. Cedervall, "Effect of biased measurement errors on accuracy of position location methods," in *Proc. IEEE Global Telecomm. Conf.*, vol. 3, Sydney, NSW, 1998, pp. 1497–1502.

[52] B. Van Veen and K. Buckley, "Beamforming: a versatile approach to spatial filtering," *IEEE Signal Processing Mag.*, vol. 5, no. 2, pp. 4–24, 1988.

[53] H. Krim and M. Viberg, "Two decades of array signal processing research: the parametric approach," *IEEE Signal Processing Mag.*, vol. 13, no. 4, pp. 67–94, 1996.

[54] R. Engelbrecht, "Passive source localization from spatially correlated angle-of-arrival data," *IEEE Trans. Signal Processing*, vol. 31, no. 4, pp. 842–846, 1983.

[55] C.-C. Chong, C.-M. Tan, D. I. Laurenson, S. McLaughlin, M. A. Beach, and A. R. Nix, "A new statistical wideband spatio-temporal channel model for 5-GHz band WLAN systems," *IEEE J. Select. Areas Commun.*, vol. 21, no. 2, pp. 139–150, Feb. 2003.

[56] P. Deng and P. Fan, "An AOA assisted TOA positioning system," in *Proc. of Int. Conf. on Commun. Technol.*, vol. 2, Beijing, 2000, pp. 1501–1504.

[57] L. Cong and W. Zhuang, "Hybrid TDOA/AOA mobile user location for wideband CDMA cellular systems," *IEEE Trans. Wireless Commun.*, vol. 1, no. 3, pp. 439–447, 2002.

[58] C. Chang and A. Sahai, "Estimation bounds for localization," in *Proc. of the First Annual IEEE Communications Society Conference on Sensor and Ad Hoc Communications and Networks, SECON 2004*, S. Clara, CA, USA, Oct. 2004, pp. 415–424.

[59] M. Hamilton and P. Schultheiss, "Passive ranging in multipath dominant environments. i. known multipath parameters," *IEEE Trans. Signal Processing*, vol. 40, no. 1, pp. 1–12, 1992.

[60] J. Lee and S. Yoo, "Large error performance of UWB ranging," in *Proc. of IEEE International Conference on Ultra Wideband (ICUWB)*, Zurich, Switzerland, 2005, pp. 308–313.

[61] A. A. Saleh and R. A. Valenzuela, "A statistical model for indoor multipath propagation," *IEEE J. Select. Areas Commun.*, vol. 5, no. 2, pp. 128–137, Feb. 1987.

[62] I. Reuven and H. Messer, "A Barankin-type lower bound on the estimation error of a hybrid parameter vector," *IEEE Trans. Inform. Theory*, vol. 43, no. 3, pp. 1084–1093, May 1997.

[63] R. A. Horn and C. R. Johnson, *Matrix Analysis*, 1st ed. Cambridge, NY: Cambridge University Press, 1985.

[64] R. A. Scholtz, "How do you define bandwidth?" in *Proc. International Telemetering Conference*, Oct. 1972, pp. 281–288, los Angeles, California, Invited Paper.

[65] D. B. Jourdan, D. Dardari, and M. Z. Win, "Position error bound for UWB localization in dense cluttered environments," in *Proc. IEEE Int. Conf. on Commun.*, vol. 8, Istanbul, TURKEY, June 2006, pp. 3705–3710.

[66] S. W. Golomb and R. A. Scholtz, "Generalized Barker sequences," *IEEE Trans. Inform. Theory*, vol. IT-11, no. 4, pp. 533– 537, Oct. 1965.

[67] S. W. Golomb and M. Z. Win, "Recent results on polyphase sequences," *IEEE Trans. Inform. Theory*, vol. 44, no. 2, pp. 817–824, Mar. 1998.

[68] S. W. Golomb and G. Gong, *Signal Design for Good Correlation : For Wireless Communication, Cryptography, and Radar.* Cambridge University Press, 2005.